

University of Louisville

ThinkIR: The University of Louisville's Institutional Repository

Electronic Theses and Dissertations

12-2023

Adaptive personalized drug delivery method for warfarin and anemia management: Modeling and control.

Affan Affan
University of Louisville

Follow this and additional works at: <https://ir.library.louisville.edu/etd>



Part of the [Biomedical Commons](#), and the [Controls and Control Theory Commons](#)

Recommended Citation

Affan, Affan, "Adaptive personalized drug delivery method for warfarin and anemia management: Modeling and control." (2023). *Electronic Theses and Dissertations*. Paper 4227.
<https://doi.org/10.18297/etd/4227>

This Doctoral Dissertation is brought to you for free and open access by ThinkIR: The University of Louisville's Institutional Repository. It has been accepted for inclusion in Electronic Theses and Dissertations by an authorized administrator of ThinkIR: The University of Louisville's Institutional Repository. This title appears here courtesy of the author, who has retained all other copyrights. For more information, please contact thinkir@louisville.edu.

ADAPTIVE PERSONALIZED DRUG DELIVERY METHOD FOR WARFARIN
AND ANEMIA MANAGEMENT: MODELING AND CONTROL

by
Affan Affan,
B. Eng, M.Sc.

A Dissertation

Submitted to the Faculty of the
J.B. Speed School of Engineering of the University of Louisville
for the degree of

Doctor of Philosophy
in Electrical and Computer Engineering.

Department of Electrical and Computer Engineering,
University of Louisville,
Louisville, Kentucky, USA.

December 2023

©November, 2023
Affan Affan
All rights reserved

ADAPTIVE PERSONALIZED DRUG DELIVERY METHOD FOR WARFARIN
AND ANEMIA MANAGEMENT: MODELING AND CONTROL

By

Affan Affan

A Dissertation Approved on

11/10/2023

By the following Dissertation Committee

Tamer Inanc, Ph.D., Dissertation Chair

Jacek M. Zurada, Ph.D., Committee member

Christopher Richards, Ph.D., Committee member

Michael McIntyre, Ph.D., Committee member

John Naber, Ph.D., Committee member

DEDICATION

To my late parents, Mr. & Mrs. Muhammad Razzaq, who always believed in me and worked hard to provide me with opportunities for a better life against all odds.

ACKNOWLEDGEMENTS

I would like to thank my supervisor, Dr. Tamer Inanc for his support and guidance throughout my research work here at the University of Louisville. Without his support and trust, I would not have been able to succeed in this endeavor. I would also like to thank Dr. Jacek M. Zurada for his support in conducting my research and providing feedback on research work which helped improve the quality of the work. I would like to thank all my friends, both in the United States and elsewhere who have been a tremendous support to me during my time in Louisville. They were like a family away from home. Finally, I would like to say thanks to my family, who have supported me throughout thick and thin. First and foremost my late parents, my mother Mumtaz Akhtar and father Muhammad Razzaq. They through their hard work and determination left no stone unturned to provide me with the best upbringing anyone can provide to their children. My wife Joudat Bint Khalil, has always been a pillar of support for me. My siblings, Sadaf Amir, Adnan, and Rizwan have been the best brothers and a sister anyone can ask for. My lovely nieces and nephews are a cause of much joy in our lives.

ABSTRACT

ADAPTIVE PERSONALIZED DRUG DELIVERY METHOD FOR WARFARIN AND ANEMIA MANAGEMENT: MODELING AND CONTROL

Affan Affan

November 10, 2023

Personalized precision medicine aims to develop the appropriate treatments for suitable patients at the right time to obtain optimal results. Personalized medicine is challenging due to inter- and intra-patient variability, narrow therapeutic window, the effect of other medications, comorbidity (more than one disease at a time), nonlinear patient dynamics, and time-varying patient dose response characteristics which include bleeding (internal and external). This research aims to develop a framework for an adaptive personalized modeling and control method with minimum clinical patient specific dose response data for optimal drug dosing. The proposed methodology is applied to anemia and warfarin management. It is challenging in practice to achieve an optimal dosage of erythropoietin (EPO) to maintain Hemoglobin (Hgb) levels between 10-12 *g/dl* in case of anemia management and the optimal dosage of warfarin to maintain an International Normalized Ratio (INR) between 2.0 to 3.0 in case of warfarin management, based on population-based models due to inter-and intra-variability of the patients. For personalized patient modeling, semi-blind robust system identification incorporates the effect of non-zero initial conditions and uses the minimum number of patient specific clinical data. The model (In)validation technique and Kalman filter are used for adaptation. Furthermore, Adaptive Model Predictive Control (AMPC), Extremum-Seeking Control (ESC), Model-Free Reinforcement Learning (MFRL), and Model-Based Reinforcement Learning (MBRL) control policies are defined for Virtual Chronic Kidney Disease (VCKD) patients. These methods are tested for the events of bleeding and missing dosages. The results conclude that data-driven adaptive control methods, such as AMPC and DQN-RL, can handle serious conditions of bleeding and missing dosage for virtual CKD patients which have a narrow therapeutic window. However, one major drawback of the MFRL methods is the requirement of a high number of patient specific data points to train the agent. This requirement is not suitable for personalized medicine. To reduce the number of patient specific data points required for training the agent, MBRL is introduced. However, MB-DQN-RL faces challenges in providing steady EPO dosages. Therefore, AMPC along with semi-blind robust model identification with Kalman filter provides a complete practical framework to provide personalized optimal dosages.

TABLE OF CONTENTS

ACKNOWLEDGEMENTS	iv
ABSTRACT	v
List of Figures	vii
List of Tables	xi
1 PERSONALIZED MEDICINE	1
1.1 Personalized Anemia Management	1
1.2 Personalized Warfarin Management	2
2 SYSTEM IDENTIFICATION METHODS FOR PERSONALIZED MEDICINE	4
2.1 Semi-Blind Robust System Identification	4
2.1.1 Model (In)validation based Adaptive Model Identification	6
2.1.1.1 Algorithm	8
2.1.1.2 Anemia Management Results	11
2.1.1.3 Warfarin Management Results	19
2.1.2 Kalman Filter based Adaptive Model Identification	25
2.1.2.1 Anemia Management Results	26
2.1.2.2 Warfarin Management Results	32
3 VIRTUAL CHRONIC KIDNEY DISEASE (V-CKD) PATIENT MODEL	37
4 OPTIMAL CONTROL DESIGN FOR PERSONALIZED MEDICINE	40
4.1 Adaptive Model Predictive Control (AMPC)	40
4.2 Extremum Seeking Control	42
4.2.1 Results	44
4.3 Reinforcement Learning for Personalized Medicine	46
4.3.1 Model-Free Deep Q-Learning for Optimal EPO Dosing	46
4.3.1.1 Results	47
4.3.2 Model-Based Deep Q-Learning for Optimal EPO Dosing	49
4.3.2.1 Results	50
5 CONCLUSION AND FUTURE WORK	53
5.1 Summary	53
5.2 Future Work	53
References	55

LIST OF FIGURES

2.1	Framework for semi-blind identification.	5
2.2	The (In)validation framework for semi-blind robust identification. . . .	7
2.3	The convex relaxed Model (In)validation framework for semi-blind robust identification.	8
2.4	Recursive adaptive model identification with Model (In)validation. . . .	9
2.5	Prediction results for patient-1 model obtained by semi-blind robust identification with model (In)validation.	11
2.6	Prediction results for patient-1 model obtained by semi-blind robust identification without model (In)validation.	12
2.7	Prediction results for patient-13 model obtained by semi-blind robust identification without model (In)validation.	13
2.8	Prediction results for patient-13 model obtained by semi-blind robust identification with model (In)validation.	14
2.9	Prediction results for patient-19 model obtained by semi-blind robust identification without a model (In)validation.	15
2.10	Prediction results for patient-19 model obtained by semi-blind robust identification with a model (In)validation.	16
2.11	Prediction results for patient-21 model obtained by semi-blind robust identification with a model (In)validation.	17
2.12	Prediction results for patient-21 model obtained by semi-blind robust identification without a model (In)validation.	18
2.13	Error Comparison between semi-blind robust identification with and without model (In)validation for anemia management.	19
2.14	Error comparison of personalized Warfarin-INR dose-response models obtained with and without model (In)validation	20
2.15	Prediction results for patient-7 model obtained by semi-blind robust identification without model (In)validation for Warfarin dosing.	21
2.16	Prediction results for patient-7 model obtained by semi-blind robust identification with model (In)validation for Warfarin dosing.	21
2.17	Prediction results for patient-3 model obtained by semi-blind robust identification without model (In)validation for Warfarin dosing.	23
2.18	Prediction results for patient-3 model obtained by semi-blind robust identification with model (In)validation for Warfarin dosing.	24
2.19	Prediction results for patient-10 model obtained by semi-blind robust identification without model (In)validation or Warfarin dosing.	25
2.20	Prediction results for patient-10 model obtained by semi-blind robust identification with model (In)validation or Warfarin dosing.	26
2.21	Prediction results of semi-blind robust system identification with the Kalman filter for Patient-1 of anemia management.	27

2.22	Prediction results of ARX with the Kalman filter for Patient-1 of anemia management.	27
2.23	Prediction results of semi-blind robust system identification with the Kalman filter for Patient-13 for anemia management.	28
2.24	Prediction results of ARX with the Kalman filter for Patient-13 of anemia management.	28
2.25	Prediction results of semi-blind robust system identification with the Kalman filter for Patient-19 of anemia management.	29
2.26	Prediction results of ARX with the Kalman filter for Patient-19 of anemia management.	29
2.27	Prediction results of ARX with the Kalman filter for Patient-19 of anemia management.	30
2.28	Prediction results of ARX with the Kalman filter for Patient-19 of anemia management.	30
2.29	Prediction results of semi-blind robust system identification with the Kalman filter for Patient-21 for anemia management.	31
2.30	Prediction results of ARX with the Kalman filter for Patient-21 for anemia management.	31
2.31	MMSE values for anemia management for; (1) Semi-blind with model(In)validation (2) Semi-blind without model(In)validation, (3) Semi-blind with Kalman Filter, (4) ARX with Kalman Filter.	32
2.32	Prediction results of ARX with the Kalman filter for Patient-3 of warfarin management.	33
2.33	Prediction results of semi-blind robust system identification with the Kalman filter for Patient-3 of warfarin management.	33
2.34	Prediction results of ARX with the Kalman filter for Patient-7 for warfarin management.	34
2.35	Prediction results of semi-blind robust system identification with the Kalman filter for Patient-7 for warfarin management.	34
2.36	Prediction results of ARX with the Kalman filter for Patient-10 for warfarin management.	35
2.37	Prediction results of semi-blind robust system identification with the Kalman filter for Patient-10 for warfarin management.	35
2.38	MMSE values for Warfarin management for; (1) Semi-blind with model(In)validation (2) Semi-blind without model(In)validation, (3) Semi-blind with Kalman Filter, (4) ARX with Kalman Filter.	36
4.1	Block diagram for Adaptive MPC (AMPC) with online parameter estimation for virtual CKD Patient.	41
4.2	Block diagram for Extremum Seeking Control (ESC) with online parameter estimation for V-CKD Patient.	42
4.3	<i>In-silicio</i> results of AMPC and ESC for V-CKD Patient-1.	44
4.4	<i>In-silicio</i> results of AMPC and ESC for V-CKD Patient-2.	45
4.5	Block diagram for DQN-RL for virtual CKD Patient.	46
4.6	Results of DQN-RL and AMPC for the V-CKD Patient-1.	48
4.7	Results of DQN-RL and AMPC for the V-CKD Patient-2.	49
4.8	Block diagram for Model-Based DQN Reinforcement Learning (MB-DQN-RL) for V-CKD Patient.	50

4.9	Results of MB-DQN-RL and AMPC for the V-CKD Patient-1.	51
4.10	Results of MB-DQN-RL and AMPC for the V-CKD Patient-2.	52

LIST OF TABLES

2.1	Model (In)Validation Results of Patient-1	12
2.2	Model (In)Validation Results of Patient-13	14
2.3	Model (In)Validation Results of Patient-19	16
2.4	Model (In)Validation Results of Patient-21	18
4.1	Virtual CKD Patient Model Parameters [1, 2]	43

CHAPTER 1

PERSONALIZED MEDICINE

Personalized or precision medicine is an innovative approach to disease treatment that considers differences in people's genes, environments, and lifestyles. Precision medicine aims to target the right treatments to the right patients at the right time to obtain optimal results. For drug administration, the five rights, which are the right patient, the right drug, the right time, the right dose, and the right route, are well known [3]. However, many dosing errors occur due to the current trial-and-error approach resulting in insufficient guidance of medication and dose-response data. This chapter discusses the field of personalized medicine for anemia management and warfarin management and the role of control theory in this field.

1.1 Personalized Anemia Management

In Chronic Kidney Disease (CKD), the functionality of the patient's kidneys is compromised to produce a hormone called erythropoietin (EPO) [4, 5]. This affects erythropoiesis, a process to produce red blood cells (RBCs), and leads to low hemoglobin (Hgb) levels [6]. This medical condition is called anemia and it affects more than 3 million people in the US alone. Statistically, there were about 890,000 visits to emergency departments due to anemia across the US as per the database of Centers for Disease Control and Prevention (CDC) for 2018 [7].

The optimal dosing of external EPO is challenging due to its narrow therapeutic window, the effect of other medications, comorbidity (more than one disease at a time), nonlinear patient dynamics, and time-varying patient-dose response characteristics due to bleeding (internal and external), aging, weight and dietary habits [8, 9, 10]. This emphasizes that the one-size-fits-all model approach may not work best, and therefore personalized and adaptive drug delivery methods are required.

Many researchers have proposed different techniques to develop dose-response models for a number of different diseases. Bayesian-based drug delivery using population patient data is discussed in [11]. In [12], control-oriented models are developed for Type-1 Diabetes to capture the intra-patient variability of insulin drug patients. Artificial Intelligence-based neural network models are discussed in [13, 14, 15]. Some researchers attempted to identify individual patient models in [16]. In [17] the focus was to predict the value for EPO instead of Hgb, which is not desired as predicting the Hgb level gives values of EPO but it is not true for vice versa. However, most of these models are based on predetermined model structure and noise distribution, which are not suitable for anemia management as each patient has different characteristics. The models obtained by the classical system identification techniques do not yield good re-

sults as they assume that predefined model structure and model order are close to the actual system (patient) and one fixed mathematical model works for all dynamics regardless of the complexity and uncertainties existing in the system (patient). Therefore, the modeling stage should include the effect of disturbances and uncertainties that are being introduced during operations. In contrast to classical identification techniques, robust system identification considers system (patient) uncertainties, unmodeled dynamics, and model complexity, i.e., there is no assumption on the model order, type of uncertainties, and noise affecting the data.

Recently, [18] has reported a feedback control approach for optimal EPO dosing and reported that patient models obtained through system identification suffer performance degradation over time. This indicates that an adaptive modeling approach is needed to avoid this kind of degradation. Semi-blind robust system identification-based adaptive modeling framework for CKD patients is reported in [19, 20]. Model Predictive Control (MPC) based approach has been proposed for optimal EPO dosing in [21, 22]. The proposed approach is highly effective, however, there is room for testing the ability of MPC in the event of bleeding and missing dosage. Nonlinear MPC is proposed for optimal EPO dosing in [1]. This research has a significant contribution, however, the model used in this work is not adaptive and the results show a long recovery time after bleeding.

1.2 Personalized Warfarin Management

Warfarin is an oral anticoagulant used to decrease blood clotting and avoid thromboembolic events in the human body. The main reason for the thrombotic events is the blood clots that break loose and are stuck in narrow vessels. The effect of warfarin is monitored by measuring the International Normalized Ratio (INR). INR is the ratio between the patient's prothrombin time (PT) and the mean normal PT [23]. The desired range of INR values is between 2.0 to 3.0 [24]. In addition to the narrow therapeutic range of INR, the INR is highly affected by genetics, change in diet, and the use of other medications throughout treatment. These fluctuations can lead to under-anticoagulation, increasing the risk of clotting, and over-anticoagulation, increasing the risk of release of blood from broken blood vessels [25].

The dosage of warfarin is affected by dietary interactions, drug interactions, demographic effects, and genetics[26]. Vitamin K is a natural antidote to warfarin and most dark green vegetables such as broccoli consist of a high level of vitamin K [27]. On average, a human takes around 60-200 $\mu\text{g}/\text{day}$ of vitamin K, while the intake of 100 $\mu\text{g}/\text{day}$ of vitamin K for 4 consecutive days can lower the INR value by 0.2 [28]. One of the major factors which influence the INR value in the human body are interactions of other drugs with warfarin [29]. Drugs such as amiodarone used to treat heart rhythm problems interact with warfarin to increase the anticoagulant effect [30]. On the other hand, drugs like aspirin increase the risk of bleeding by eliminating warfarin [31, 32, 33]. The aforementioned factors lead to the ineffective warfarin dosage, which is the common cause of most hospital visits in the USA and UK [34, 35].

The narrow therapeutic range of Warfarin and the risk of bleeding due to unintentional overdosing of Warfarin urge the need for a robust, adaptive, and patient-specific warfarin management system that represents true patient status in the event of a change diet and life habits [26]. Another challenge for the applications of precise drug delivery is the slow sampling rate as often measurement sampling time is of days and weeks. It

can slow the process of data collection and result in small data sets. Therefore, a modeling algorithm is needed that can identify the model at an early stage and recursively improve the model capabilities as the new measurement data is received. Also, due to swift changes in factors related to warfarin, the prediction models must show the true status of the patients using a limited number of available patient-specific clinical data. Therefore, the model must learn the change in the dose-response characteristics of each patient and adapt to the wavering status within an equitable time frame.

Many researchers have proposed dose-response models to predict the dosage of warfarin using different model identification techniques. Numerous prediction models have been proposed in the literature that use the Bayesian approach to predict the warfarin dosage [36, 37, 38, 39, 36]. The Bayesian approach is prominent in model identification due to its ability to take full account of uncertainties related to the model and parameter values. However, Bayesian methods require the selection of probability distributions of disturbances and noise, which can be time-consuming and may lead to erroneous dose-response models if the prior distributions are imprecise [40, 41]. Several artificial intelligence (AI)-based predictive models have been proposed using different methods [42, 43, 44]. The AI-based models can efficiently predict warfarin dosage to reduce the risk of overdosing or under-dosing. The main challenge in AI-based models is the requirement of a large data set, which is a drawback as patient-specific clinical dose-response data for warfarin is usually not available in high volume. Moreover, the AI-based models are typically trained using population-based data sets. This is very pivotal because, with the use of population-based data sets, the inter-and intra-variability among the patients can not be effectively addressed.

Inspired by the methods and challenges discussed in the literature, the next section discusses the semi-blind robust system identification method. It uses the effect of non-zero initial conditions and the minimum number of patient-specific dose-response data points to find the patient model.

CHAPTER 2

SYSTEM IDENTIFICATION METHODS FOR PERSONALIZED MEDICINE

2.1 Semi-Blind Robust System Identification

The patient (system) model is a set of mathematical equations that describes the patient's behavior in response to the medication over time. In this research work, system identification aims to develop a low-order model of the patient from finite, noisy measurements of clinical dose-response data. The following result from the literature will provide the foundation for the existence of linear time-invariant (LTI) models with relevant features.

Lemma 1. *Given a matrix-valued sequence $\{G_i\}_{i=0}^{n-1}$, there exists a discrete LTI model, $G(z) \in \mathcal{BH}_\infty$, such that*

$$G(z) = G_0 + Gz + G_2z^2 + \cdots + G_{n-1}z^{n-1}, \quad (2.1)$$

if and only if $(T_G^n)^T T_G^n \leq I$.

where \mathcal{BH}_∞ denotes the open ball in an infinity normed space and T_G is the Toeplitz matrix. The patient model is required to be stable, controllable, and observable. By considering stability margin $(\rho - 1)$ and input bound by K , the patient model of form \mathcal{S} is defined as follows [45, 46]:

$$\mathcal{S} \doteq \{G(z) = G_p(z) + G_{np}(z)\}, \quad (2.2)$$

which consists of non-parametric portion, $G_{np} \in \mathcal{BH}_{\infty,\rho}(K)$ for $\rho \geq 1$ and parametric portion, G_p , of form \mathcal{P} is defined as follows:

$$\mathcal{P} \doteq \{G_p(z) = \mathbf{p}^T \mathbf{H}(z), \mathbf{p} \in \mathcal{R}^{N_p}\}, \quad (2.3)$$

where \mathbf{p} is affine parameter. The N_p components of vector $H(z)$ are known as linearly independent, rational transfer functions as shown in Fig. 2.1. The model $G(z) \in \mathcal{S}$, that maps input sequence, \mathbf{u} , to output sequence, \mathbf{y} , in the presence of noise, η with noise bound, $\epsilon \in \mathcal{N}$, can be obtained by the following condition.

Lemma 2. *There exists an operator $G \in \mathcal{S}$ such that $\mathbf{y} = G\mathbf{u} + \eta$, given that K , ρ , and measurement data (\mathbf{u}, \mathbf{y}) are provided, if and only if a parameter vector \mathbf{g} exists, which satisfy:*

$$M(g) \doteq \begin{bmatrix} KR^{-2} & (T_g^N)^T \\ T_g^N & KR^2 \end{bmatrix} \geq 0, \quad (2.4)$$

$$\mathbf{y} = T_u^N P \mathbf{p} + T_u^N \mathbf{g},$$

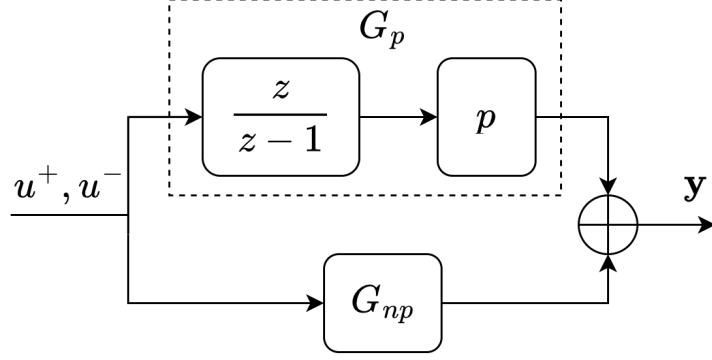


Figure 2.1: Framework for semi-blind identification.

where $P_k = \{h_k^1, h_k^2, \dots, h_k^{N_p}\}$, here h_k^i is the k -th Markov parameter of the i -th transfer function $H(z)$. g_k is the k -th Markov parameter of the non-parametric portion G_{np} and $R = \text{diag}[1, \rho, \rho^2, \dots, \rho^{N-1}]$. T_u^N and T_g^N are the lower Toeplitz matrix associated with parameter vector, g , and input measurements \mathbf{u} . Relation of T_g^N with measurement data (\mathbf{u}, \mathbf{y}) is defined as follows:

$$\begin{bmatrix} y_0 \\ y_1 \\ y_2 \\ \vdots \\ y_{N-1} \end{bmatrix} = \begin{bmatrix} g_0 & 0 & 0 & \cdots \\ g_1 & g_0 & 0 & \cdots \\ g_2 & g_1 & g_0 & 0 \\ \vdots & \vdots & \ddots & \vdots \\ g_{N-1} & g_{N-2} & \cdots & g_{2N-1} \end{bmatrix} \begin{bmatrix} u_0 \\ u_1 \\ u_2 \\ \vdots \\ u_{N-1} \end{bmatrix}. \quad (2.5)$$

In most applications of system identification zero initial conditions are considered. However, a patient might already have a medical history, which can affect the prediction of the identified model. It is also important to mention that for this application, the patient data is not steady-state data, therefore, the effect of past inputs is still present. The response of the patient model is highly affected by their initial state at $t = 0$. The semi-blind robust identification technique incorporates the effect of initial conditions of the patient (system) as follows [47, 48, 46]:

Problem 1. Given a priori set of candidate models, \mathcal{S} , noise bound, ϵ , and posteriori measurement data, (\mathbf{u}, \mathbf{y}) , and maximum stability gain, ρ , determine $G(z)$, which is compatible with priori information and posteriori measurement data, such that τ is a non-empty set. Given the state space model, $G = \begin{bmatrix} A_g & B_g \\ C_g & D_g \end{bmatrix}$, τ is defined as:

$$\tau(\mathbf{y}) \doteq \left\{ G \in \mathcal{S} : y_k - \sum_{i=0}^N q_i u_{k-i} + C_g A_g^{k-1} \mathbf{x}_0 \in \mathcal{N}, k = 0, \dots, N-1 \right\} \quad (2.6)$$

where $q_0 = D_g$; $q_i = C_g (A_g)^{i-1} B_g$. The solution to (2.6) involves solving a non-convex Bilinear Matrix Inequalities (BMIs) in g_i and initial conditions, \mathbf{x}_0 , which is a non-convex and NP-hard problem. The above problem can be converted to the convex problem by assuming that past inputs, u^- , belong to some set, \mathcal{U}_- [47]. Therefore, the initial condition, \mathbf{x}_0 , can be replaced by the effect of past inputs. Equation (2.6) can be modified as follows:

$$\tau(\mathbf{y}) \doteq \{ G(z) \in \mathcal{S} : y_k - (T_g u^+)_k + (\Gamma_g u^-)_k, k = 0, \dots, N-1 \}, \quad (2.7)$$

where $u^+ = u_0, u_1, \dots, u_{N-1}$ and Γ_g is the Hankel matrix, which maps the past inputs to the output as follows:

$$\begin{bmatrix} y_0 \\ y_1 \\ y_2 \\ \vdots \\ y_{N-1} \end{bmatrix} = \begin{bmatrix} g_1 & g_2 & \cdots & g_N \\ g_2 & g_3 & \cdots & g_{N+1} \\ \vdots & \vdots & \ddots & \vdots \\ g_N & g_{N+1} & \cdots & g_{2N-1} \end{bmatrix} \begin{bmatrix} u_{-1} \\ u_{-2} \\ u_{-3} \\ \vdots \\ u_{-N} \end{bmatrix}. \quad (2.8)$$

The first part of the τ set corresponds to the plant (patient) response for input u and the latter part provides information for the system response for past inputs u^- [47, 48]. The term $(\Gamma_g u^-)_k$ can be reduced to $x_k = (\Gamma_g u^-)_k \in \mathcal{X}_0$, by assuming that set of past input has the form, $\mathcal{U} = \mathcal{Bl}(K_u)$, and a bound, $\|\Gamma_g\|_{l^p \rightarrow l^\infty} \leq \gamma$, is available as priori information. Here, $\mathcal{Bl}(K_u)$ denotes the open K_u -ball in a normed space l and \mathcal{Bl} is the open unit ball in space l . The modified problem statement can be written as follows:

Problem 2. *Given priori set of candidate models, past inputs and noise $(\mathcal{S}, \mathcal{U}, \mathcal{N})$ and N measurement (\mathbf{u}, \mathbf{y}) data points, determine $G(z) \in \mathcal{S}$, which is compatible with a priori information and a posteriori measurement data (\mathbf{u}, \mathbf{y}) , such that τ is a non-empty set:*

$$\tau(\mathbf{y}) \doteq \{G(z) \in \mathcal{S} : y_k - (T_g u^+)_k - x_k, k = 0, \dots, N-1\}, \quad (2.9)$$

where $|x|_k \leq \gamma K_u$. By using Lemma 2, following result can be deduced:

Proposition 1. *Problem 2 can be solved by finding a feasible solution of the following LMIs in g and \mathbf{x} :*

$$\begin{aligned} M(g) &= \begin{bmatrix} KR^{-2} & (T_g^N)^T \\ (T_g^N) & KR^2 \end{bmatrix} \geq 0, \\ |y - (T_u^N pP + T_u^N g) - \mathbf{x}| &\in \mathcal{N}, \\ -\gamma K_u &\leq \mathbf{x} \leq \gamma K_u, \end{aligned} \quad (2.10)$$

where γ, K_u, p, P represent γ -ball in a normed space, bound on the norm of the sequence u^- , affine parameters, and the parametric portion of the model, respectively.

Heretofore, we have discussed the semi-blind robust system identification to obtain individualized patient models using a limited number of patient-specific clinical data points, possibly corrupted by noise. However, as time passes the patient's characteristics may change due to aging, change in food habits, and new medication for another disease (comorbidity). The change in the patient's status may reflect in the patient's drug-dose response, and the model identified at an early stage may not match the patient's current dose-response characteristics. Therefore, this model may not be suitable anymore for the controller as time passes. To adapt the model to the patient's current status, the next sub-sections discuss the two model adaptation techniques: (1) Model (In)validation based Adaptive Model Identification, which provides mathematical evidence about the suitability of the model by testing the model on data unseen by the identification process and (2) Kalman Filter based Adaptive Model Identification, which updates the model parameters based on prediction error.

2.1.1 Model (In)validation based Adaptive Model Identification

To use an individualized patient model identified by semi-blind robust system identification, it is important to validate the identified model. Therefore, the identified model is

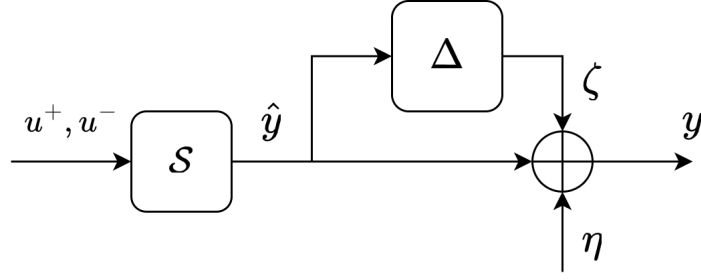


Figure 2.2: The (In)validation framework for semi-blind robust identification.

tested against the patient's new measurement data points, which have not been used in system identification to avoid biases. This method indicates when an identified model is no longer compatible with the patient's measurement data and the model needs to be updated by re-identification using semi-blind robust system identification. This also helps to cover system uncertainties, unmodeled dynamics, and model complexity in the system. By assuming multiplicative uncertainty and additive noise, the problem can be stated as follows:

Problem 3. Given M new measurement data points, $(\mathbf{y}^+, \mathbf{u}^+)$, the nominal model, $G(z) \in \mathcal{S}$, descriptions of admissible noise, \mathcal{N} , uncertainty, Δ , and initial conditions, \mathcal{X}_0 , determine if there exists at least one triple $(\eta, \Delta, x_0) \in \mathcal{N} \times \Delta \times \mathcal{X}_0$ that can reproduce the available experimental data by the following equation [47]:

$$y = (I + \Delta) (T_g u^+ + T_g^{ic} x_0) + \eta, \quad (2.11)$$

where u^+ is the input after, $t = 0$. T_g maps the input to the output, whereas, T_g^{ic} , maps the initial conditions to the output. The above problem has a term, $T_g^{ic} x_0$, where x_0 is the unknown initial condition. During the identification, this term can be replaced with some term representing the effect of these initial conditions such as $u^- \in \mathcal{U}_-$. Therefore, (2.11) can be modified as follows:

$$y = (I + \Delta) (T_g u^+ + \Gamma_g u^-) + \eta. \quad (2.12)$$

Figure 2.2 shows the framework for the model (In)validation, which shows the model is validated by the new measurement data if and only if there exists, $\Delta \in \Delta$, such that, $y - \hat{y} - \eta \doteq \zeta = \Delta \hat{y}$. Using Lemma 1, $\Delta = \mathcal{BH}_\infty(\delta)$ is equal to the feasible solution of following inequalities:

$$\begin{aligned} (T_\zeta^M)^T T_\zeta^M &\leq \delta^2 (T_{\hat{y}}^M)^T T_{\hat{y}}^M, \\ \delta^2 (T_{\hat{y}}^M)^T T_{\hat{y}}^M - (T_y^M - T_{\hat{y}}^M - T_\eta^M)^T (T_y^M - T_{\hat{y}}^M - T_\eta^M) &\geq 0, \end{aligned} \quad (2.13)$$

where $T_{\hat{y}} \doteq T_g^M T_{u^+}^M + \Gamma_g^M T_{u^-}^M$. Here, due to cross terms, $T_\eta^M \Gamma_g^M T_{u^-}^M$, (2.13) is non-convex. To avoid solving the non-convex problem, the following convex relaxation is considered as shown in Fig. 2.3 [47, 48]. The measurement noise is affected by Δ , $\eta \doteq (1 + \Delta) \tilde{\eta}$, in this alternative setup for the model (In) validation. Equation (2.12) can be modified as follows:

$$y = (I + \Delta) (T_g u + \Gamma_g u^- + \tilde{\eta}) \quad (2.14)$$

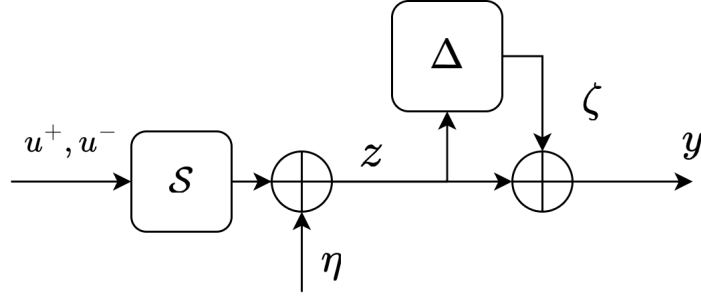


Figure 2.3: The convex relaxed Model (In)validation framework for semi-blind robust identification.

Equation (2.14) is satisfied if a triple $(u^-, \tilde{\eta}, \Delta)$ exists, where $\|\tilde{\eta}\|_2 \leq \tilde{\epsilon}$, $\|\Delta\|_\infty \leq \delta$ and $\tilde{\epsilon} = \frac{\epsilon}{1+\delta}$. The solution of (2.14) satisfies the (2.12) with triple $(\mathbf{u}^-, \eta, \Delta)$, where $\eta \doteq (1 + \Delta)\tilde{\eta}$. By assuming $\|\Delta\|_\infty \ll 1$, (2.14) can be solved by following LMI problem [46].

Theorem 1. Equation (2.14) is satisfied if there exists $\delta < 1$, $\tilde{\eta} \in \tilde{\mathcal{N}}$ and $\mathbf{u}^- \in \mathcal{U}_-$, such that following LMI are satisfied:

$$\begin{aligned}
 A &\doteq \begin{bmatrix} X(\mathbf{u}^-) & (T_\omega)^T \\ (T_\omega) & (\delta^2 - 1)^{-1}I \end{bmatrix} \leq 0, \\
 T_\omega &\doteq T_g T_u + \Gamma_g T_{u^-}, \\
 X &\doteq (T_y)^T T_y - (T_y)^T T_\omega - (T_\omega)^T T_y.
 \end{aligned} \tag{2.15}$$

This concludes the mathematical discussion about Mode (In)validation for adaptation of models identified using semi-blind robust system identification. The next subsection discusses the algorithmic implementation of the model (In)validation framework with semi-blind robust system identification for adaptive system identification.

2.1.1.1 Algorithm

This section combines model (In)validation with semi-blind robust system identification to develop an adaptive model identification framework, which improves the prediction accuracy and ensures the identified models are suitable for controller design as well. The general framework of the proposed adaptive model identification method is shown in Fig. 2.4 [49]. The proposed adaptive identification starts by collecting a few data points till time step T as shown in step-A of Fig. 2.4. The acquired data set is divided into two parts. The first part indicated by the blue box has N_t data points to be used for the identification step using semi-blind robust system identification. The second part shown with the pink box has M_t data points equal to the number of parameters in the identified model, to be used by the model (In)validation framework discussed in the previous section. For example, if the reduced model order is 3^{rd} order model then only four data points are required for model (In)validation. However, if the 3^{rd} order model is not validated and a reduced model of order 4, 5 or 6 is used then six or seven data points are required for model (In)validation. At time step T , the patient model is identified and the model is tested for model (In)validation which completes step-A.

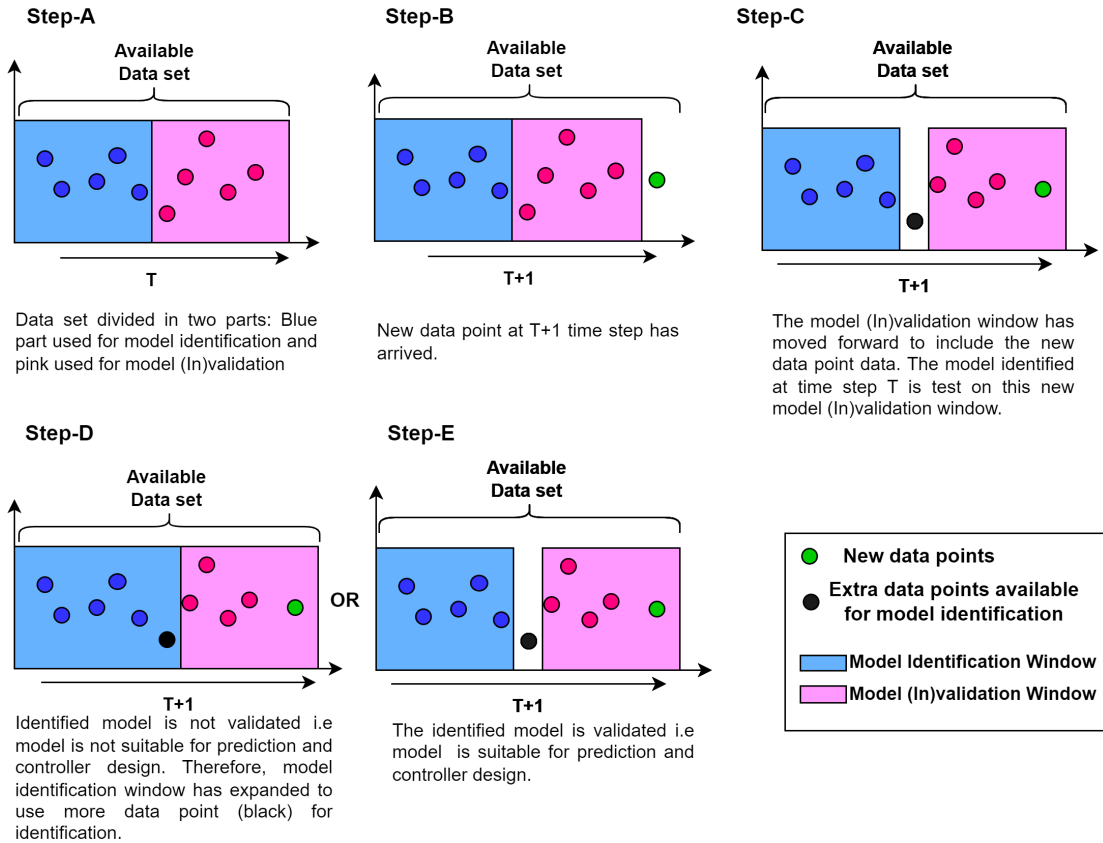


Figure 2.4: Recursive adaptive model identification with Model (In)validation.

At the $T + 1$ time step, a new data point (green) has been acquired shown in step-B. In step-C, the model (In)validation window has moved forward to include the new data point in the window leaving a past data point (black) available to be used for identification in the future if needed. The model identified in step-A is tested on this new model (In)validation window. Now, there can be two outcomes: (i) the model is validated, i.e model is suitable for future predictions and controller design or the model is invalid for future predictions. If the model is validated then step-E in Fig. 2.4 is followed. (ii) if the model is (In)validated then step-D is followed, where the model identification window has expanded to include the extra available data point (black) in the window which makes the total data points equal to $N_t + 1$ available for re-identification. The model is updated by re-identification through semi-blind robust system identification. The newly identified model is then tested on the model (In)validation window before it is used for prediction. This procedure is followed recursively at each time step.

The practical implementation of the aforementioned adaptive individualized patient modeling framework to develop personalized patient models representing patients' true dose-response characteristics is given in Algorithm 1. The user input to initialize the algorithm is the patient data which includes patient ID and patient-specific dose-response data, stability margin ρ , the minimum number of patient's clinical data for the identification N_t , initial and maximum acceptable reduced model order, O and O_{max} , respectively. The full-order model is identified in steps 1-2. Step 3 reduces the model order based on the initial value of O . The identified personalized patient model is processed through model (In)validation at step 6. The data points M_t are selected at step 5 to be used for model (In)validation. The amount of data points M_t is equal to the coefficients

Algorithm 1: Adaptive personalized patient dose-response modelling.

Input: Patient-ID, clinical data, N_t, ρ_{max}, O_{max} .
Output: Discrete-time individualized patient model, G_r

```
1 function Semiblind( $N_t, \rho$ , clinical data, ID);
2   return(G)
3 function ReduceModelorder(G, O);
4   return( $G_r$ )
5 Select,  $M_t$ , data points for model (In)validation.
6 function ModelInvalidation( $G_r, M_t$ );
7   if  $\|\Delta\|_\infty < 1$  then
8     print(model validated.)
9     return( $G_r$ )
10  else
11    print(model invalidated.)
12    If  $O < O_{max}$  then
13       $O = O + 1$ ; repeat step 4.
14    else
15      if  $\rho < \rho_{max}$ 
16        Set default  $O$ ; Increase  $\rho$ ;
17        repeat step 2.
18      else
19        Set default  $O$  and  $\rho$ ; Increase  $N_t$ ;
20        repeat step 2.
21      endif
22    endif
23  endif
24 exit
```

of the reduced-order model obtained in step 4.

If the model (In)validation requirements are met, the algorithm shows the verified personalized patient model. Otherwise, the model is not suitable for prediction and controller design, and the reduced model order, O , is raised for the same value of ρ . ρ is raised if the order of the model is higher than O_{max} . The amount of data points, N_t , utilized for the identification process is increased if $\rho > \rho_{max}$, and the algorithm returns to step 1.

It is important to mention that for model adaptation through re-identification, the most recent available N_t data points are used. Although the maximum low-order model limit can be extended, low-order models are favored for controller design since they have fewer parameters to adjust. Low-order models have also been favored in clinical applications due to the ease with which the resulting models can be explained.

This concludes the algorithmic implementation of the Model (In)validation based adaptive model identification. The next subsection discusses the prediction results for the above-discussed algorithm.

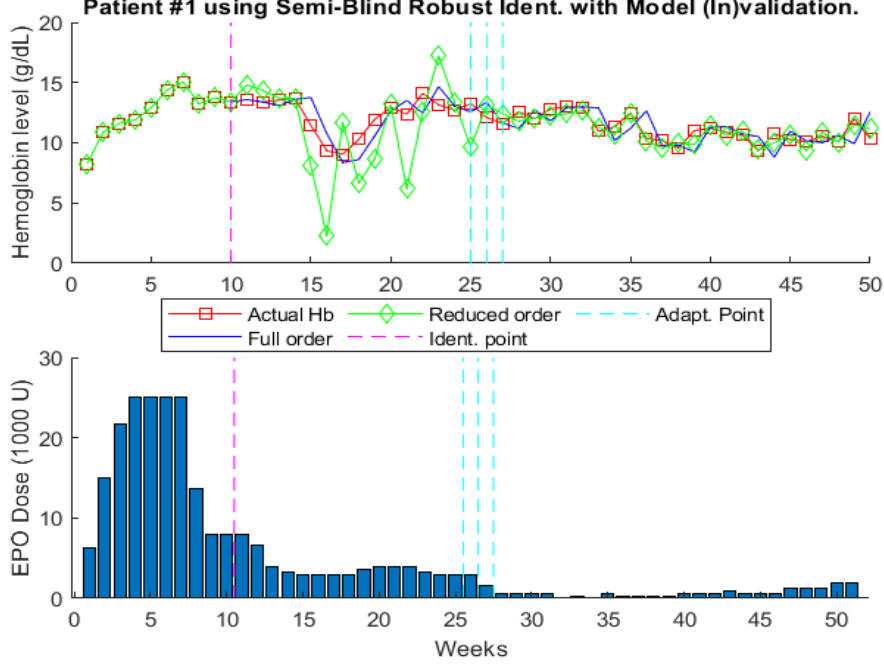


Figure 2.5: Prediction results for patient-1 model obtained by semi-blind robust identification with model (In)validation.

2.1.1.2 Anemia Management Results

This study is IRB approved by the Human Subjects Protection Program Office at the University of Louisville. For simulation purposes, clinical data of 50 patients, previously collected at the University of Louisville, Kidney Disease Program were used. These patients represent the good, average and bad responders to the medication. Each patient received three EPO dosages per week and the Hgb level was tested once a week. To match the input-output data dimension, the average of three EPO dosages is used as input. One-step-ahead prediction is used to show the predicting capabilities of the identified models. The performance of patient models obtained by the semi-blind robust identification technique is analyzed by calculating minimum mean squared error (MMSE) between measured clinical Hgb data and predicted Hgb level using the reduced-order models. The performance of semi-blind robust identification with model (In)validation is compared to semi-blind robust identification without model (In)validation by computing the MMSE values as well. The model is checked for model (In)validation at each time step and updated if the model is not validated. The mathematical expressions for patient-1 models using semi-blind robust identification with model (In)validation are given below:

$$G_1(z) = \begin{cases} \frac{0.9z^4+0.07z^3+0.02z^2-0.1z+0.45}{z^4-0.56z^3-0.26z^2-0.15z+0.01} & 10 \leq n \leq 24 \\ \frac{3.3z^4+1.26z^3-1.29z^2-1.6z+0.27}{z^4-0.58z^3-0.77z^2-0.05z+0.41} & n = 25 \\ \frac{2.2z^4+4z^3-1.63z^2-0.98z+2.3}{z^4-0.99z^3-0.46z^2+z-0.5} & n = 26 \\ \frac{-0.1z^5-0.1z^4+0.6z^3-0.2z^2-0.3z+0.2}{z^5-0.9z^4-0.4z^3+0.4z^2-0.4z+0.3} & 27 \leq n \leq 50, \end{cases} \quad (2.16)$$

where n refers to week. The model prediction results of the above model for patient-1 are shown in Fig. 2.6. In the following figures of semi-blind robust identification simulation results, the red line with square markers shows the actual clinical Hgb values

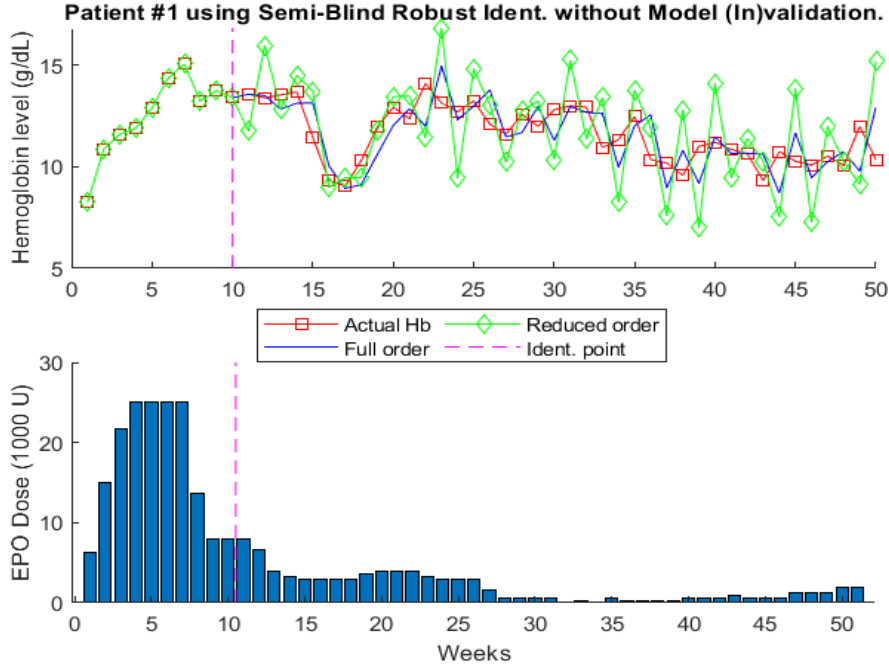


Figure 2.6: Prediction results for patient-1 model obtained by semi-blind robust identification without model (In)validation.

of the patient, the solid blue line shows the model prediction results of the full order model obtained using semi-blind robust identification technique, the green line with diamond markers shows the prediction results of the reduced-order model, the magenta vertical dashed line shows the number of data points, N_t , used in the identification process for the first time and the cyan vertical dashed line represents the points where the model is (In)validated and then updated (i.e., the model could not be validated with the recent patient data through the model (In)validation algorithm and therefore model identification algorithm is rerun as shown in Algorithm-1). Finally, the vertical blue bars show the weekly EPO dosages.

It is important to mention that whenever the model is (In)validated, all available data points are used to update the model. The full order model is equal to the $N_t + 2$, the model consists of parametric and non-parametric portion, and the reduced order model range from 3^{rd} order to 6^{th} order model (not limited). The selection of the reduced-order model is based on model (In)validation conditions, the model order which satisfies the model (In)validation condition of $\|\Delta\|_\infty < 1$ is selected as the final reduced-order

Table 2.1: Model (In)Validation Results of Patient-1

Data Range (Weekly)	$\ \Delta\ _\infty$
10-24	0.93
25	0.99
26	0.84
27-50	0.86

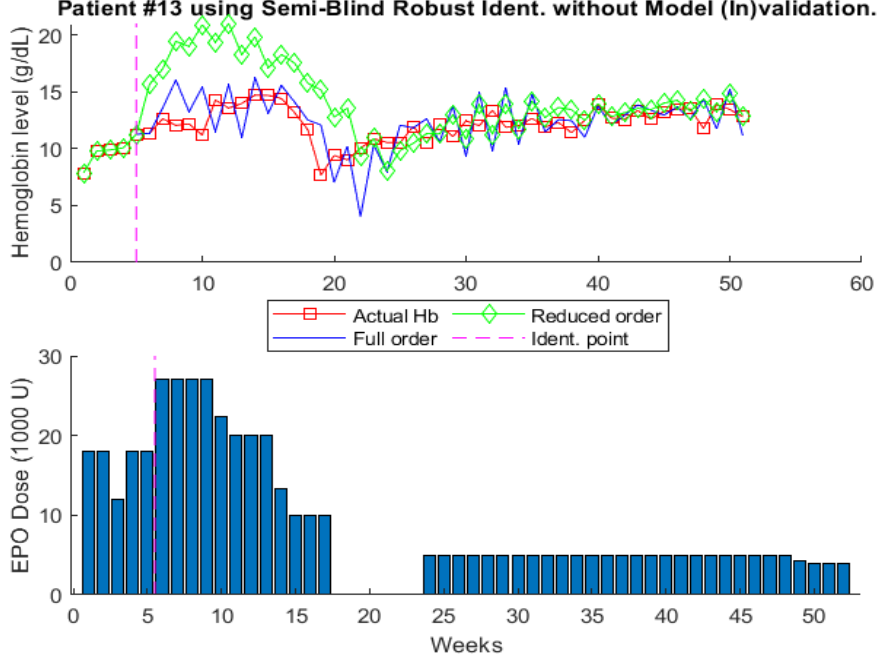


Figure 2.7: Prediction results for patient-13 model obtained by semi-blind robust identification without model (In)validation.

model. The identified model is checked for model (In)validation at each time step (week) and updated as the model is (In)validated. The model (In)validation results for patient-1 are given in TABLE 2.1. All values of $\|\Delta\|_\infty$ are less than one for patient-1, which satisfies the condition for model (In)validation. It is important to mention that in clinical applications personalized drug dose-response models from as few numbers of clinical data as possible are desired.

In this application, only 5-10 data points corresponding to 5–10-week data collection time from anemia patients are used in the identification algorithm. Therefore, more data points are not used in the identification algorithm since it would cause a delay in the treatment (through the proposed algorithm) of patients. The identified model by the semi-blind identification for patient-1 does (In)validate, i.e., the resulting individualized model is updated three times at weeks 25, 26, and 27. This is represented in Fig. 2.5 with the presence of three cyan vertical lines. It is worth mentioning that all the previously available data points are used to update the model whenever a model is (In)validated e.g., at week 25, the previous 24 data points are used in the identification process to update the model. For comparison, the mathematical model of patient-1 using the identification process without a model (In)validation is shown in (2.17) and prediction results are shown in Fig. ??.

$$G_1(z) = \frac{0.5z^5 - 0.3z^4 + 0.1z^3 - 0.1z^2 - 0.01z + 0.002}{z^5 - 1.7z^4 + 0.8z^3 - 0.3z^2 + 0.14z - 0.01} \quad (2.17)$$

The model of patient-1 shown in (2.17) is identified using 10 data points. As this model is not processed through model (In)validation, it is, therefore, not possible to confirm that the model is suitable for controller design as time passes. This is an alarming situation because the patient’s condition may change over time due to the spread of the disease or the patient suffers from another disease. However, model (In)validation can

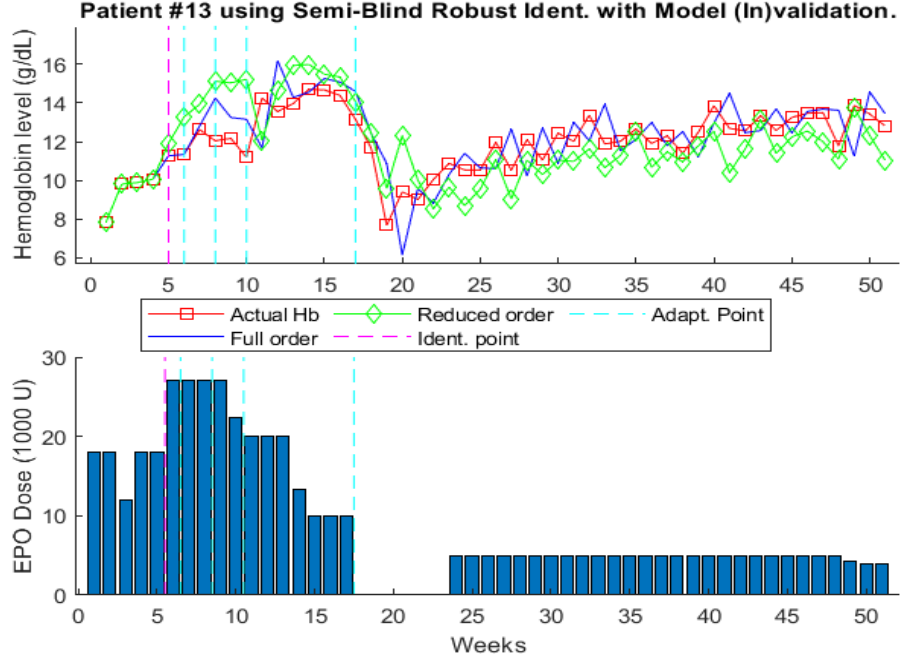


Figure 2.8: Prediction results for patient-13 model obtained by semi-blind robust identification with model (In)validation.

provide an alert for situations where a model is not suitable for prediction and controller design anymore. The benefit of model (In)validation can be seen in the sense of prediction error as shown in Fig. 2.13. The prediction error for models obtained using model (In)validation is lower than the model obtained without model (In)validation. The mathematical expressions for patient-13 models obtained by semi-blind robust identification with model (In)validation are as follows:

$$G_{13}(z) = \begin{cases} \frac{0.6s^3+0.4s^2+0.1s+0.2}{s^3-0.7s^2-0.1s-0.1} & n = 5 \\ \frac{0.6s^5+0.2s^4-0.2s^3+0.1s^2+0.1s-0.03}{s^5-0.8s^4-0.2s^3+0.004s^2+0.01s+0.004} & 6 \leq n \leq 7 \\ \frac{0.7s^3-0.2s^2-0.1s+0.2}{s^3-1.3s^2+0.4s-0.1} & 8 \leq n \leq 9 \\ \frac{0.1s^4+0.5s^3+0.4s^2+0.5s+0.2}{s^4-0.9s^3+0.3s^2-0.3s-0.03} & 10 \leq n \leq 16 \\ \frac{-0.2s^4-0.1s^3-0.03s^2-0.2s+0.1}{s^4-0.8s^3+0.5s^2-0.03s-0.6} & 17 \leq n \leq 51 \end{cases} \quad (2.18)$$

Patent-13 is a challenging patient model because the values of Hgb are varying between $8g/dl$ and $14g/dl$ and hence EPO dosages are also varying significantly. This

Table 2.2: Model (In)Validation Results of Patient-13

Data Range (Weekly)	$\ \Delta\ _{\infty}$
5	0.96
6-7	0.81
8-9	0.96
10-16	0.98
17-51	0.99

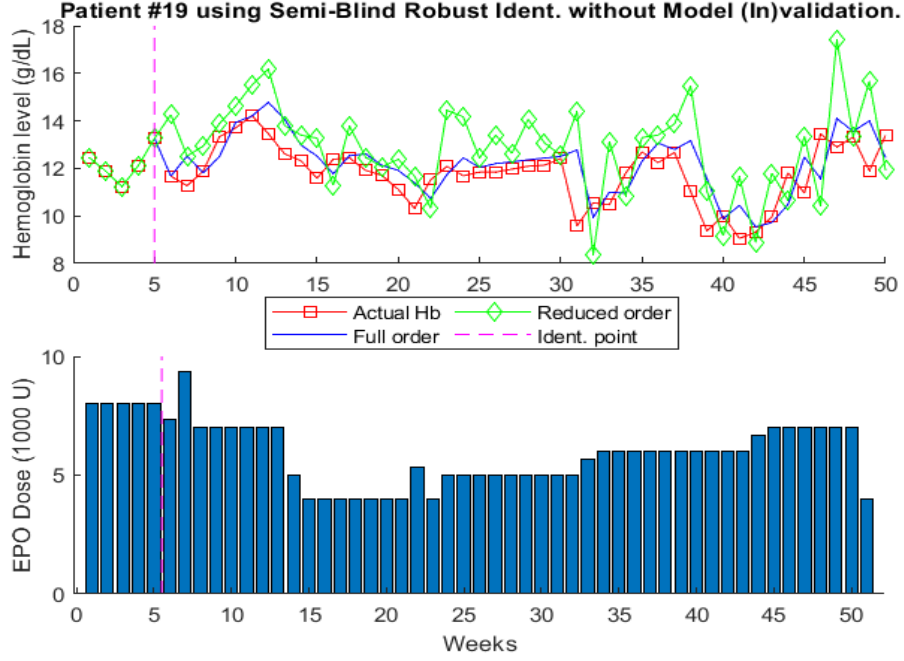


Figure 2.9: Prediction results for patient-19 model obtained by semi-blind robust identification without a model (In)validation.

can indicate that the patient is a poor responder to the medication and finding an optimal dosage is a difficult task for this patient. The prediction results of patient-13 in Fig. 2.8 show that it was difficult to find an appropriate model which satisfies all the conditions even at earlier time steps, the model is updated three times within the first 10 weeks. The interesting part is between weeks 17 and 23 when the EPO dosages are zero. This phenomenon is challenging for the identification algorithm as the model identified is for non-zero EPO dosages, therefore, it will be challenging for the model to be validated for zero EPO dosages. However, the semi-blind robust identification technique updated the model to capture the dynamics of this direction of zero EPO doses as soon as the identification algorithm sensed this trend in the data. The model (In)validation results for patient-13 are shown in TABLE 2.2. All values of $\|\Delta\|_\infty$ are less than one which satisfies the conditions of model (In)validation. To compare the performance of models shown in (2.18), the mathematical model of patient 13 using the identification process without a model (In)validation is shown in (2.19) and prediction results are shown in Fig. 2.7.

$$G_{13}(z) = \frac{0.7z^5 - 0.5z^4 + 0.1z^3 - 0.1z^2 - 0.03z + 0.003}{z^5 - 2z^4 + 1.3z^3 - 0.5z^2 + 0.2z - 0.02} \quad (2.19)$$

The prediction error in models identified by semi-blind robust identification with model (In)validation is smaller than the ones obtained by semi-blind robust identification without model (In)validation. It can be seen by the prediction results that semi-blind robust identification with the model (In)validation performed better by incorporating the fluctuations in the patient characteristics which is not possible without a model (In)validation. The mathematical expressions for patient-19 models obtained by semi-

blind robust identification with model (In)validation are as follows:

$$G_{19}(z) = \begin{cases} \frac{0.9z^5 - 0.5z^4 - 0.02z^3 + 0.04z^2 - 0.1z + 0.01}{z^5 - 2.1z^4 + 1.6z^3 - 0.7z^2 + 0.2z - 0.02} & n = 5 \\ \frac{0.5z^5 + 0.2z^4 - 0.6z^3 + 0.3z^2 - 0.1z + 0.004}{z^5 - 2.1z^4 + 1.6z^3 - 0.6z^2 + 0.1z - 0.005} & 6 \leq n \leq 10 \\ \frac{0.6z^4 - 0.3z^3 + 0.4z^2 - 0.6z + 1.3}{z^4 - 1.3z^3 + 0.5z^2 - 0.3z + 0.04} & 11 \leq n \leq 12 \\ \frac{0.7z^5 - 0.01z^4 + 0.5z^3 + 0.9z^2 - 0.7z + 0.6}{z^5 - 1.2z^4 + 0.5z^3 - 0.04z^2 - 0.5z + 0.2} & 13 \leq n \leq 50 \end{cases} \quad (2.20)$$

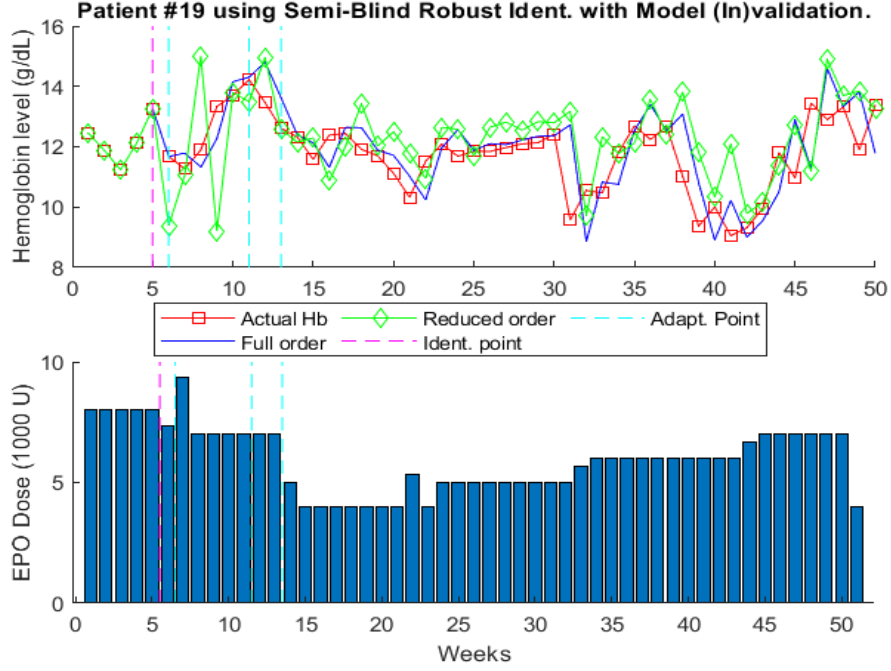


Figure 2.10: Prediction results for patient-19 model obtained by semi-blind robust identification with a model (In)validation.

Patient-19 is a very interesting case as the EPO dosage has frequent changes and Hgb values are ranging between 8 g/dl and 14 g/dl as shown in Fig. 2.10. This patient does not qualify as a poor responder to medication because the change between EPO dosages is low even though Hgb values vary significantly. Therefore, it becomes an interesting scenario where the patient's response is not ordinary. However, the identification process with the model (In)validation can identify the model and timely update the model to represent the true dose-response characteristics of the patient. TABLE 2.3 shows the model (In)validation results for patient-19. The values of $\|\Delta\|_\infty$ are less than

Table 2.3: Model (In)Validation Results of Patient-19

Data Range (Weekly)	$\ \Delta\ _\infty$
5	0.93
6-10	0.96
11-12	0.96
13-50	0.88

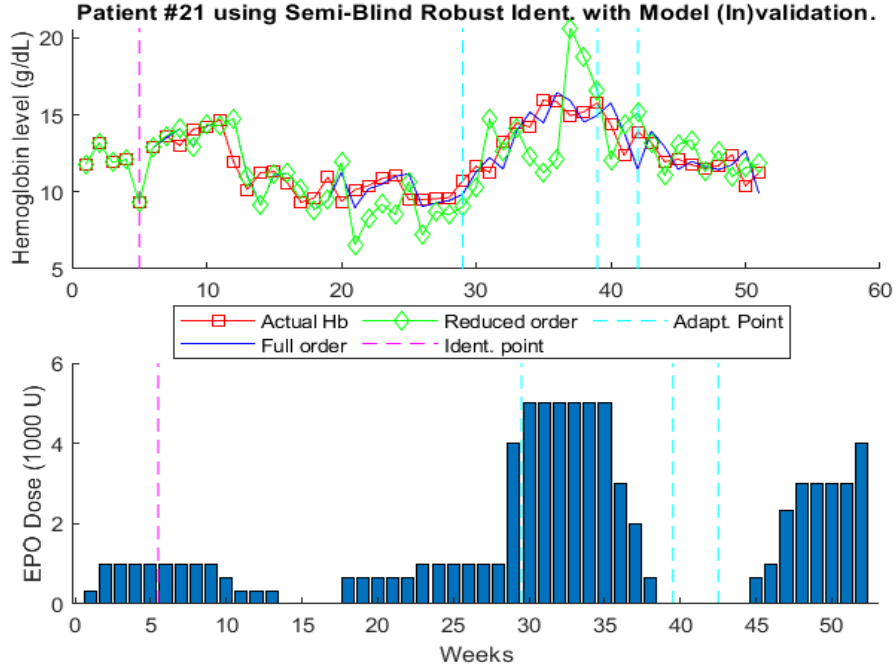


Figure 2.11: Prediction results for patient-21 model obtained by semi-blind robust identification with a model (In)validation.

one which satisfies the condition for the model (In)validation. For the sake of comparison, the model of patient-19 without model (In)validation is as follows:

$$G_{19}(z) = \frac{1.1z^5 - 0.9z^4 + 0.2z^3 - 0.08z^2 - 0.1z - 0.0004}{z^5 - 2z^4 + 1.5z^3 - 0.6z^2 + 0.2z + 0.00014} \quad (2.21)$$

The dose-response for the above model for patient 19 is shown in Fig. 2.9. The model shown in (2.21) is identified using 5 initial data points and the reduced model order is 5th order. The model orders in (2.20) and (2.21) are almost similar however the difference is the model (In)validation and the advantage of it can be seen in Fig. 2.13 in the sense of prediction error values. The error between actual clinical Hgb data and predicted Hgb by the model is 5.6 and 8.6 given by (2.20) and (2.21), respectively.

Patient-21 models obtained by semi-blind robust identification with model (In)validation are shown in (2.22) and without model (In)validation are shown in (2.23). The prediction results for models (2.22) and (2.23) are shown in Fig. 2.11 and Fig. 2.12, respectively. For the initial model identification, only five data points are used as shown in Fig. 2.11 with the magenta color vertical lines. In Fig. 2.11, the model has been updated three times. It is interesting to discuss that between weeks 14 and 17, the model is validated for zero EPO dosages even though non-zero EPO dosages are used for initial model identification. On the other hand, between weeks 38 and 44, the model is updated two times. This can be explained by observing the change in EPO dosages. As the change in EPO dosages is high between weeks 38 and 44, the identification process, therefore, has to go through an extensive search to find the model which can be used to accommodate such fluctuations in the EPO dosages. However, the change in EPO dosages between weeks 14 and 17 is small, therefore, the model is easily validated during this period.

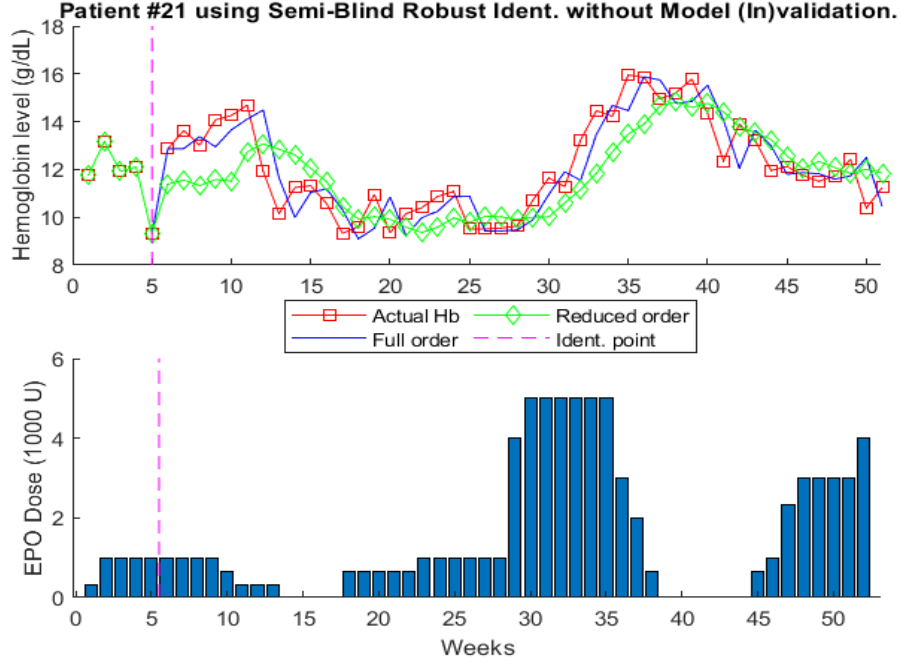


Figure 2.12: Prediction results for patient-21 model obtained by semi-blind robust identification without a model (In)validation.

$$G_{21}(z) = \begin{cases} \frac{0.9z^5 - 0.3z^4 - 0.1z^3 + 0.002z^2 - 0.2z + 0.1}{z^5 - 1.3z^4 + 0.2z^3 + 0.1z^2 + 0.03z + 0.03} & 5 \leq n \leq 28 \\ \frac{-0.3z^4 + 0.3z^3 + 3z^2 + 0.02z - 2}{z^4 - 0.3z^3 - 1.2z^2 - 0.03z + 0.4} & 29 \leq n \leq 38 \\ \frac{0.6z^4 + 0.1z^3 - 1.5z^2 + 1.4z + 2.4}{z^4 + 0.2z^3 - 1.2z^2 - 0.2z + 0.3} & 39 \leq n \leq 41 \\ \frac{-1.7z^3 + 4.9z^2 - 5.6z + 3}{z^3 - 1.9z^2 + 1.2z - 0.24} & 42 \leq n \leq 51 \end{cases} \quad (2.22)$$

$$G_{21}(z) = \frac{0.9z^5 - 0.3z^4 - 0.1z^3 - 0.01z^2 - 0.2z + 0.1}{z^5 - 1.3z^4 + 0.2z^3 + 0.1z^2 + 0.02z + 0.03} \quad (2.23)$$

The model (In)validation results are shown in TABLE 2.4 and the prediction error is shown in Fig. 2.13. As documented in these figures and tables, the semi-blind robust identification technique identified individualized patient models and updated the model to capture the time-varying patient dynamics with low error within an appropriate time frame for each patient. This is especially important for efficient controller design and hence for finding an individualized drug-dose regimen for the patients. The MMSE values for the identified models using model (In)validation are considerably smaller

Table 2.4: Model (In)Validation Results of Patient-21

Data Range (Weekly)	$\ \Delta\ _\infty$
5-28	0.87
29-38	0.92
39-41	0.94
42-51	0.34

than those of models identified without model (In)validation. This shows that the semi-blind robust identification performs better with the model (In)validation to identify the individualized models by using a considerably lower number of clinical patient-specific data points and by updating the models as well using time-domain clinical patient-specific data.

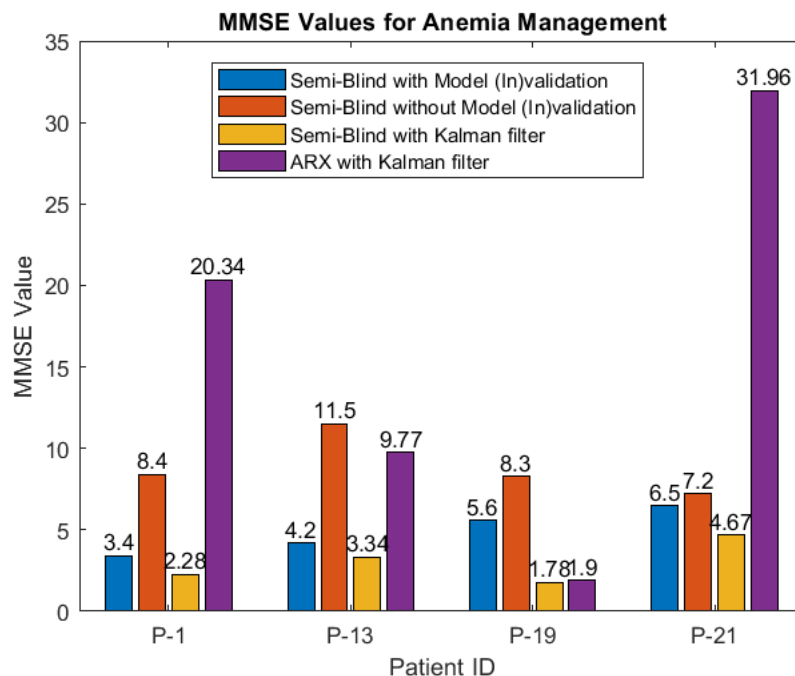


Figure 2.13: Error Comparison between semi-blind robust identification with and without model (In)validation for anemia management.

2.1.1.3 Warfarin Management Results

This section shows the one-step-ahead prediction results of personalized patient models produced with and without model (In)validation using the semi-blind robust model identification approach. The MMSE between predicted and clinically obtained INR levels is used to assess the model's accuracy and also used to compare the performance of patient models with and without a model (In)validation. The clinical dose-response data of Warfarin-INR of forty-four patients were gathered at the Robley Rex Veterans Administration Medical Center.

Dr. Brier (mentioned in the acknowledgment) was funded by the Department of Veterans Affairs to look at the pharmacogenetics of warfarin. This dataset consists of dose and INR data from patients collected from 2008-2012. Dose and INR data were abstracted from pharmacy records for all subjects, additionally, using an informed consent process, genetic information was determined for CYP2C9 and VKORC1. Data provided for this project will be an incrementing time field starting a 1 (day), dose schedule (ie 5mg MonWedFri, 7.5mg TueThuSatSu), INR, and CYP2C9 and VKORC1 status. The Human Subjects Protection Program Office at the University of Louisville has given this project IRB approval. The data set contains patient ID, warfarin dosage, and INR values. Identifying patient models at the earliest stages of treatment is desired for precise drug delivery. It is worth mentioning that model identification with model

(In)validation requires some extra data points depending on the order of the identified model.

In the following results for the model (In)validation process, the model order is selected which satisfies the conditions of model (In)validation, $\|\Delta\|_\infty < 1$, ranging between 3rd and 5th order models. However, for models identified without model (In)validation, we will be using the Akaike Information Criterion, $AIC = 2K \times 2\ln(L)$, to select the appropriate model order. Here, L is the log-likelihood of the model best fit and K is the independent variable of the model. As there is no adaptation involved in models identified without model (In)validation, the model order will not change once selected through the Akaike information criterion.

Figure 2.14 shows the MMSE results of the identified model for each patient. The blue bars show the MMSE values of models identified without model (In)validation and the orange textured bars show the MMSE value of models identified with model (In)validation. The figure shows that MMSE values for models identified with model (In)validation are less than the ones without model (In)validation. It shows that the prediction capabilities of the model increase along with confidence in the model to be used for controller design. To analyze these patients, we are showing the one-step-ahead prediction results obtained by the identified models of patients 3, 7, and 10. In these prediction results, we show the comparison between models identified with and without model (In)validation.

Figure 2.15 shows the one-step-ahead prediction results for patient - 7 with 4th order model shown in (2.24) identified using semi-blind robust system identification without model (In)validation process.

$$G_7(z) = \frac{0.09z^4 + 0.13z^3 + 0.12z^2 + 0.08z + 0.001}{z^4 + 0.50z^3 - 0.09z^2 - 0.45z - 0.86} \quad (2.24)$$

The clinically obtained actual INR levels and warfarin dosages are shown by a red line

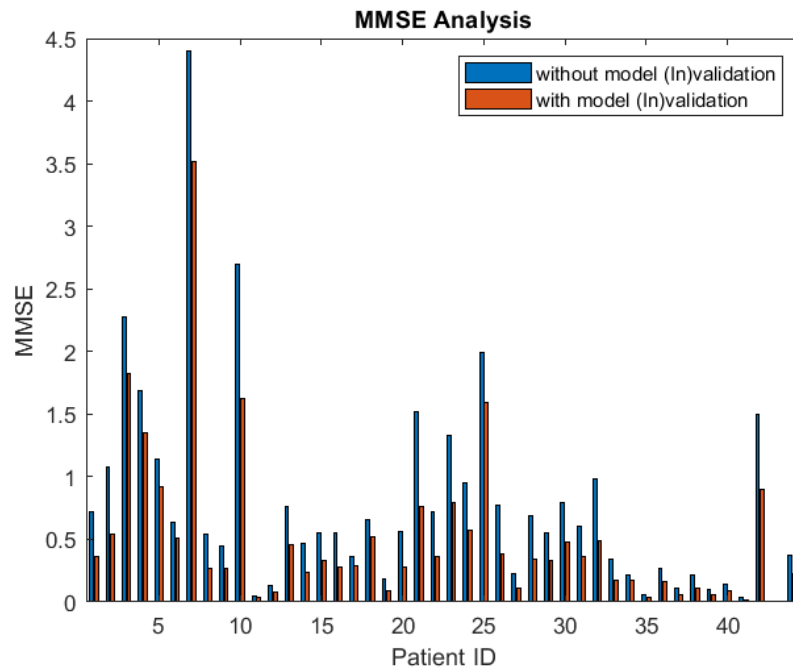


Figure 2.14: Error comparison of personalized Warfarin-INR dose-response models obtained with and without model (In)validation

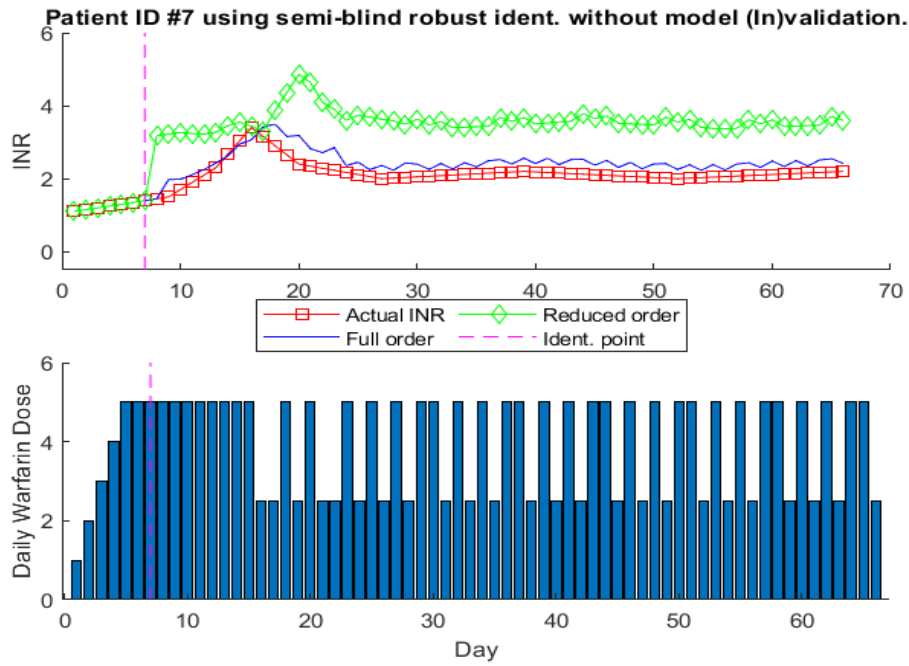


Figure 2.15: Prediction results for patient-7 model obtained by semi-blind robust identification without model (In)validation for Warfarin dosing.

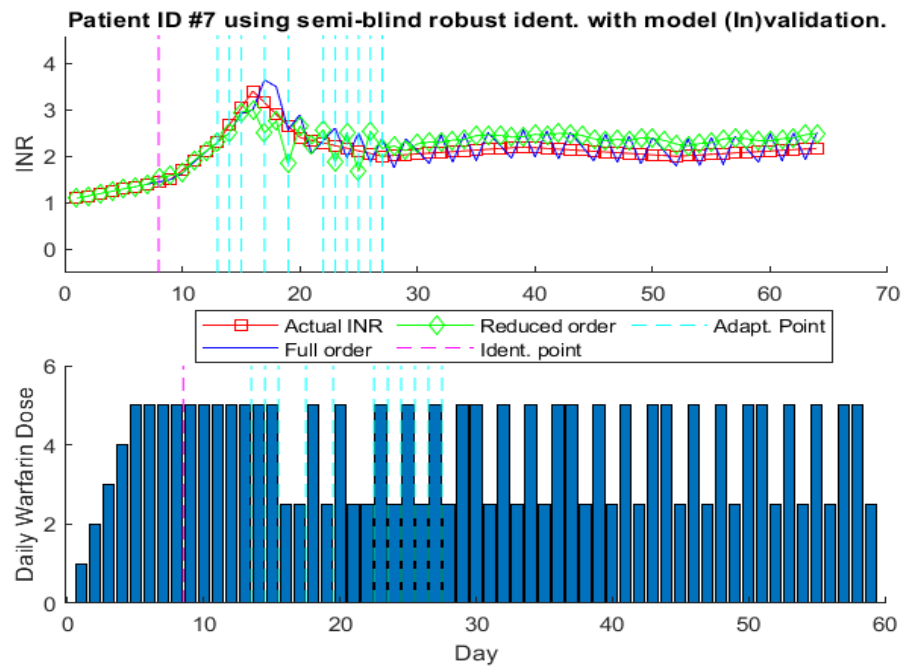


Figure 2.16: Prediction results for patient-7 model obtained by semi-blind robust identification with model (In)validation for Warfarin dosing.

with squared markers and blue bars (bottom), respectively. The predicted INR levels, in response to clinically obtained warfarin dosage, using identified full-order model and reduced-order model are shown with a blue line and green line with diamond markers, respectively. The model is identified using seven data points, $N_t = 7$, highlighted with a pink dotted vertical line. It can be seen that identified 4th order model is not

able to completely mimic the clinically obtained INR values. However, the 6th order model, equal to one less of data points used for identification, can predict the INR values close to actual INR values with slightly low error. It shows that this identified model is not able to predict the does-response with better accuracy. Therefore, we observe the prediction results of the patient-7, however, this time we introduce the model (In)validation process along with semi-blind robust system identification. Similar to Fig. 2.15 seven data points are used for initial identification and the model is processed through model (In)validation as shown in Fig. 2.16 and mathematical model structure is shown in (2.25). Here, n represents days.

$$G_7(z) = \begin{cases} \frac{0.12z^3 - 0.13z^2 + 0.04z - 2.677e^{-5}}{z^3 - 1.48z^2 + 0.5z - 0.008} & 8 \leq n \leq 12 \\ \frac{0.064z^4 - 0.122z^3 + 0.09z^2 - 0.023z + 4.012e^{-3}}{z^4 - 2.75z^3 + 2.81z^2 - 1.18z + 0.13} & n = 13 \\ \vdots & \vdots \\ \frac{0.03z^5 + 0.05z^4 + 0.04z^3 + 0.01z^2 - 0.02z - 0.013}{z^5 + 0.42z^4 - 0.45z^3 - 0.82z^2 - 0.49z + 0.4} & 27 \leq n \leq 64 \end{cases} \quad (2.25)$$

Figure 2.16 shows that the model is adapted multiples times (eleven times), represented with the vertical dotted cyan line. This shows that the previously identified model is not valid and it is needed to be updated through re-identification using a semi-blind robust system identification method. For patient-7, there will be twelve model equations as the model is updated eleven times within sixty-four days of treatment. It can be seen that model identified with model (In)validation predicts the INR values close to clinically obtained INR values. This highlights the benefit of the recursive adaptive model identification algorithm to increase the accuracy of the model prediction. It is interesting to note that after the thirty data points, there is no need for model adaptation. This illustrates that with the passage of time and the arrival of new data, the adaptive algorithm has identified a model which can define the dose response of the patient at later stages as all the variations to be experienced in the latter part of the treatment are already captured by the model.

Furthermore, one-step-ahead prediction results for patient-3 based on model identification without model (In)validation are shown in Fig. 2.17. The mathematical model identified without model (In)validation is shown in (2.26).

$$G_3(z) = \frac{0.09z^5 + 0.02z^4 + 0.003z^3 + 0.02z^2 + 0.05z - 2e^{-4}}{z^5 - 0.78z^4 - 0.17z^3 + 0.16z^2 + 0.31z - 0.49} \quad (2.26)$$

For model identification without model (In)validation, 5th order model is used based on *AIC*. To improve the prediction results, (2.27) shows the mathematical model for patient -3 obtained using model (In)validation-based proposed adaptive identification algorithm.

$$G_3(z) = \begin{cases} \frac{0.1356z^3 - 0.1867z^2 + 0.1011z - 0.01912}{z^3 - 1.827z^2 + 1.024z - 0.1909} & 8 \leq n \leq 12 \\ \frac{0.0697z^3 + 0.01878z^2 - 0.002374z - 0.04851}{z^3 - 1.044z^2 + 0.1159z - 0.05208} & 13 \leq n \leq 14 \\ \vdots & \vdots \\ \frac{0.02z^5 + 0.069z^4 + 0.059z^3 - 0.02z^2 - 0.04z - 0.01}{z^5 + 1.54z^4 - 0.52z^3 - 1.6z^2 - 0.43z + 0.07} & 53 \leq n \leq 59 \end{cases} \quad (2.27)$$

Figure 2.18 shows prediction results for this model. The initial model is identified using 7 data points. The initial reduced model, selected by the adaptive algorithm discussed in Section 2.1.1.1, is 3rd order model. It can be seen that model is updated multiple

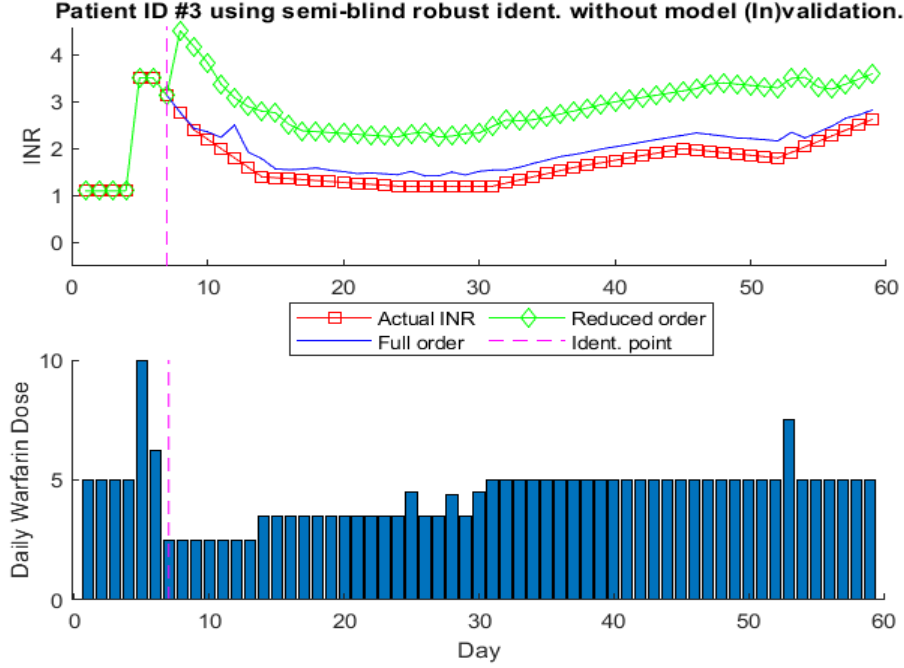


Figure 2.17: Prediction results for patient-3 model obtained by semi-blind robust identification without model (In)validation for Warfarin dosing.

times to reduce the prediction error throughout the treatment. It shows the effect of the model (In)validation-based model adaptation.

Figure 2.19 shows a one-step-ahead prediction for the model identified without a model (In)validation for patient-10. Here, seven data points and 5th order model, selected based on Akaike Information Criterion, is used for semi-blind robust model identification as shown in (2.28). It can be seen that identified model predicted the INR values has some error. It can be seen that predicted INR values using the full order model, shown in the solid blue line, are off as well.

$$G_{10}(z) = \frac{0.1z^5 - 0.02z^4 + 0.04z^3 - 0.01z^2 + 0.03z + 0.8e^{-3}}{z^5 - 1.4z^4 + 1.28z^3 - 1.09z^2 + 0.9z - 0.62} \quad (2.28)$$

For comparison, we include the model (In)validation in the identification process to use the adaptive model identification algorithm for patient-10 as shown in (2.29). The prediction results with model (In)validation for patient-10 are shown in Fig. 2.20. The model is updated four times within sixty days of treatment and this patient's behavior is not changing over time, which shows that finding the model for the patient-10 is easier than for patient-3. It can be seen that model adaptation increases prediction accuracy by capturing all the fluctuations. It is interesting to note that the model is updated at the last period of treatment. During the last period of treatment clinically obtained warfarin dosages are constant. However, INR values are changing which makes the model to be updated. This highlights the need for model (In)validation to be introduced in the model identification process to increase the prediction accuracy and reliability of the

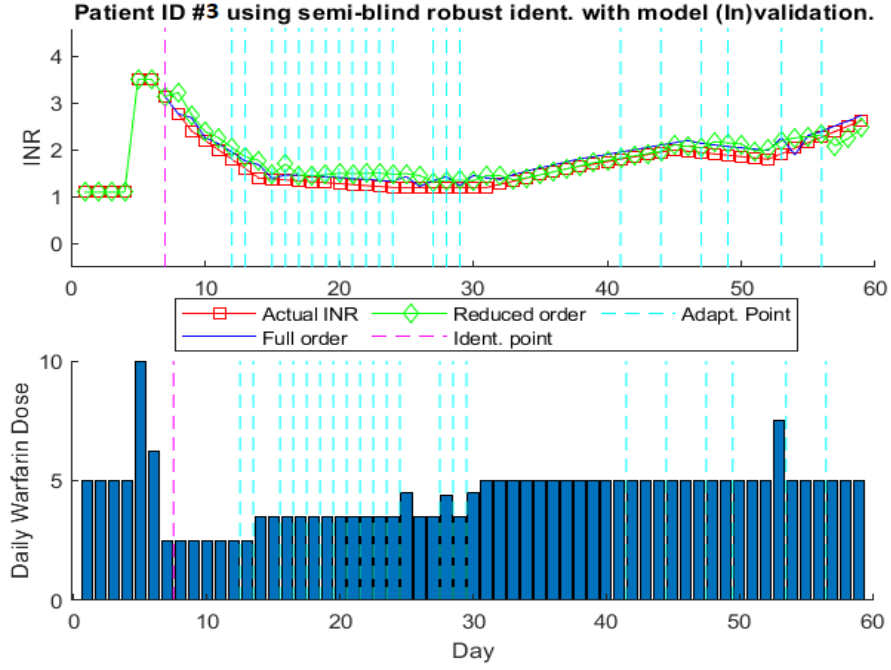


Figure 2.18: Prediction results for patient-3 model obtained by semi-blind robust identification with model (In)validation for Warfarin dosing.

model for controller design in the event of a change in dose-response characteristics.

$$G_{10}(z) = \begin{cases} \frac{0.07z^3 - 0.1z^2 + 0.06z - 0.009826}{z^3 - 1.9z^2 + 1.1z - 0.21} & 8 \leq n \leq 14 \\ \frac{0.04z^3 - 0.05z^2 + 0.02z - 0.001499}{z^3 - 1.9z^2 + z - 0.1} & n = 15 \\ \vdots & \vdots \\ \frac{0.01z^5 + 0.01z^4 + 0.001z^3 - 1.7e^{-05}z^2 - 0.01z - 0.002}{z^5 - 0.4z^4 - 0.4z^3 - 0.3z^2 - 0.63z + 0.7} & 59 \leq n \leq 63 \end{cases} \quad (2.29)$$

This concludes the adaptive system identification using semi-blind robust system identification with model (In)validation. By MME error analysis for warfarin management and anemia management, it can be concluded that semi-blind robust system identification by incorporating the effect of non-zero initial conditions reduces the number of data points required for personalized model identification and model (In)validation helps to validate the model and improve the prediction error. However, this approach involves solving two optimization problems based on LMIs and inherently requires more data points for model (In)validation. The requirement of more data points for model (In)validation is major drawback because in medical applications measurement sampling frequency is generally low such as weekly or daily. Furthermore, simultaneously solving these LMI problems can lead to unfeasible solution, which can lead to higher computational time as much as 50-60 minutes for processing 80 data points. This can limit the implementation of the proposed method in a clinical setting. Therefore, in the next section, semi-blind robust system identification is combined with Kalman Filter for model adaptation. Kalman filter updates the model parameters based on prediction error in real-time with minimum possible computational time.

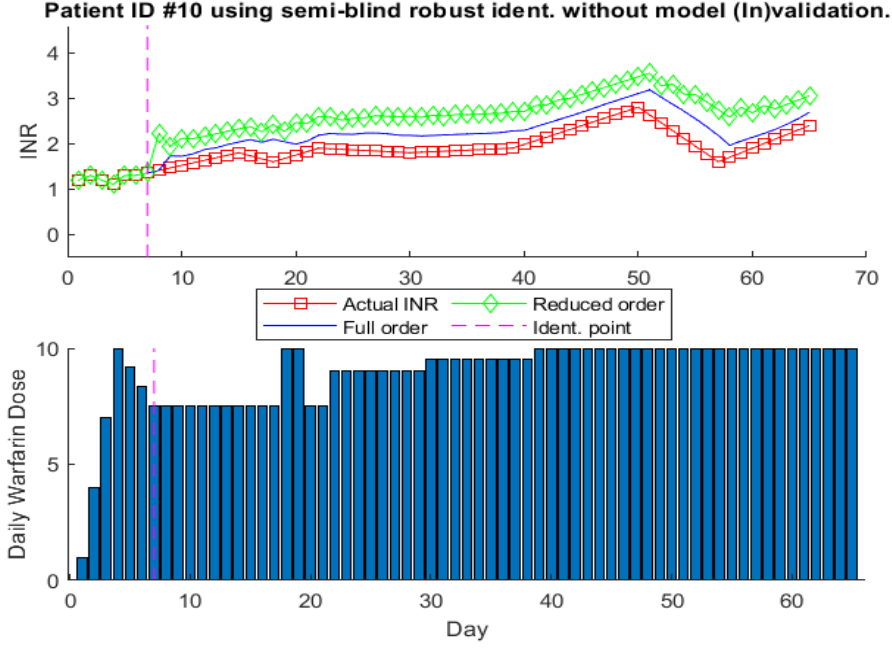


Figure 2.19: Prediction results for patient-10 model obtained by semi-blind robust identification without model (In)validation or Warfarin dosing.

2.1.2 Kalman Filter based Adaptive Model Identification

The parameters of the model given in (2.2) need to be updated to represent the patient's current characteristics as the treatment progresses. Ideally, the response of the model defined in (2.2) should mimic the response of an actual patient as time progresses during the treatment. We propose using online system identification with the Kalman filter to meet this objective. For online system identification, let's assume that the true patient model can be written as following linear regression model [50]:

$$y(t) = \psi^T \phi(t) + e(t), \quad (2.30)$$

where $y(t)$ is the true output of the patient, ψ^T is the regression vector formed based on input and output measurements of the patient, $\phi(t)$ is a vector of true model parameters, and $e(t)$ is the noise source. Let the predicted output, $\hat{y}(t)$, provided by the identified model, $\hat{y}(t) = \psi^T \hat{\phi}(t-1)$. Here $\hat{\phi}(t)$ contains the currently estimated model parameters. It is assumed that $\phi(t) = \phi(t-1) + w(t)$ and $w(t)$ is the white Gaussian noise. Recursive infinite history estimation with Kalman filter is written as [50]:

$$\hat{\phi}(t) = \hat{\phi}(t-1) + K(t)[y(t) - \hat{y}(t)], \quad (2.31)$$

where $K(t) = Q(t)\psi(t)$ is the Kalman gain and $Q(t)$ is defined as follows:

$$Q(t) = \frac{P(t-1)}{R_2 + \psi^T(t)P(t-1)\psi(t)}, \quad (2.32)$$

where R_2 is the variance of error term in (2.30) and $P(t)$ is computed as follows:

$$P(t) = P(t-1) + R_1 - \frac{P(t-1)\psi(t)\psi^T(t)P(t-1)}{R_2 + \psi^T(t)P(t-1)\psi(t)}, \quad (2.33)$$

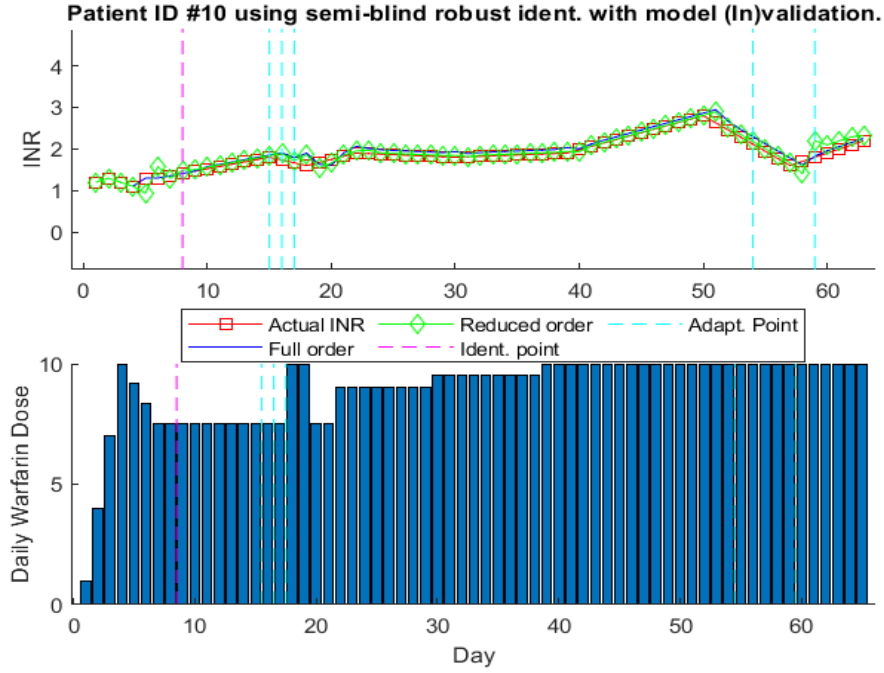


Figure 2.20: Prediction results for patient-10 model obtained by semi-blind robust identification with model (In)validation or Warfarin dosing.

where $R_1 = E[w(t)w^T(t)]$. This concludes the mathematical description of the Kalman filter for adaptive model identification. The next section discusses the results of the Kalman filter with semi-blind robust system identification for anemia and warfarin management.

2.1.2.1 Anemia Management Results

This section provides the simulation results for semi-blind robust system identification with the Kalman filter for anemia management. The clinical data set discussed in section 2.1.1.2 is used for this simulation. The prediction results for patient-1 using semi-blind robust system identification with Kalman filter are shown in Fig. 2.21. For these prediction results, 5 data points are used for identification, and the 4th order model is used. The model parameters are updated based on prediction errors using the Kalman filter at each time step. The prediction error for results shown in Fig. 2.21 is 1.23 ± 0.718 and the minimum mean squared error (MMSE) is 2.28 as shown by Fig. 2.31. For comparison, the benchmark recursive 4th order ARX model with the Kalman filter is used. Figure 2.22 shows the one-step-ahead prediction results for the recursive ARX model for patient-1. The prediction error for the ARX model is 2.70 ± 13.33 and the MMSE value is 20.34, which shows the significance of using the effect of non-zero initial conditions in semi-blind robust system identification.

Figure 2.23 shows the prediction results for patient-13 from anemia management using semi-blind robust system identification with Kalman filter. For this patient, 8 data points are used for identification, and the 4th order model is used for prediction results shown Fig 2.23. Figure 2.24 shows the prediction results for patient 13 using the 4th order ARX model with the Kalman filter. The interesting part of these results is between weeks 15 and 24. During this time period, EPO dosages are zero, which

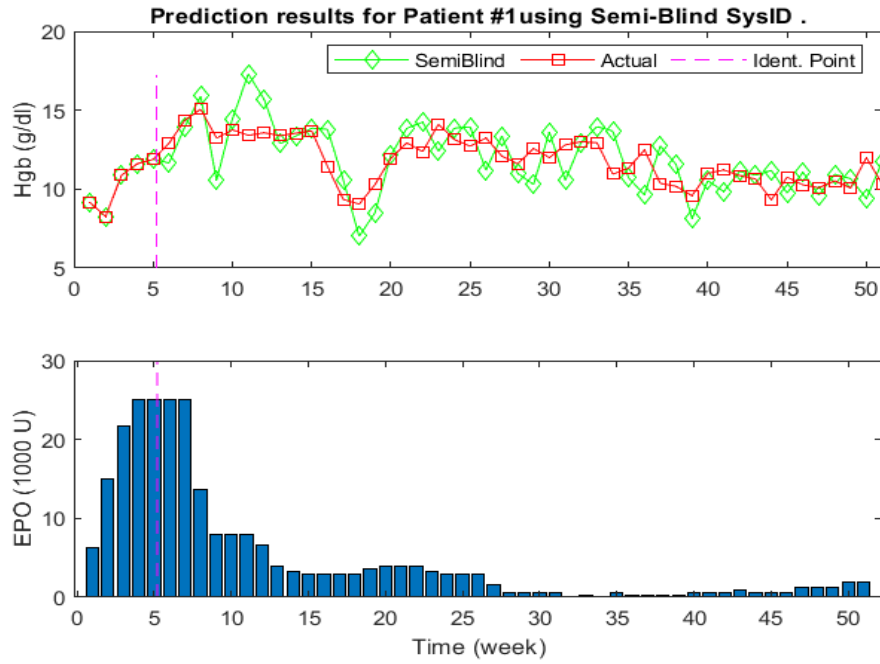


Figure 2.21: Prediction results of semi-blind robust system identification with the Kalman filter for Patient-1 of anemia management.

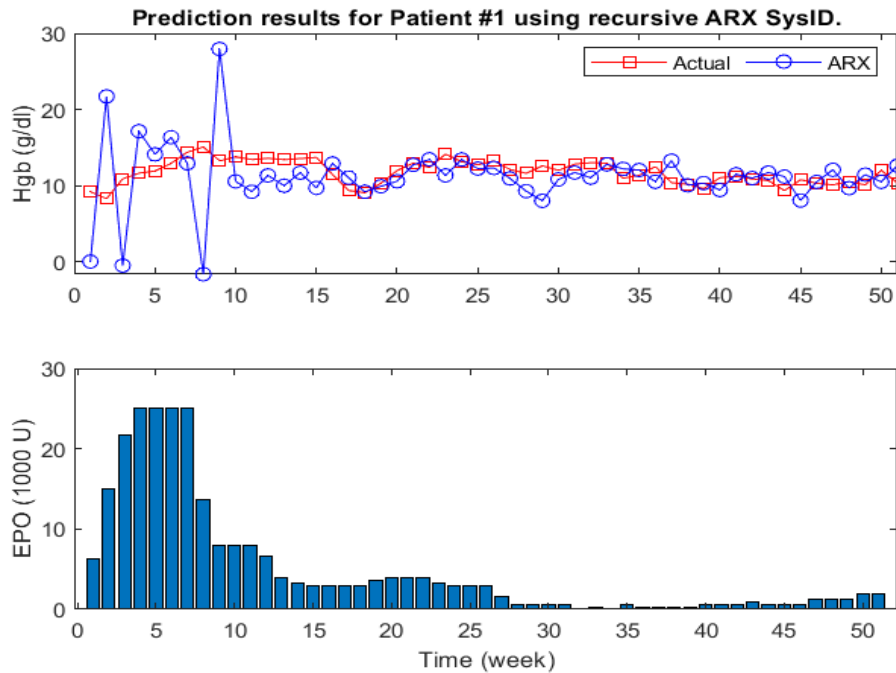


Figure 2.22: Prediction results of ARX with the Kalman filter for Patient-1 of anemia management.

indicates missing dosages or intentional zero dosages by a physician to control the Hgb.

During this period, both models suffer significant prediction errors because of discontinuity in actual data, and identified models are linear. However, the model identified using semi-blind robust system identification is able to adapt and suffers low error. This is due to the fact that the parameters of this model are obtained after optimization in

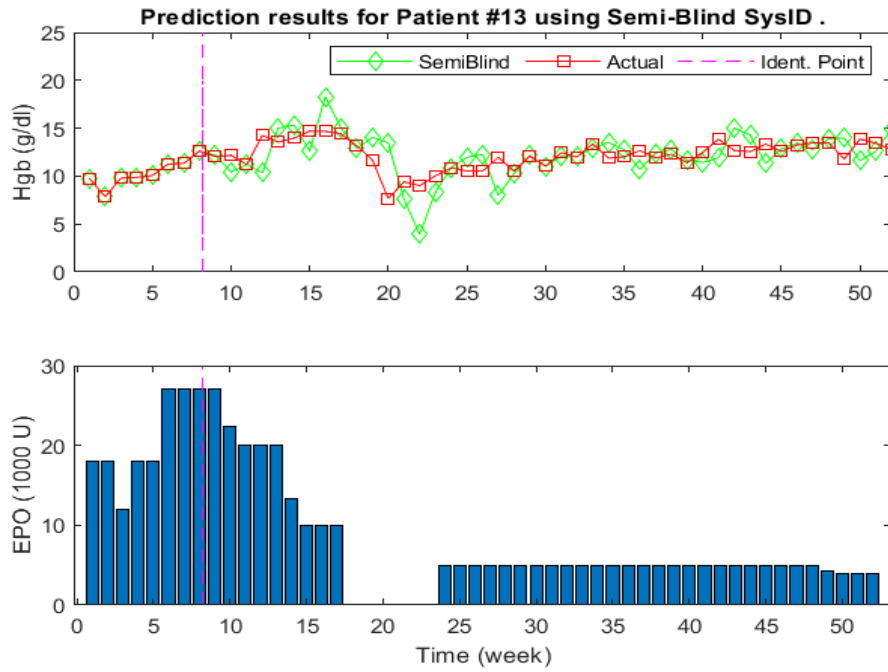


Figure 2.23: Prediction results of semi-blind robust system identification with the Kalman filter for Patient-13 for anemia management.

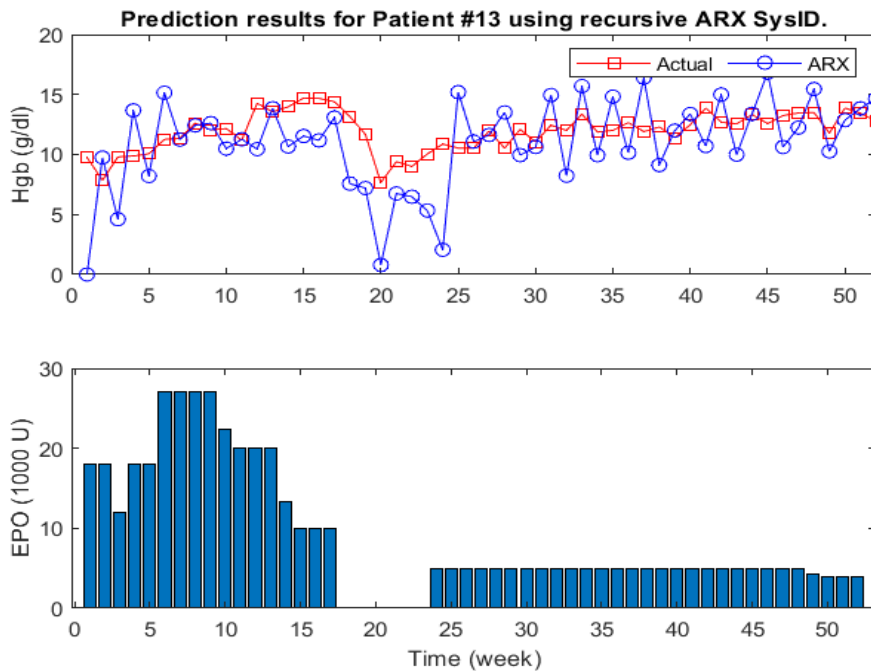


Figure 2.24: Prediction results of ARX with the Kalman filter for Patient-13 of anemia management.

the first place which reduces the number of candidate models suitable for this patient, making it easier for Kalman filter to adapt at later stages. The prediction error for the ARX model is 1.42 ± 1.87 and 2.54 ± 3.40 for the model identified using semi-blind robust system identification. The MMSE values are 3.34 and 9.77 for the semi-blind robust system identification and ARX model, respectively, as shown by Fig. 2.31.

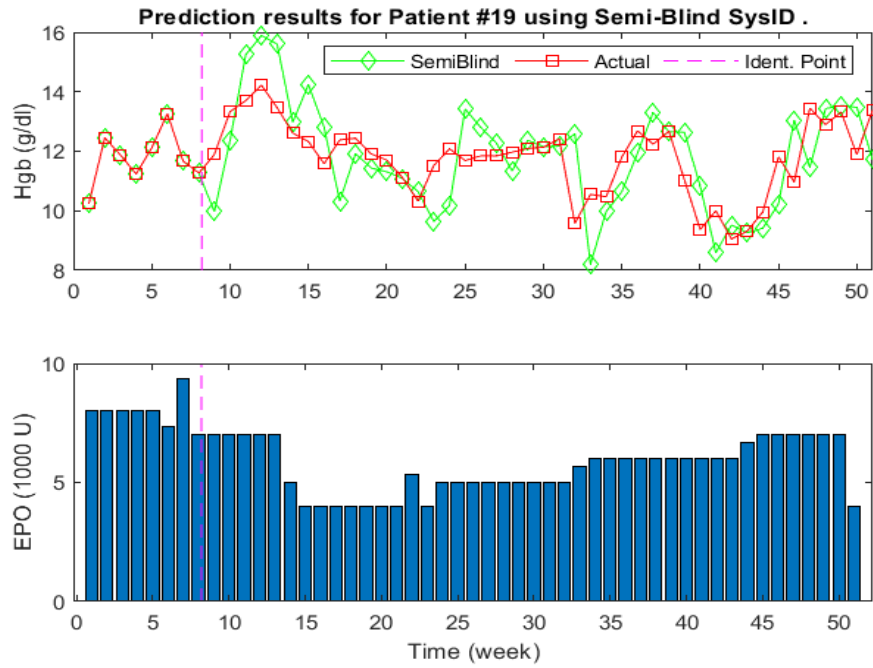


Figure 2.25: Prediction results of semi-blind robust system identification with the Kalman filter for Patient-19 of anemia management.

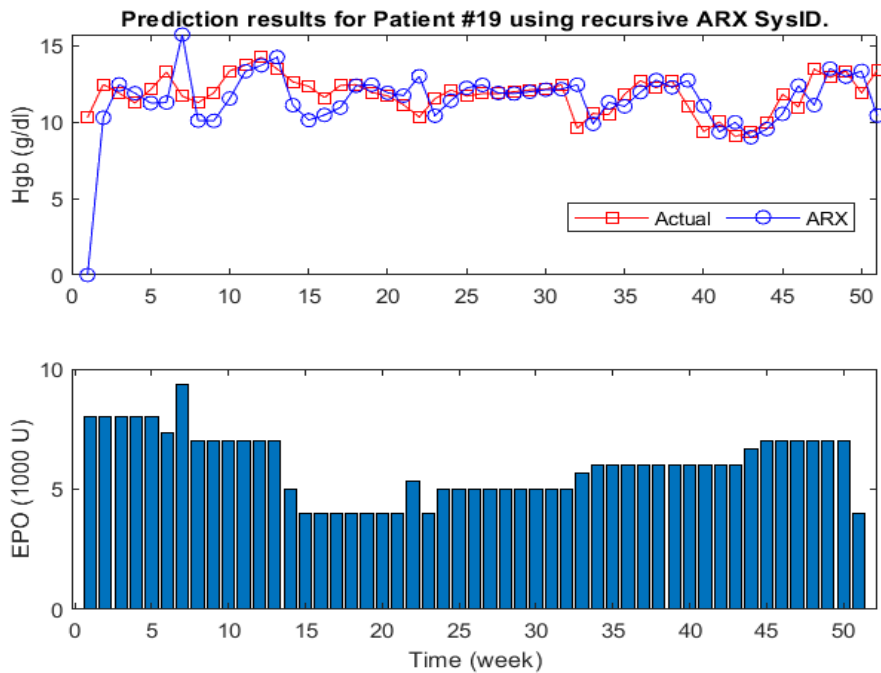


Figure 2.26: Prediction results of ARX with the Kalman filter for Patient-19 of anemia management.

Figure 2.25 shows the prediction results for patient-19 for the model identified using semi-blind robust system identification with Kalman filter. The prediction error for this model is 1.08 ± 0.61 and the MMSE value is 1.78 as shown by Fig. 2.31. For this model, 8 data points are used and the 4th order model is used. This patient's EPO dosage trend is interesting, since it changes more often. However, there is no zero (missing) dosage.

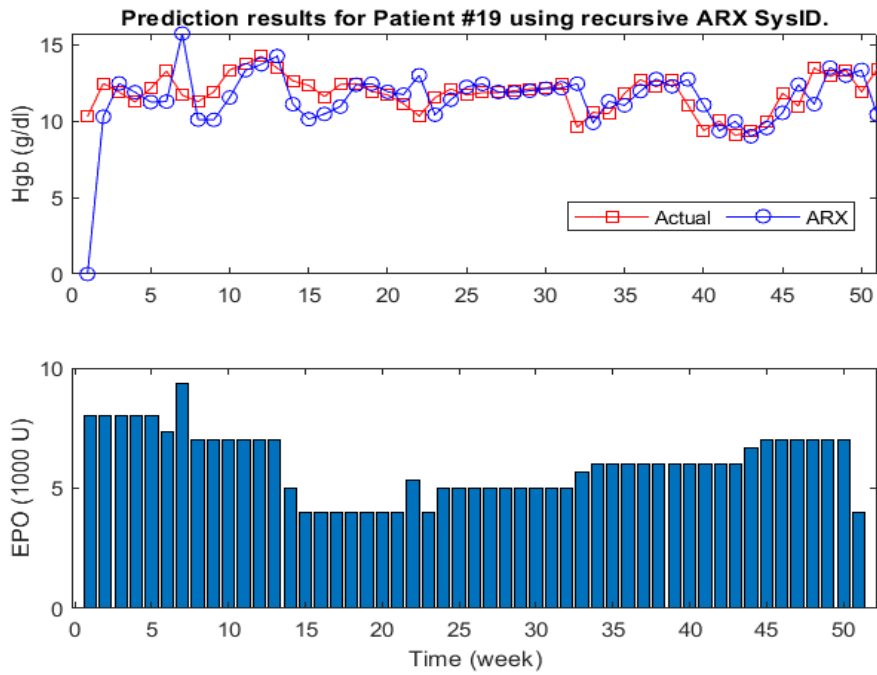


Figure 2.27: Prediction results of ARX with the Kalman filter for Patient-19 of anemia management.

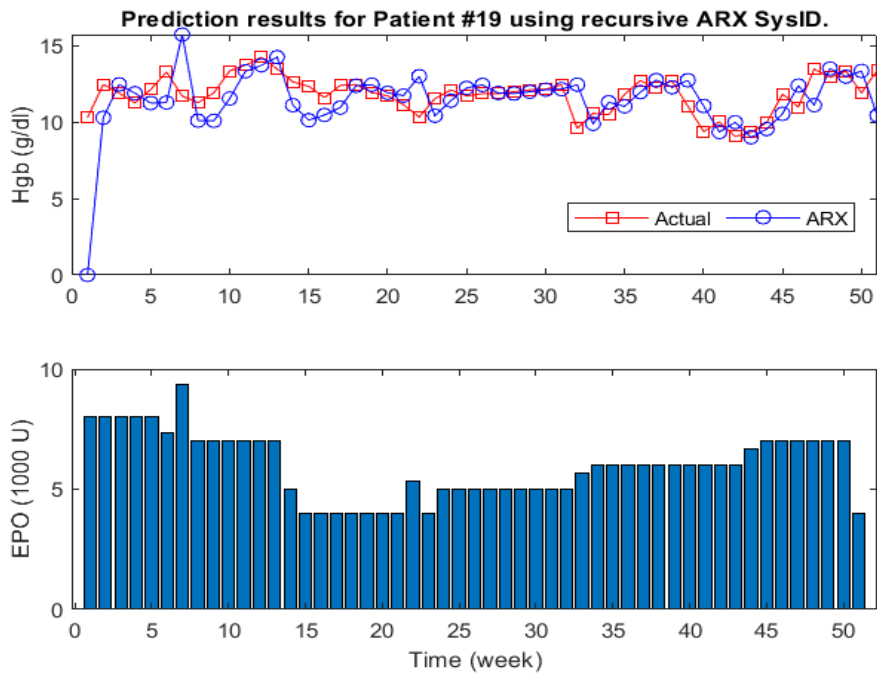


Figure 2.28: Prediction results of ARX with the Kalman filter for Patient-19 of anemia management.

The change in EPO dosage makes it more difficult to find the optimal parameters for the model. Figure 2.28 shows the prediction results for the 4th order ARX model for patient 19. The prediction error for the ARX model is 1.07 ± 0.765 and the MMSE value is 1.9 as shown by Fig. 2.31.

Figure 2.29 shows the prediction results for patient-19 for the model identified using

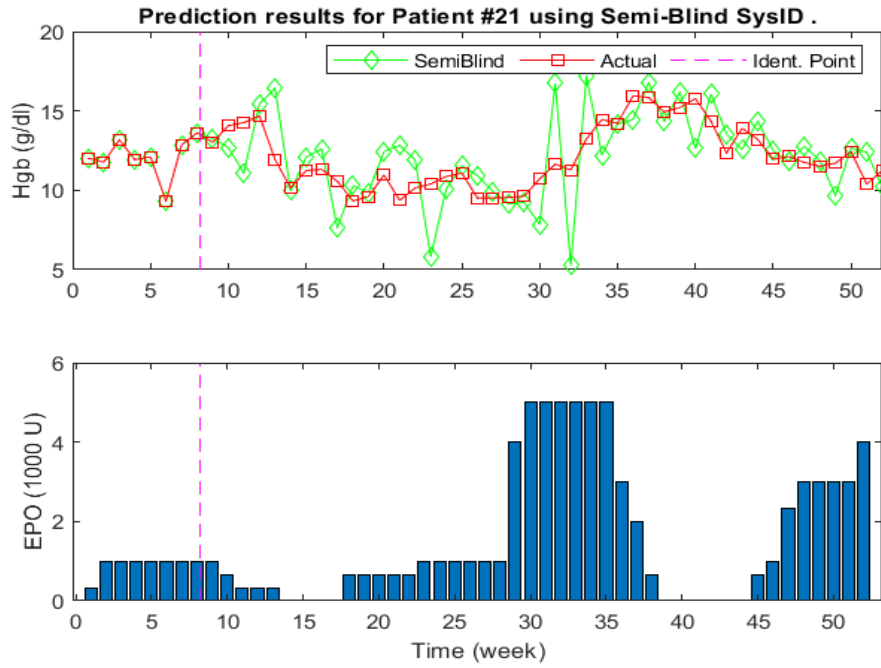


Figure 2.29: Prediction results of semi-blind robust system identification with the Kalman filter for Patient-21 for anemia management.

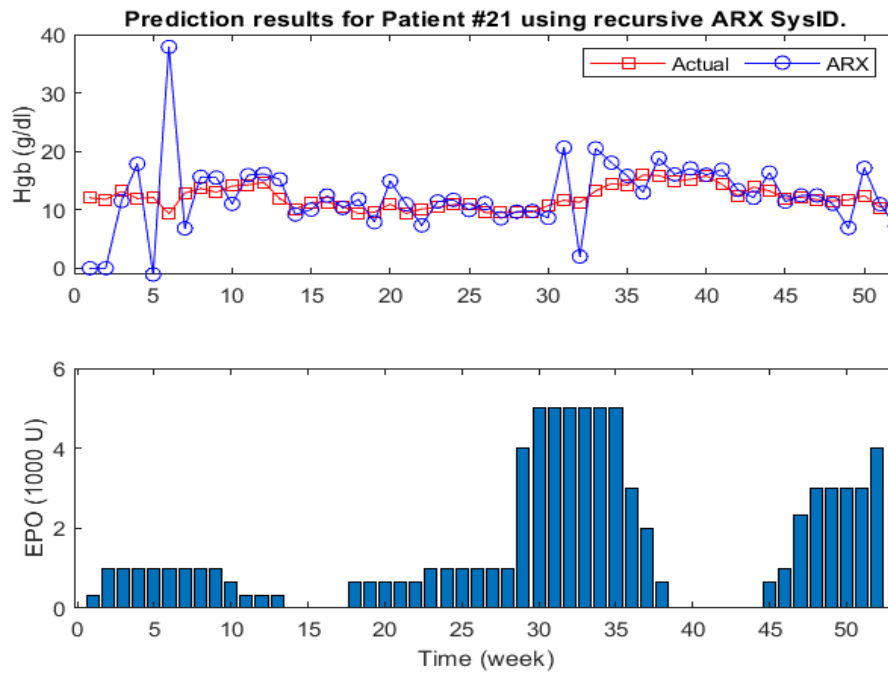


Figure 2.30: Prediction results of ARX with the Kalman filter for Patient-21 for anemia management.

semi-blind robust system identification with Kalman filter. The prediction error for this model is 1.6 ± 2.16 and the MMSE value is 4.67. For this model, 8 data points are used and the 4th order model is used. Figure 2.30 shows the prediction results for the 5th order ARX model for patient-19. The prediction error for the ARX model is 3.33 ± 21.29 and the MMSE value is 31.96.

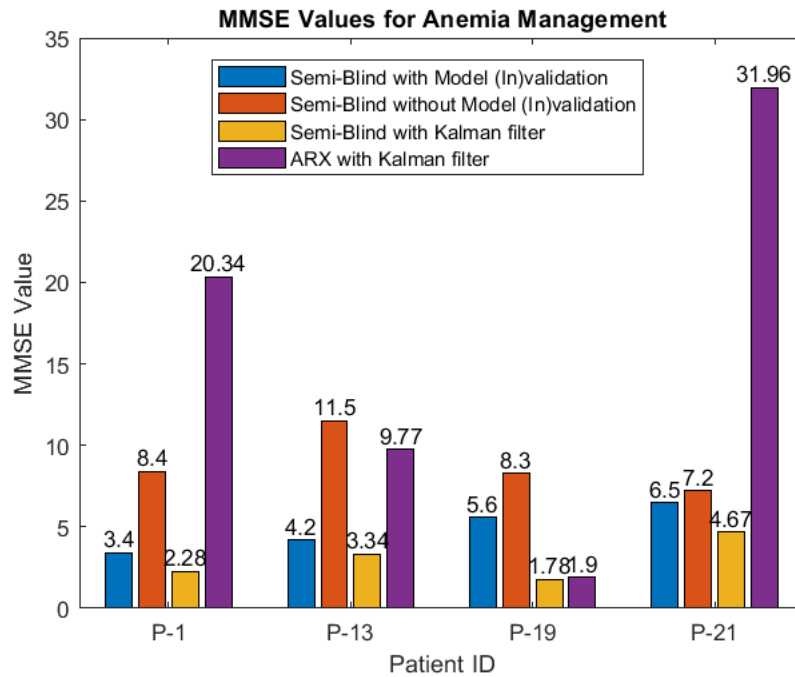


Figure 2.31: MMSE values for anemia management for; (1) Semi-blind with model(In)validation (2) Semi-blind without model(In)validation, (3) Semi-blind with Kalman Filter, (4) ARX with Kalman Filter.

Figure 2.31 shows the comparison of MMSE values of all methods. It shows that semi-blind robust system identification with the Kalman filter has outperformed all other methods for anemia management.

2.1.2.2 Warfarin Management Results

This section provides the simulation results for semi-blind robust system identification with the Kalman filter for warfarin management. The clinical data set discussed in section 2.1.1.3 is used for this simulation. The prediction results for patient-3 using semi-blind robust system identification with Kalman filter are shown in Fig. 2.33. For these prediction results, 7 data points are used for identification, and the 4th order model is used. The model parameters are updated based on prediction errors using the Kalman filter at each time step. The prediction error for results shown in Fig. 2.33 is 0.10 ± 0.05 and the minimum mean squared error (MMSE) is 0.058 as shown in Fig. 2.38. For comparison, the benchmark recursive 4th order ARX model with the Kalman filter is used. Figure 2.32 shows the one-step-ahead prediction results for the recursive ARX model for patient-1. The prediction error for the ARX model is 0.13 ± 0.12 and the MMSE value is 0.131 as shown in Fig. 2.38, which shows the significance of using the effect of non-zero initial conditions in system identification.

Figure 2.35 shows the prediction results for patient-7 from warfarin management using semi-blind robust system identification with Kalman filter. For this patient, 7 data points are used for identification, and the 4th order model is used for prediction results shown Fig 2.35. Figure 2.34 shows the prediction results for patient-7 using the 4th order ARX model with the Kalman filter.

The prediction error for the ARX model is 0.31 ± 0.42 and 0.13 ± 0.059 for the model

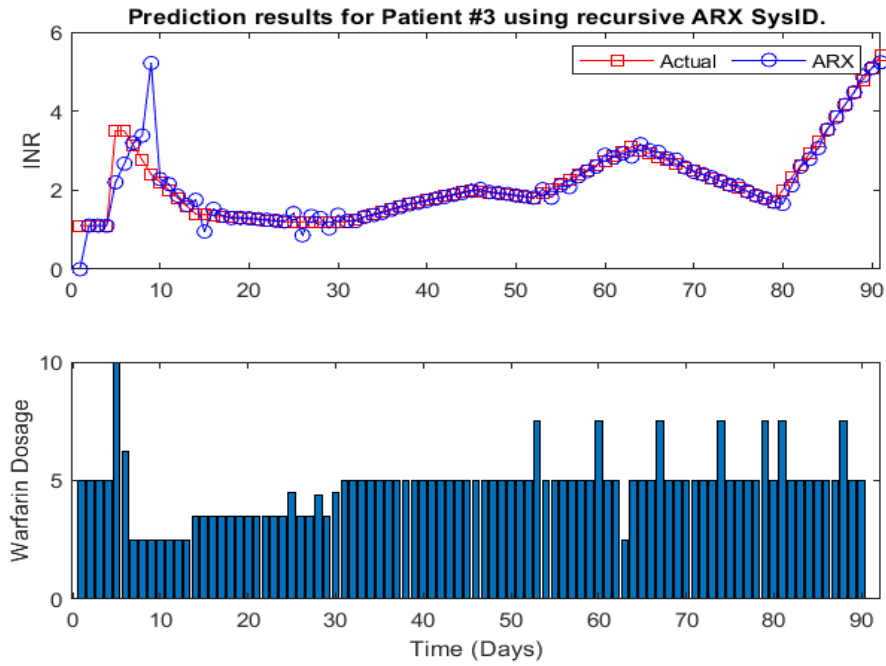


Figure 2.32: Prediction results of ARX with the Kalman filter for Patient-3 of warfarin management.

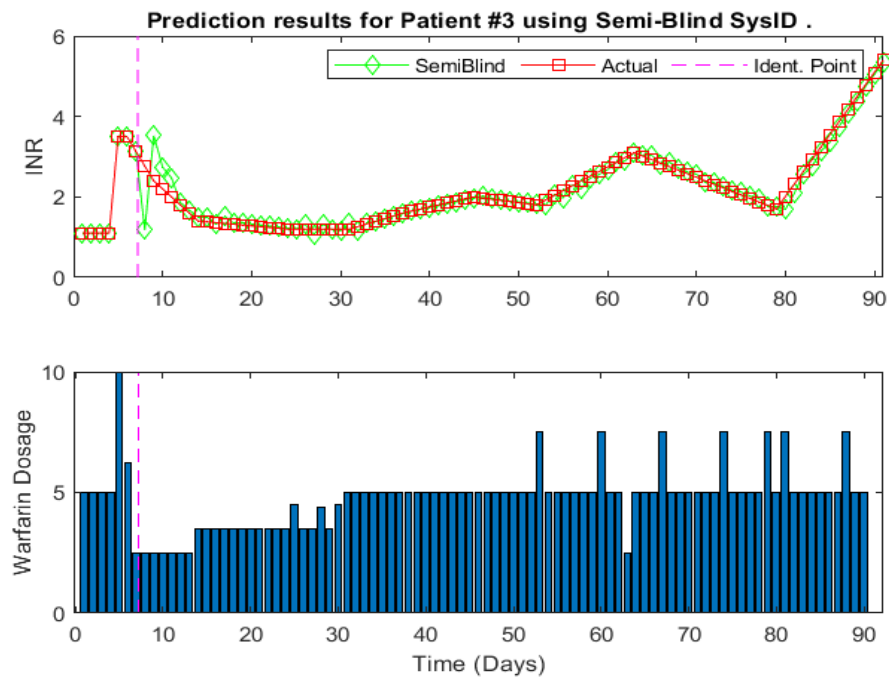


Figure 2.33: Prediction results of semi-blind robust system identification with the Kalman filter for Patient-3 of warfarin management.

identified using semi-blind robust system identification. The MMSE values are 0.073 and 0.51 for the semi-blind robust system identification and ARX model, respectively, as shown in Fig. 2.38.

Figure 2.37 shows the prediction results for patient-10 for the model identified using semi-blind robust system identification with Kalman filter. The prediction error for this

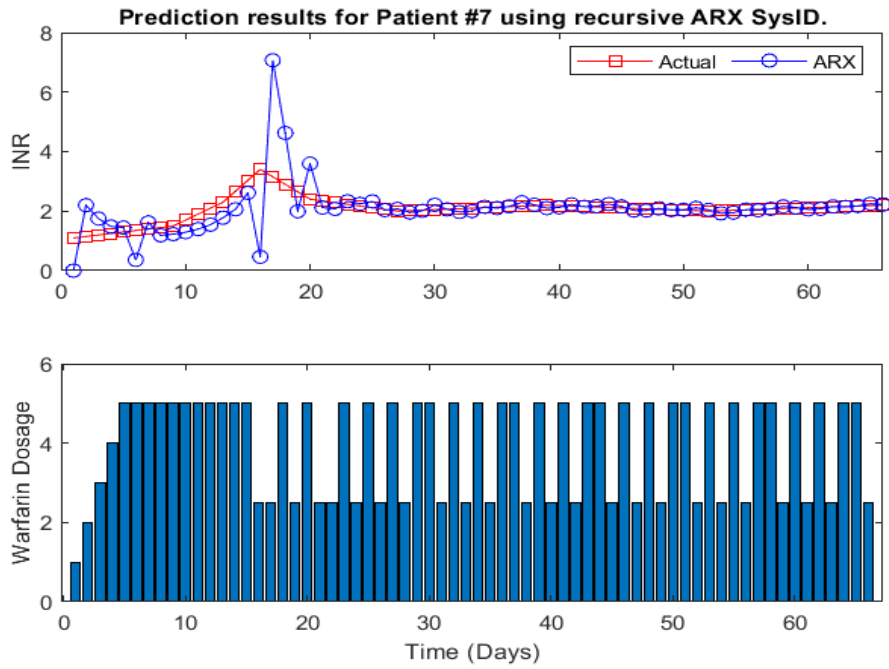


Figure 2.34: Prediction results of ARX with the Kalman filter for Patient-7 for warfarin management.

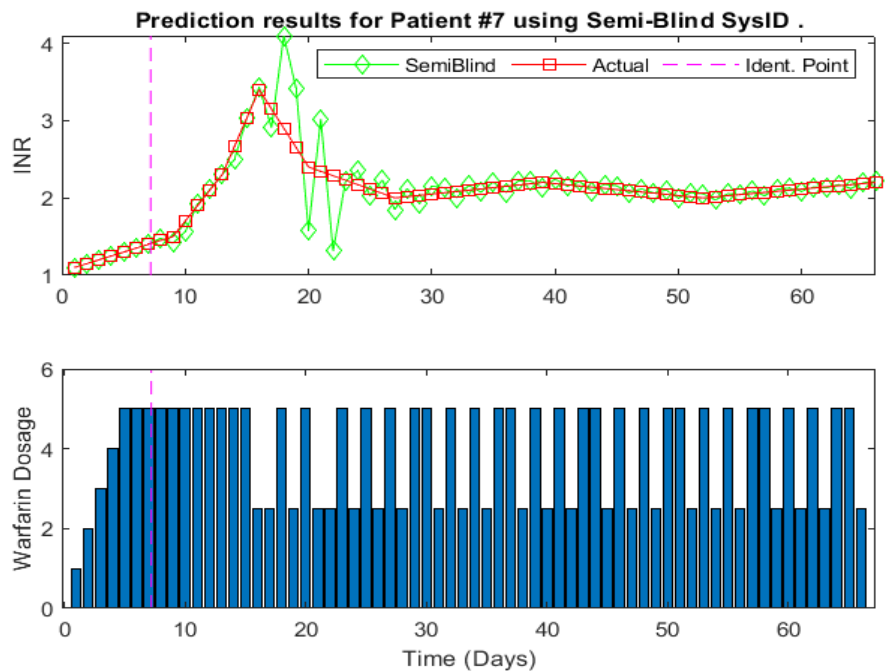


Figure 2.35: Prediction results of semi-blind robust system identification with the Kalman filter for Patient-7 for warfarin management.

model is 0.0812 ± 0.0069 and the MMSE value is 0.0133. For this model, 7 data points are used and the 4th order model is used. Figure 2.36 shows the prediction results for the 4th order ARX model for patient-10. The prediction error for the ARX model is 0.497 ± 0.769 and the MMSE value is 1.00 as shown in Fig. 2.38.

The error comparison of warfarin management and anemia management for all the

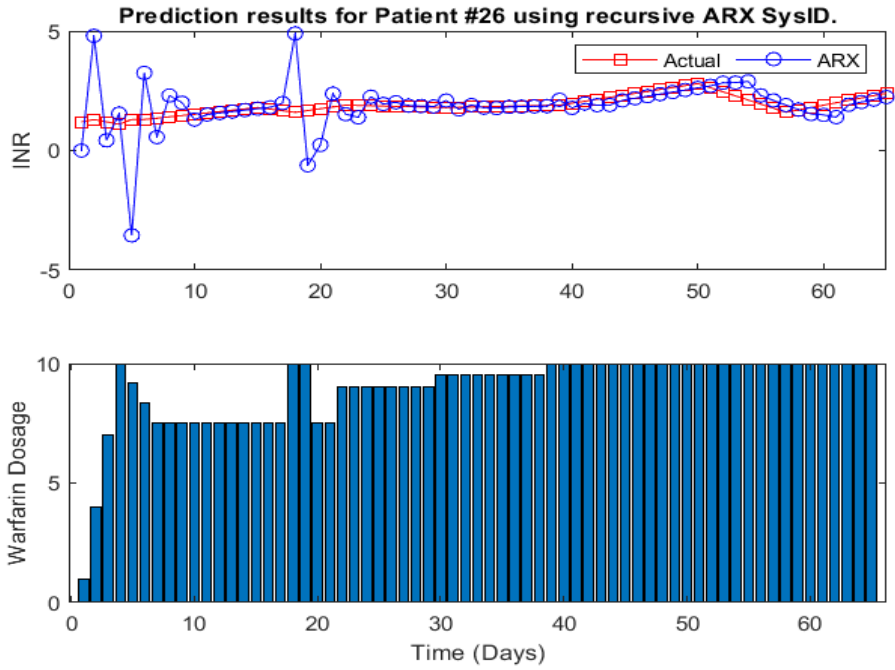


Figure 2.36: Prediction results of ARX with the Kalman filter for Patient-10 for warfarin management.

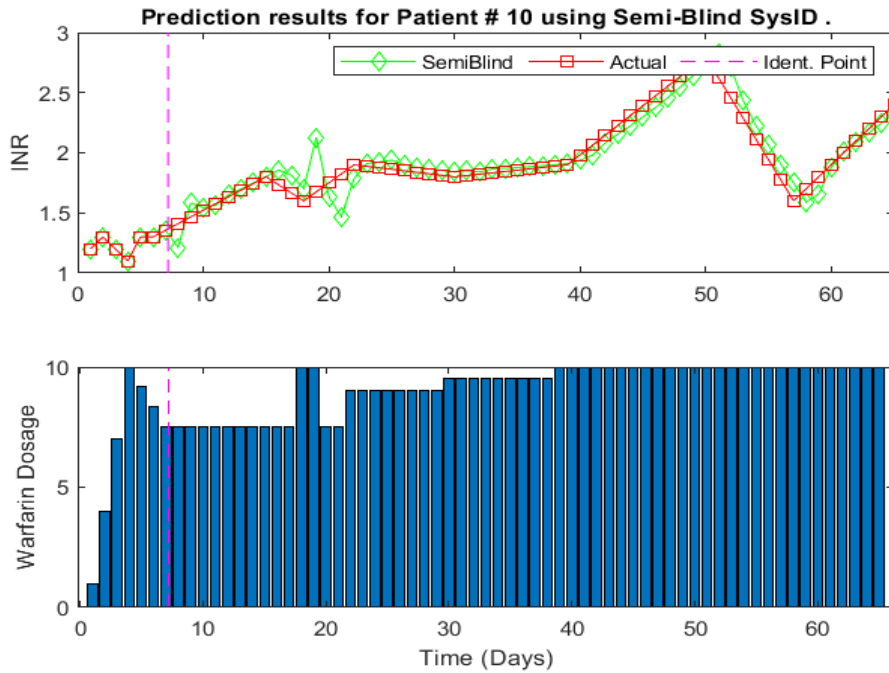


Figure 2.37: Prediction results of semi-blind robust system identification with the Kalman filter for Patient-10 for warfarin management.

methods is shown in Fig. 2.31 & Fig. 2.38. It shows that the Kalman filter with semi-blind robust system identification is able to provide personalized patient dose-response models with low prediction error and able to update the model parameters with low computational time. The next task is to design the control method for optimal dosage. To test the controller, an actual patient or virtual patient model is required. Based on

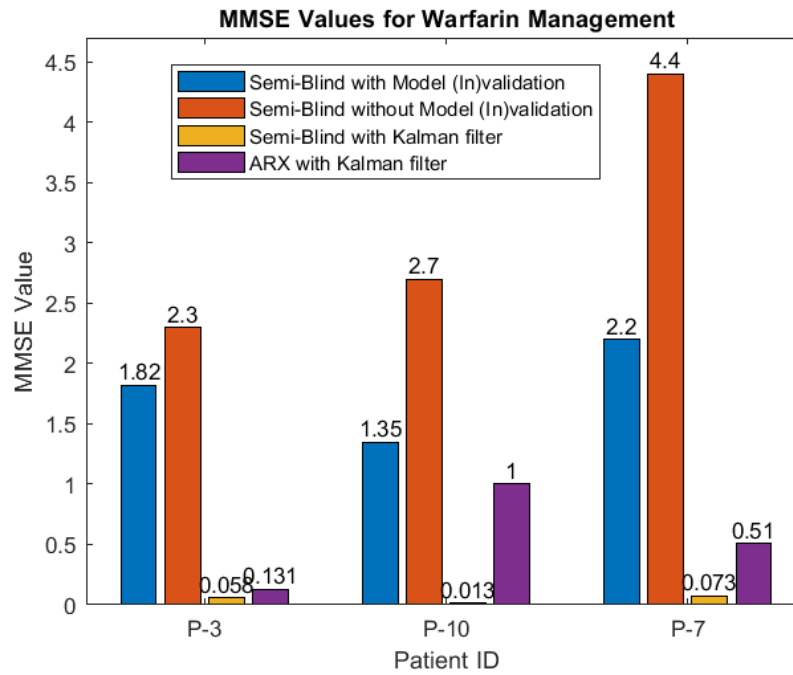


Figure 2.38: MMSE values for Warfarin management for; (1) Semi-blind with model(In)validation (2) Semi-blind without model(In)validation, (3) Semi-blind with Kalman Filter, (4) ARX with Kalman Filter.

the literature review, only the virtual chronic kidney disease (V-CKD) patient model is available. Therefore, in the next chapters, the V-CKD patient model is discussed and the adaptive control method is tested on it.

CHAPTER 3

VIRTUAL CHRONIC KIDNEY DISEASE (V-CKD) PATIENT MODEL

A virtual patient model of erythropoiesis for adults with sufficient iron is used [2, 1] to analyze the performance of controllers *in silico* experiments. In this model, the process of erythropoiesis is divided into five stages: (1) Burst-forming unit erythroids (BFU-E), (2) colony-forming unit erythroids CFU-E, (3) Erhythroblasts, (4) Marrow reticulocytes, and (5) Erythrocytes. Equation (3.1) shows the dynamics for BFU-E where stem cells enter the erythropoiesis lineage [1, 2]:

$$\begin{aligned} \frac{\partial}{\partial t}p(\mu^p, t) + \frac{\partial}{\partial \mu^p}p(\mu^p, t) &= \beta^p p(\mu^p, t), \\ p(0, t) = S_0, \quad p(\mu^p, 0) &= p_0(\mu^p), \end{aligned} \quad (3.1)$$

where p is the cell population in BFU-E stage, $0 \leq \mu^p \leq 7$ is the maturity of cells, t is time step for overall erythropoiesis and β^p is proliferation rate. S_0 is the rate at which stem cells commit to erythropoiesis lineage and $p_0(\mu^p)$ is the initial condition for cell population in the BFU-E stage. By using the finite difference method with Δt as the time step and $\Delta \mu$ as the discretization step for the maturity of the cell, the discretized form for the BFU-E stage is given as follows:

$$\begin{aligned} \beta^p p(\mu_j^p, t_i) &= \frac{p(\mu_j^p, t_{i+1}) - p(\mu_j^p, t_i)}{\Delta t} + \\ &\quad \frac{p(\mu_j^p, t_i) - p(\mu_{j-1}^p, t_i)}{\Delta \mu}, \end{aligned} \quad (3.2)$$

where i is the time index and j is the index for the cell maturity step. The cell evolution dynamics for the CFU-E stage are as follows [2, 1]:

$$\begin{aligned} \frac{\partial}{\partial t}q(\mu^q, t) + \frac{\partial}{\partial \mu^q}q(\mu^q, t) &= [\beta^q - \alpha^q(E(t))]q(\mu^q, t), \\ q(\mu_{min}^q, t) = p(\mu_{max}^q, t), \quad q(\mu^q, 0) &= q_0(\mu^q), \end{aligned} \quad (3.3)$$

where q is cell population and $7 \leq \mu^q \leq 13$ is cell maturity in the CFU-E stage. β^q is the constant proliferation rate, (μ_{min}^q, t) is the boundary condition value provided by the output of the BFU-E stage, and $q_0(\mu^q)$ is the initial value of cell density of in stage CFU-E stage. Rate of apoptosis, $\alpha^q(E(t))$, based on EPO concentration in plasma, $E(t)$, is defined as follows:

$$\alpha^q(E(t)) = \frac{a_1 - b_1}{1 + e^{k_1 E(t) - c_1}} + b_1, \quad (3.4)$$

where, variables a_1 , b_1 , c_1 and k_1 are medically suggested patient specific variables. The discretized form for (3.3) can be found as follows:

$$\beta^q - \alpha^q(E(t_i))q(\mu_j^q, t_i) = \frac{q(\mu_j^q, t_{i+1}) - q(\mu_j^q, t_i)}{\Delta t} + \frac{q(\mu_j^q, t_i) - q(\mu_{j-1}^q, t_i)}{\Delta \mu}. \quad (3.5)$$

Dynamical evolution of cell density in the third stage of erythropoiesis named Erythroblasts is governed by [2, 1]:

$$\begin{aligned} \frac{\partial}{\partial t}r(\mu^r, t) + \frac{\partial}{\partial \mu^r}r(\mu^r, t) &= \beta^r r(\mu^r, t), \\ r(\mu_{min}^r, t) &= q(\mu_{max}^q, t), \quad r(\mu^r, 0) = r_0(\mu^r), \end{aligned} \quad (3.6)$$

where r is the cell population in the erythroblast stage with a cell maturity range of $13 \leq \mu^r \leq 18$. β^r is the constant proliferation rate, $r_0(\mu^r)$ is the initial cell population in this stage at $t = 0$ and $r(\mu_{min}^r, t)$ is the boundary condition value provided by the output of CFU-E stage. The discretization of (3.6) can be found as follows:

$$\beta^r r(\mu_j^r, t_i) = \frac{r(\mu_j^r, t_{i+1}) - r(\mu_j^r, t_i)}{\Delta t} + \frac{r(\mu_j^r, t_i) - r(\mu_{j-1}^r, t_i)}{\Delta \mu}. \quad (3.7)$$

The dynamical relation of cell evolution in the stage of marrow reticulocytes is given as follows [2, 1]:

$$\begin{aligned} \frac{\partial}{\partial t}s(\mu^s, t) + v^s(E(t))\frac{\partial}{\partial \mu^s}s(\mu^s, t) &= -\alpha_0^s s(\mu^s, t), \\ v^s(E(t))s(\mu_{min}^s, t) &= r(\mu_{max}^r, t), \quad s(\mu^s, 0) = s_0(\mu^s), \end{aligned} \quad (3.8)$$

where s is the cell population density in marrow reticulocytes with cell maturity range $18 \leq \mu^s \leq 21$ and α_0^s is the rate of ineffective erythropoiesis. The term $v^s(E(t))s(\mu_{min}^s, t)$ describes the rate at which the cell enters in marrow reticulocyte stage from erythroblast stage. $s_0(\mu^s)$ is initial cell density in marrow reticulocytes at $t = 0$ and $v^s(E(t))$ is the maturity velocity calculated based on EPO as follows:

$$v^s(E(t)) = \frac{a_2 - b_2}{1 + e^{k_2 E(t) - c_2}} + b_2, \quad (3.9)$$

where a_2 , b_2 , c_2 and k_2 are patient specific variables. The discretized form for (3.8) can be found as:

$$\begin{aligned} -\alpha_0^s s(\mu_j^s, t_i) &= \frac{s(\mu_j^s, t_{i+1}) - s(\mu_j^s, t_i)}{\Delta t} \\ &+ v^s(E(t_i))\frac{s(\mu_j^s, t_i) - s(\mu_{j-1}^s, t_i)}{\Delta \mu}. \end{aligned} \quad (3.10)$$

The model for erythrocytes cell stage is given by [2, 1]:

$$\begin{aligned} \frac{\partial}{\partial t}m(\mu^m, t) + \frac{\partial}{\partial \mu^m}m(\mu^m, t) &= -\alpha^m(E(t), \mu^m)m(\mu^m, t), \\ m(0, t) &= v^s(E(t))s(\mu_{max}^s, t), \quad m(\mu^m, 0) = m_0(\mu^m), \end{aligned} \quad (3.11)$$

where m is the cell population in the erythrocytes cell stage with cell maturity $0 \leq \mu^m \leq 120$, $s(\mu_{max}^s, t)$ is the number of the cells provided by the previous stage and $m_0(\mu^m)$ is the initial cell population in erythrocytes cell stage. $\alpha^m(E(t), \mu^m)$ is the mortality rate of RBCs due to low EPO in plasma, and it is defined as follows:

$$\alpha^m = \begin{cases} \alpha_r^m + \min\left(\frac{c_E}{E(t)^{k_E}}, b_E\right) & \text{for } E(t) < \tau_E, \\ \alpha_r^m & \text{otherwise,} \end{cases} \quad (3.12)$$

where, α_r^m is daily random breakdown. c_E , k_E , b_E are constants. τ_E is the threshold for $E(t)$ below which neocytolysis, selective destruction of the youngest population of erythrocytes in blood, is triggered. The discretized form for (3.11) can be found as follows:

$$-\alpha^m(E(t_i), \mu_j^m) m(\mu_j^m, t_i) = \frac{m(\mu_j^m, t_{i+1}) - m(\mu_j^m, t_i)}{\Delta t} + \frac{m(\mu_j^m, t_i) - m(\mu_{j-1}^m, t_i)}{\Delta \mu}. \quad (3.13)$$

Equations (3.1) through (3.13) summarize the dynamical model for Virtual CKD (V-CKD) patients. For this V-CKD patient model, the EPO is first introduced in the second stage in (3.3). The EPO concentration in the human body is the sum of endogenously produced erythropoietin, E^{end} , and external dosage, $E^{ex}(t_{i+1})$. It is defined as follows:

$$E(t_{i+1}) = E^{end}(t_{i+1}) + E^{ex}(t_{i+1}). \quad (3.14)$$

The human kidneys adjust the production of EPO according to the oxygen partial pressure in the blood and the number of RBCs. The dynamics of endogenous EPO concentration, $E^{end}(t)$, in plasma are defined by the following ordinary partial differential equation.

$$\dot{E}^{end}(t) = \frac{1}{TBV} E_{in}^{end}(t) - c_{deg}^{end} E^{end}(t), \quad (3.15)$$

where, c_{deg}^{end} is the degradation rate of endogenous EPO, TBV is total blood volume, and $E_{in}^{end}(t)$ is endogenous erythropoietin released by kidneys, defined as a sigmoid function as follows:

$$E_{in}^{end}(t) = \frac{a_3 - b_3}{1 + e^{k_3 \tilde{M}(t) - c_3}} + b_3, \quad (3.16)$$

where $\tilde{M}(t) = \frac{10^{-8} M(t)}{TBV}$ and $M(t) = \int_0^{\mu_{max}^m} m(\mu^m, t) d\mu^m$ is the total number of RBCs. Given the above dynamics of EPO in plasma and cells at each stage, the Hgb value can be calculated as follows:

$$Hgb = \frac{M(t) \times MCH}{TBV \times 10^{10}}, \quad (3.17)$$

where $MCH = 29 \text{ pg}$ is the mean corpuscular hemoglobin. This concludes the V-CKD patient model, i.e., mimicking an actual CKD patient treated for anemia. As discussed in the next sections, this model is to be used as an actual plant model for validation of the controllers *in silico* experiments.

CHAPTER 4

OPTIMAL CONTROL DESIGN FOR PERSONALIZED MEDICINE

4.1 Adaptive Model Predictive Control (AMPC)

Traditional MPC uses a linear-time-invariant (LTI) model to predict the next control input. However, AMPC is suitable for highly nonlinear models or time-varying models, such as CKD patients [51]. Since the change in model parameters in the future cannot be known beforehand, therefore, linear-time varying MPC or gain-scheduled MPC is not suitable for the application of personalized EPO dosing. As the parameters of the CKD patient model change over time, therefore, the controller has enough time to update the model and predict the next dosage (control input) before the next scheduled dosing time.

In general, AMPC consists of two parts: (1) system identification/online parameter estimation, and (2) traditional MPC as shown in Fig. 4.1. Let's define the time-varying state-space form of the dynamical model in the MPC framework as follows [52, 53, 54]:

$$\begin{aligned} x_{k+1} &= A_k x_k + B_k^u u_k + B_v^v k + B_k^d d_k, \\ y_k &= C_k x_k + D_k^v v_k + D_k^d d_k, \end{aligned} \quad (4.1)$$

where A_k is the state transition matrix associated with state vector, x_k , B_k^u is the input matrix associated with input vector, u_k , to be controlled. B_v^v is the input matrix associated with measured disturbances, v_k . B_k^d is the matrix associated with unmeasured disturbances, d_k . C_k is the state-to-output matrix for output, y_k . D_k^v is the matrix associated with measured disturbance to output dynamics and D_k^d is the matrix associated with unmeasured disturbances to output dynamics. These matrices are subject to change and obtained through online system identification, discussed earlier.

Given the plant model structure for online parameter estimation, we define the cost function and constraints for MPC for optimal EPO dosage in CKD patients. It is important to mention that for AMPC, cost function and constraints are defined like traditional MPC. The standard cost function is defined as follows [52, 53]:

$$\min \quad J(z_k) = J_{Hgb}(z_k) + J_{\Delta u}(z_k) + J_\epsilon(z_k), \quad (4.2)$$

where $J_{Hgb}(z_k)$ is the Hgb reference tracking cost function to achieve the target value of Hgb, Hgb^{Target} . $J_{\Delta u}(z_k)$ is the cost function for the change in EPO dosage, Δu , and $J_\epsilon(z_k)$ is the cost function for the constraint violation. The constraints for this optimization problem are as follows:

$$\begin{aligned} u_{min} = 0 &\leq u_k \leq 20000 = u_{max}, \\ -1000 &\leq |\Delta u_k| \leq 1000, \quad 10 \leq Hgb^{Target} \leq 12 \text{ g/dl}. \end{aligned} \quad (4.3)$$

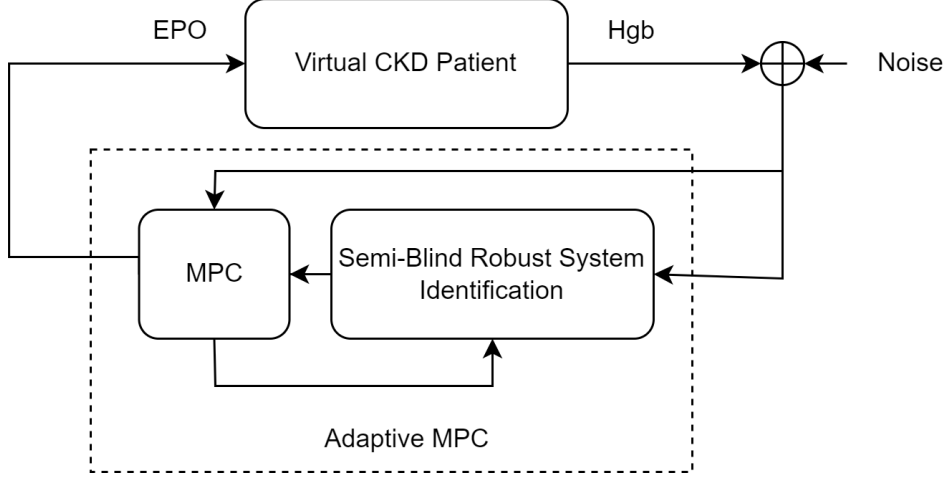


Figure 4.1: Block diagram for Adaptive MPC (AMPC) with online parameter estimation for virtual CKD Patient.

Hgb reference tracking cost function is defined as:

$$J_{Hgb}(z_k) = \sum_{i=1}^{ph} \frac{w}{s} \left[Hgb_{k+i|k}^{Target} - Hgb_{k+i|k}^{Actual} \right]^2, \quad (4.4)$$

where, Hgb^{Target} is desired hemoglobin level of the patient and Hgb^{Actual} is actual Hgb measurement. $z_k = [u_{k|k}, u_{k+1|k}, u_{k+2|k}, \dots, u_{k+ph-1|k}]$ is the input vector which contains the EPO dosage values across the prediction horizon obtained by solving a quadratic optimization problem. ph is the prediction horizon and k is the time step. w is the weight and s is the scale factor.

The cost function to regulate the change in successive EPO dosages is defined as follows:

$$J_{\Delta u}(z_k) = \sum_{i=1}^{ph-1} \frac{w}{s} \left[u_{k+i|k} - u_{k+i-1|k} \right]^2, \quad (4.5)$$

where, the goal is to minimize the difference between successive EPO dosages, provided by the optimization problem across the prediction horizon, in the input vector, $z_k = [u_{k|k}, u_{k+1|k}, u_{k+2|k}, \dots, u_{k+ph-1|k}]$. For example, at $i = 1$, $u_{k+1|k} - u_{k|k} = \Delta u$.

For the application of EPO dosing, the maximum limit on EPO dosage is a hard constraint, however, the change in successive EPO dosages is a soft constraint. Such as during bleeding the EPO dosage is required to be quickly increased but it is not suitable to violate the maximum allowed limit on EPO dosage. Therefore, the cost function for constraint violation is used as follows:

$$J_{\epsilon}(z_k) = \rho_{\epsilon} \epsilon_k^2, \quad (4.6)$$

where, ϵ_k is the slack variable and ρ_{ϵ} is the penalty weight for constraint violation. It is useful to regulate soft constraints and avoid violation of hard constraints for the optimization problem. This concludes the description of AMPC for V-CKD patients. V-CKD patient model discussed in Section-3 is used as an actual plant model for *in silicio* experiments for validation of the proposed controller designs.

4.2 Extremum Seeking Control

The requirement of the dynamical model in AMPC design increases computational complexity and incorrect nominal conditions can degrade the performance of the controller. Therefore, model-free controllers, which solely rely on measurement data instead of explicit dynamical models could be considered [55]. Extremum Seeking Controller (ESC) is one of the prominent model-free adaptive control strategies. The basic concept behind ESC is to maximize the objective function [56]. The main components of ESC design are parameter estimation, modulation, and demodulation as shown in Fig. 4.2.

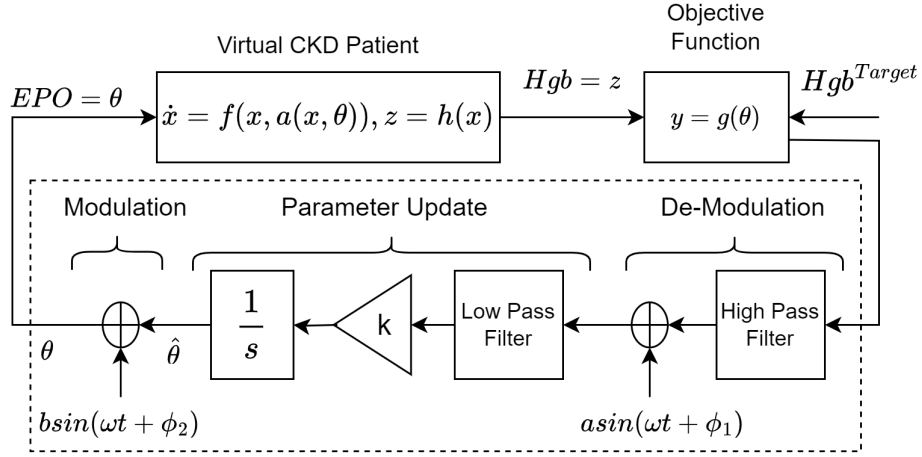


Figure 4.2: Block diagram for Extremum Seeking Control (ESC) with online parameter estimation for V-CKD Patient.

To match the notation with the literature, let

$$y = g(\theta) = g^* - \frac{g''}{2}(\theta - \theta^*)^2, \quad (4.7)$$

where $g(\theta)$ is the objective function that we wish to maximize given the variable θ and $g'' > 0$. θ is the control input provided by the controller and θ^* is the optimal control input for dynamical plant. The objective is to reduce the term $\theta - \theta^*$. $\hat{\theta}$ in Fig. 4.2 is the estimate of unknown optimal EPO input, θ^* , for virtual CKD patient and the parameter estimation error defined as $\tilde{\theta} = \theta^* - \hat{\theta}$. By focusing on the modulation part of Fig. 4.2, we derive the following mathematical relation:

$$b\sin(\omega t) - \tilde{\theta} = \theta - \theta^*, \quad (4.8)$$

By substituting (4.8) in (4.7) and using trigonometric identity:

$$g(\theta) = g^* + \frac{g''}{4}b^2 - \frac{g''}{4}\cos 2(\omega t) + \frac{g''}{2}\tilde{\theta}^2 - g''\tilde{\theta}b\sin(\omega t), \quad (4.9)$$

By applying high pass filter, $\frac{s}{s+h}$, to the (4.9) to remove term the g^* :

$$\frac{s}{s+h} [g(\theta)] = g''b\sin(\omega t)\tilde{\theta} + \frac{g''}{4}\cos 2(\omega t) - \frac{g''}{2}\tilde{\theta}^2. \quad (4.10)$$

Now modulate the signal with $a\sin(\omega t)$ as follows:

$$\zeta = g'' ab\sin^2(\omega t)\tilde{\theta} + \frac{g''}{4}a\sin(\omega t)\cos 2(\omega t) - \frac{g''}{2}\tilde{\theta}^2 a\sin(\omega t). \quad (4.11)$$

By applying trigonometric identities $2\sin^2(\omega t) = 1 - \cos 2(\omega t)$ and $2\cos 2(\omega t)\sin(\omega t) = \sin 3(\omega t) - \sin(\omega t)$ on (4.11), one can obtain:

$$\zeta = \frac{g''}{2}ab\tilde{\theta} - \frac{g''}{2}ab\cos 2(\omega t)\tilde{\theta} + \frac{g''}{8}a[\sin 3(\omega t) - \sin(\omega t)] - \frac{g''}{2}\tilde{\theta}^2 a\sin(\omega t). \quad (4.12)$$

Since θ^* is constant, therefore, $\dot{\hat{\theta}} = -\hat{\theta}$. By applying integrator and multiplying with gain, k , we get $\tilde{\theta} \approx \frac{k}{s}(\zeta)$. In (4.12), last term is quadratic in $\tilde{\theta}$. This term can be neglected as our interest lies in local analysis. The second and third terms are high-frequency terms that will be highly attenuated when passed through the integrator. These two terms can also be neglected, this results in:

$$\dot{\tilde{\theta}} \approx k \left\{ \frac{g''}{2}ab\tilde{\theta} \right\}. \quad (4.13)$$

For $kg'' < 0$, this is a stable system. This concludes that $\tilde{\theta} \rightarrow 0$ and $\hat{\theta}$ converges to optimal θ^* and hence the mathematical explanation for Extremum Seeking Control (ESC)

Parameters	Meaning	values
β^p	Proliferation rate for BFU-E cells	0.2
β^q	Proliferation rate for CFU-E cells	0.57
β^r	Proliferation rate for erythroblasts	1.024
α_0^s	Rate of ineffective erythropoiesis	0.089
α^m	Intrinsic mortality rate for erythrocytes	0.005
a_1, b_1	Constants for CFU-E cells	0.35,0.07
c_1, k_1	Constants for CFU-E cells	3,0.14
a_2, b_2	Constants for marrow reticulocytes	2,0.35
c_2, k_2	Constants for marrow reticulocytes	2.3,0.2
a_3, b_3	Constants for EPO release from kidneys	9000,10000
c_3, k_3	Constants for EPO release from kidneys	9.1,0.2
b_E, c_E, k_E	Constants for mortality rate for erythrocytes	0.1,3.5,3
τ_E	EPO threshold	9.8
c_{deg}^{end}	Degradation of kidney's EPO	25/24
c_{deg}^{ex}	Degradation of external EPO dose	8.5/24
S_0	Rate at which stem cells commit to erythroid lineage	8×10^5
Patient-specific Parameters for Patient-1		
μ^m	cell maturity duration in Erythrocytes (last stage)	14 days
Δt_{total}	Total cell maturity period	65 days
$TBV(ml)$	Total blood volume	5000
Patient-specific Parameters for Patient-2		
μ^m	cell maturity duration in Erythrocytes (last stage)	20 days
Δt_{total}	Total cell maturity period	59 days
$TBV(ml)$	Total blood volume	5500

Table 4.1: Virtual CKD Patient Model Parameters [1, 2]

used in this research. The next section discusses the results of *in silico* experiments of ESC and AMPC controllers for V-CKD patients in the scenarios of bleeding and missing dosage.

4.2.1 Results

This section discusses the results of *in silico* experiments for V-CKD patients for optimal EPO dosing. To evaluate the performance of AMPC and ESC, we analyze the patient's response in the normal routine and in the event of bleeding and missing doses. For V-CKD patients as an actual plant, we considered model parameters as shown in Table 4.1 [2, 1]. In this table, good responder patients reach desired range of Hgb quickly and EPO dosage can be found. Poor responder patients are challenging patients which show slow progress in the treatment.

For this research work, a white Gaussian noise with a power of $0.1db$ is added to the measurement of Hgb. For *in silico* experiments, the one event of bleeding is introduced at 70^{th} day of treatment and two events of consecutive missing dosages (zero EPO) are introduced through days 112 to 115 and 150 to 154. The simulation result for V-CKD patient-1 with AMPC (green plot) and ESC (red plot) are shown in Fig. 4.6. The objective is to keep the Hgb level between $10 - 12g/dl$ region shown by two solid black lines. The initial Hgb for patient 1 is around $8.3g/dl$.

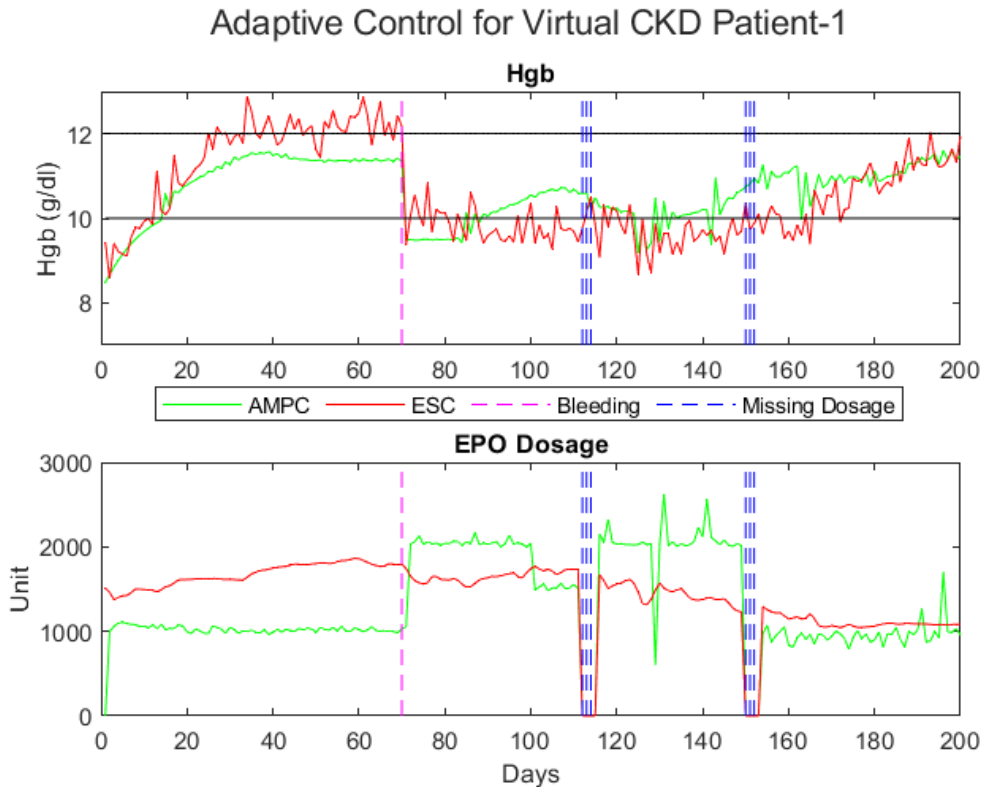


Figure 4.3: *In-silico* results of AMPC and ESC for V-CKD Patient-1.

AMPC is able to reach the Hgb level in around 18 days for patient-1 with a mean EPO dosage of 1000 units and ESC to have the first touch of desired range with a mean EPO dosage of 1500 units. AMPC is able to maintain the Hgb level in the desired range

in the presence of measurement noise, whereas, ESC-based Hgb level kept oscillating and stayed higher than 12 g/dl , which is not suitable for patients. The challenging parts of this *in silicio* experiments are the events of bleeding and missing dosages. At 70th day, the bleeding is introduced which decreased the Hgb level by a factor of 1.2 for each patient. The goal is to get the Hgb level back into the desired range without high overshoots in EPO dosing as quickly as possible. AMPC is able to achieve 11 g/dl in around 32 days, a maximum EPO dosage of 2200 units. It shows the effectiveness of AMPC with online parameter estimation in time and regulating EPO dosage in the life-threatening event of bleeding. Figure 4.6 shows the event of consecutive missing dosages through days 112 to 115 and days 150 to 154. It can be seen that AMPC is able to handle the missing dosage with minor fluctuations in the Hgb level. However, ESC suffers performance degradation because it is not able to maintain the Hgb level in the event of missing dosage because ESC has not reached EPO dosage. This shows that AMPC with recursive parameter estimation is able to maintain the desired value of Hgb in normal conditions and in events of bleeding and missing dosages.

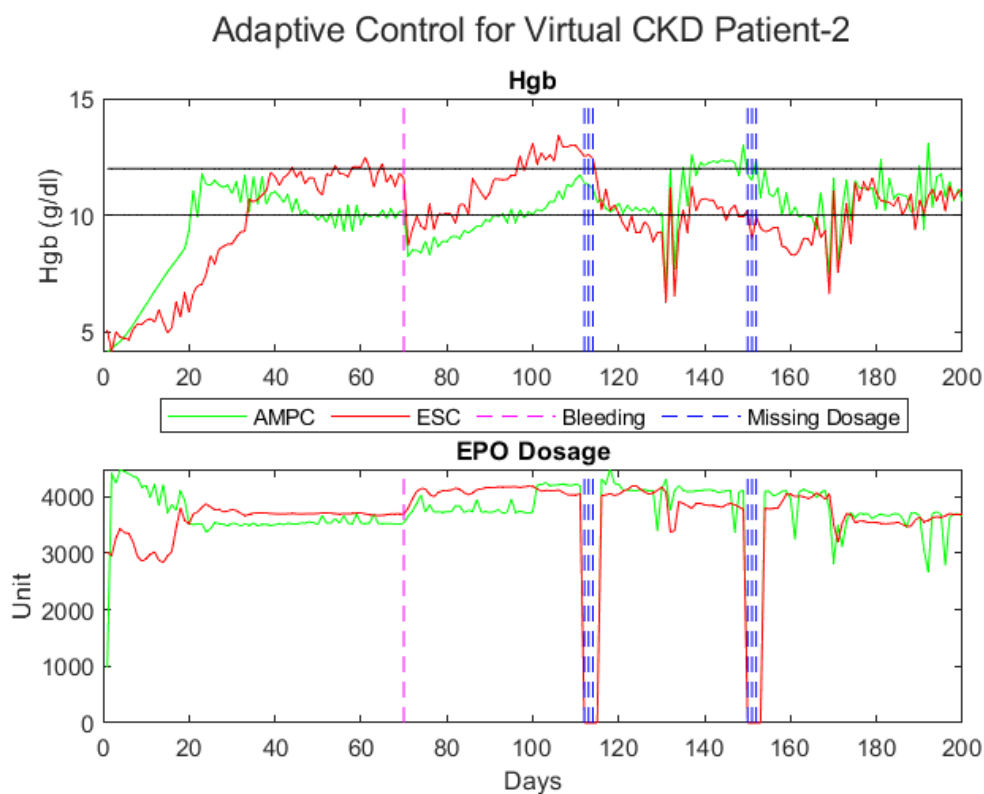


Figure 4.4: *In-silicio* results of AMPC and ESC for V-CKD Patient-2.

Figure 4.7 shows the simulation results of Hgb level and EPO dosage obtained by AMPC (green plot) and ESC (red plot) for virtual patient-2. For this patient, it took around 20 days for AMPC to reach desired Hgb level with a mean EPO dosage of 3500 units and ESC took a total of 38 days for ESC to first touch the desired range. It took 40 days for AMPC to recover the Hgb level after bleeding with a maximum EPO dosage of 7144 units and recovery time for ESC is 28 days. However, in the event of consecutive missing dosages, AMPC still outperforms ESC for V-CKD patient-2 as ESC suffers an Hgb level drop in case of missing dosage.

One of the prominent issues in the ESC results is the small oscillations in the Hgb results, which is inherited due to the perturbation to find the maximum of the objective function in ESC. The results show that AMPC is able to maintain the Hgb in the desired range without low fluctuations in events of bleeding & missing dosages as well as the normal conditions.

4.3 Reinforcement Learning for Personalized Medicine

Artificial Intelligence has been playing a vital role in the advancement of personalized medicine by using data-driven adaptive methodologies [57, 58]. In [59], a SARSA Reinforcement Learning (RL) agent is trained for optimal EPO dosage. In this research work, Takagi-Sugeno (TS) fuzzy model is used as an interactive environment to obtain the RL policy. Similarly, the Fitted Q-Iteration RL method using retrospective treatment data is developed in [60] for CKD patients. In [61], batch RL using fitted Q-iteration is proposed for optimal EPO dosage using training data from medical records. These methods proposed in the literature have shown satisfactory results. However, these studies lack the regress evaluation in the events of bleeding and missing dosages. Therefore, in this research work, we study the model-free Deep Q-learning network (DQN) RL method which takes advantage of a non-linear complex neural network to solve value function and it is evaluated for the events of bleeding and missing. Furthermore, we compare the performance of the proposed RL method to the proposed AMPC with recursive system identification to find the predictive model.

4.3.1 Model-Free Deep Q-Learning for Optimal EPO Dosing

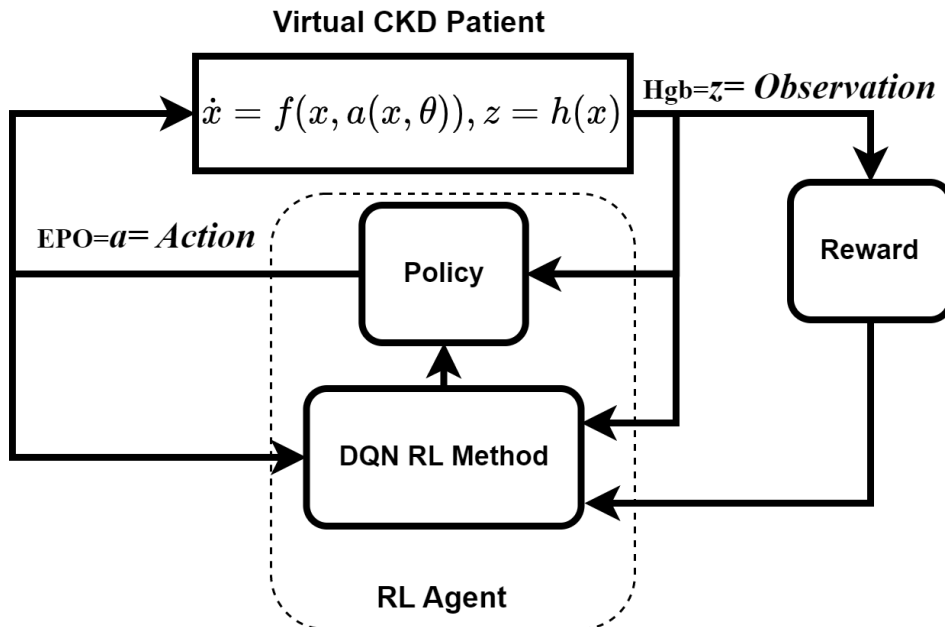


Figure 4.5: Block diagram for DQN-RL for virtual CKD Patient.

In this research work, it is considered that the RL agent interacts with the virtual CKD patient model, an environment, through an action, a sequence referring to EPO dosages and observes the output, z , in the form of Hgb levels. For V-CKD patients, the

agent has a discrete action space and continuous observation space. The agent learns from the current action and observation and all sequences terminate in a finite time step. For optimal policy, the agent interacts with the environment and maximizes a discrete reward function. The discrete reward function depends on the constraints on EPO dosages and the constraints are defined as follows:

$$\begin{aligned} a_{min} = 0 \leq a_k \leq 20000 = a_{max}, \\ -1000 \leq |\Delta a_k| \leq 1000, \quad 10 \leq z^{Target} \leq 12. \end{aligned} \quad (4.14)$$

The discrete reward function for this problem can be defined as follows:

$$\begin{aligned} R_1 &= \lambda_1(z_k \leq 10 || z_k \geq 12) \\ R_2 &= \lambda_2(|a_k - a_{k-1}| > 1000) \\ R_3 &= \lambda_3(z_k > 10 \&\& z_k < 12) \\ R_k &= -R_1 - R_2 + R_3, \end{aligned} \quad (4.15)$$

where $\lambda_1, \lambda_2, \lambda_3$ are tunable parameters. R_1 refers to the penalty if the observed Hgb is not in the desired range of $10 - 12g/dl$, R_2 is the penalty if the change in successive EPO dosages is greater than 1000 units, this part of the reward function is to avoid high jumps in the dosages. R_3 is the reward if the observed Hgb is in the desired range. R_k is the total reward at time step k . Furthermore, we define the action-value function for optimal EPO dosage as follows:

$$Q^*(z, a) = \max_{\pi} \mathbb{E}[R_t | z_k = z, a_k = a, \pi], \quad (4.16)$$

where π is a policy mapping sequences to actions. The above action-value function obeys the Bellman equation. However, instead of implementing an action-value function, an estimator $Q(z, a, \theta)$ is used. To estimate the action-value function, we have used a neural network-based approximator with weights θ . The loss function for the approximator is defined as follows:

$$L = \frac{1}{2M} \sum_{i=1}^M (y_i - Q(z_i, a_i, \pi))^2, \quad (4.17)$$

where M is the batch size and $y_i = R_i + \gamma \max_{\pi} Q_i(z_i, a_i, \pi)$. γ is the discount factor. This concludes the DQN-RL method to find the optimal EPO dosage in virtual CKD patients.

4.3.1.1 Results

In this section, *in-silico* results of two V-CKD patients are discussed. For closed-loop simulations, V-CKD patients with different parameters, such as maturity period of cells in the erythropoiesis, total blood volume, and S_0 as given in TABLE 4.1. are considered. To evaluate the performance of the DQN-RL and AMPC control policies, we have considered two life events, (1) bleeding and (2) missing dosages. *In-silico* results for the first V-CKD patient are shown in fig. 4.6. The cell maturity period of this virtual patient is 54 days, total blood volume is 5000 ml and $S_0 = 5 \times 10^5$. In simulation results, the pink dashed vertical line at 70th time step refers to the bleeding event and the vertical blue dashed line shows the two events of three consecutive missing dosages

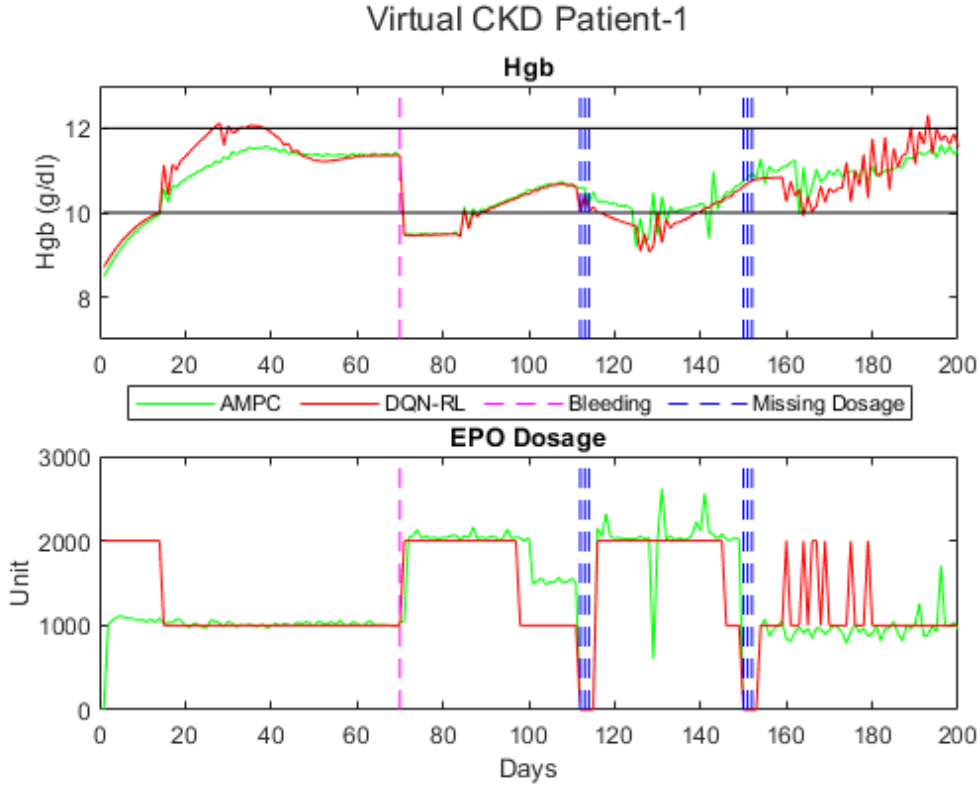


Figure 4.6: Results of DQN-RL and AMPC for the V-CKD Patient-1.

through time steps 112 to 115 and 150 to 153 days. The top plot shows the Hgb levels and the bottom plot shows EPO dosages provided by the control policies. The green plot shows the results due to DQN-RL and the red plot shows the results due to AMPC.

Figure 4.6 shows that the initial Hgb level is 9 g/dl . The AMPC provides an initial EPO dosage of 1000 units and DQN-RL suggests an EPO dosage of 2000 units, however, DQN-RL changes it to 1000 units after a few time steps. The Hgb level rises to the desired range of $10 - 12 \text{ g/dl}$. The event of bleeding is introduced at the 70^{st} time step and the Hgb level drops to the 9.4 g/dl . The AMPC and DQN-RL changed the EPO dosage to 2000 units to recover the Hgb level for the V-CKD patient. In response to this change, the Hgb level rises to the desired range and both controllers decrease the EPO dosage in order to avoid any overshoot. The events of missing dosages are introduced through time steps 112 to 115 and 150 to 153 days. The event of missing dosage means that zero EPO value in the bottom plot. Both control policies are able to recover the Hgb level due to the missing dosages, however, the frequency of EPO dosage is high in this range as expected. It shows how difficult these scenarios could be handled in the real world.

To test the proposed control policies, the results of the second V-CKD patient are shown in Fig. 4.7. The cell maturity period of this virtual patient is 54 days, total blood volume is 5100 ml and $S_0 = 5.3 \times 10^5$. The initial Hgb level for this patient is 10.68 g/dl . The AMPC provides an initial EPO dosage of 500 units and DQN-RL suggests 1000 units. The Hgb level remains in the desired range. The Hgb level drops due to the bleeding at 70^{th} time step. Both proposed control policies increase the EPO dosage to recover the Hgb level. The results show that DQN-RL has more frequency

in the change of EPO dosage as compared to AMPC. The event of missing dosage introduced through time steps 112 to 115 and 150 to 153 days results in a drop in Hgb level. However, both controllers are able to suggest acceptable EPO dosages to recover the Hgb level.

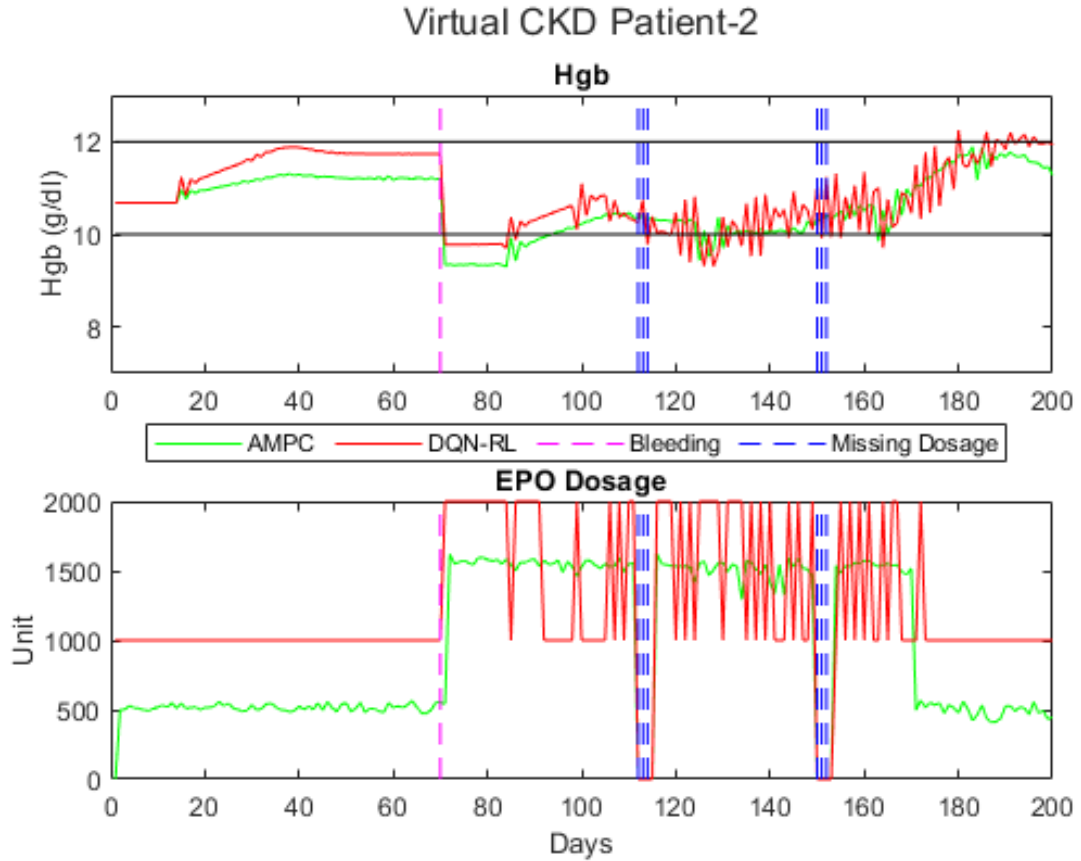


Figure 4.7: Results of DQN-RL and AMPC for the V-CKD Patient-2.

It concludes that data-driven adaptive control methods, such as AMPC and DQN-RL, are able to handle serious conditions of bleeding and missing dosage for V-CKD patients which have a narrow therapeutic window. However, one major drawback in the model-free reinforcement learning methods is the requirement of a high number of data points to train the agent. This requirement is not suitable for personalized medicine where only patient-specific data is used. To reduce the number of data points required for training the agent, Model-Based Reinforcement Learning (MBRL) is introduced in the next section.

4.3.2 Model-Based Deep Q-Learning for Optimal EPO Dosing

To reduce the number of data points required to train model-free reinforcement learning, the model identification block is introduced into Fig. 4.5. The updated block diagram for MBRL is shown in Fig. 4.8. For MBRL, data is generated from model identification in addition to measurement data points and rewards collected from the actual environment (V-CKD patient) and stored in a buffer. The stored data is used to train the agent. This reduces the number of interactions required with an actual environment by half. In this method, semi-blind robust system identification with a Kalman filter is used as

the model identification method. The results for the MBRL method are compared with AMPC and discussed in the next section.

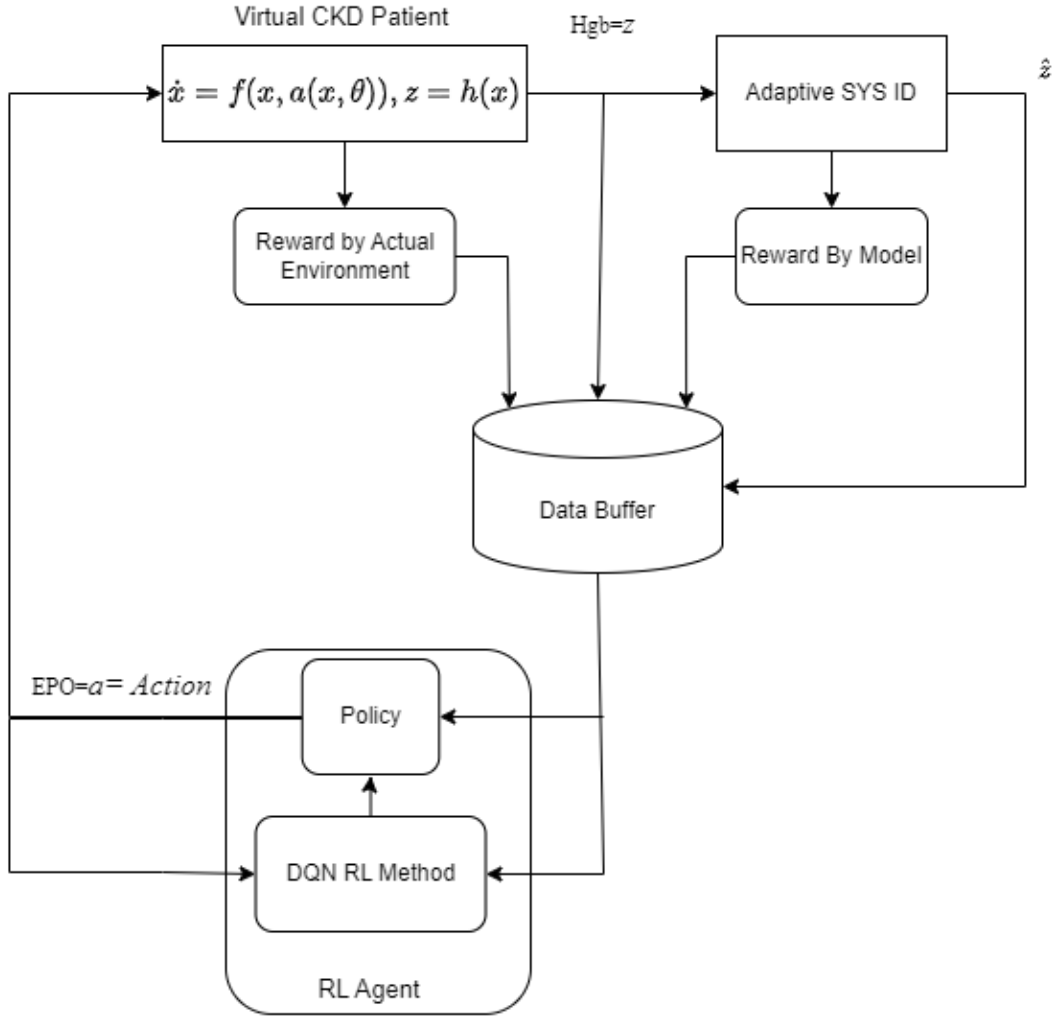


Figure 4.8: Block diagram for Model-Based DQN Reinforcement Learning (MB-DQN-RL) for V-CKD Patient.

4.3.2.1 Results

In this section, *in-silico* results of two V-CKD patients are discussed. For closed-loop simulations, V-CKD patients with different parameters, such as maturity period of cells in the erythropoiesis, total blood volume, and S_0 . are considered. To evaluate the performance of the Model-Based DQN-RL (MB-DQN-RL) and AMPC control policies, we have considered two life events, (1) bleeding and (2) missing dosages. The *in-silico* results for the first V-CKD patient are shown in Fig. 4.9. The cell maturity period of this virtual patient is 54 days, total blood volume is 5000 ml and $S_0 = 5 \times 10^5$. In simulation results, the pink dashed vertical line at 70th time step refers to the bleeding event and the vertical blue dashed line shows the two events of three consecutive missing dosages through time steps 112 to 115 and 150 to 153 days. The top plot shows the Hgb levels and the bottom plot shows EPO dosages provided by the control policies.

The green plot shows the results due to MB-DQN-RL and the red plot shows the results due to AMPC.

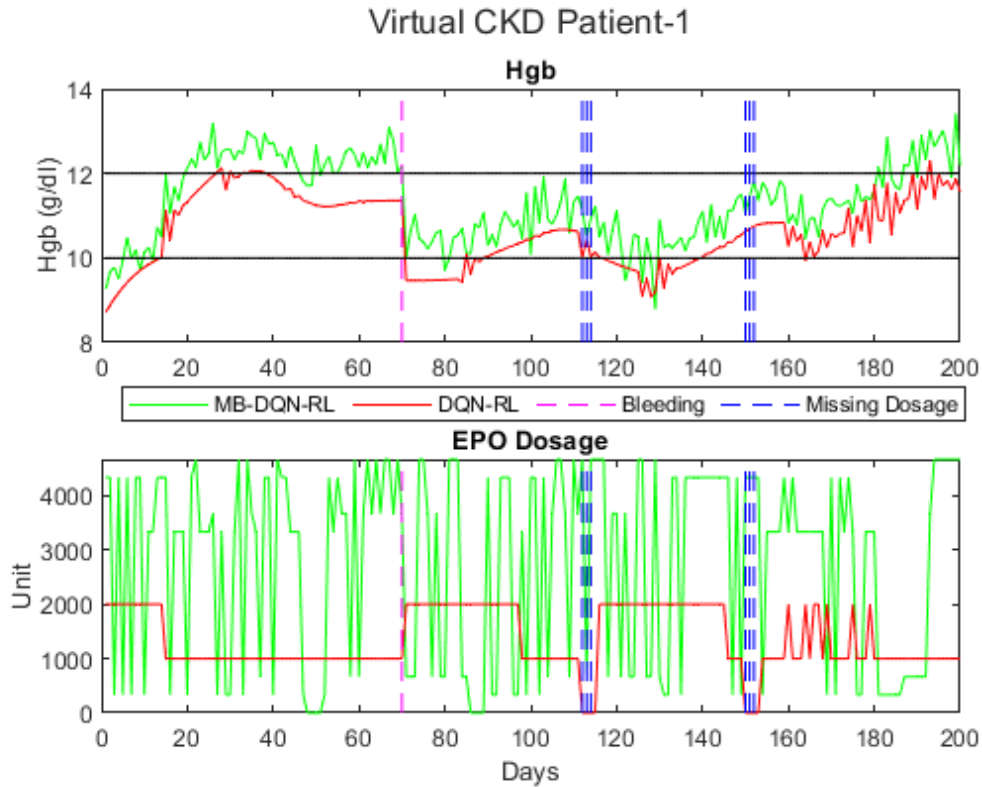


Figure 4.9: Results of MB-DQN-RL and AMPC for the V-CKD Patient-1.

Figure 4.9 shows that the initial Hgb level is 9 g/dl . The AMPC provides an initial EPO dosage of 1000 units and MB-DQN-RL suggests an EPO dosage of 20000 units, however, MB-DQN-RL shows fluctuating EPO dosages. The Hgb level rises to the desired range of $10 - 12 \text{ g/dl}$. The event of bleeding is introduced at the 70^{th} time step and the Hgb level drops. The AMPC and MB-DQN-RL changed the EPO dosage to recover the Hgb level for the virtual CKD patient. In response to this change, the Hgb level rises to the desired range and the AMPC controller decreases the EPO dosage in order to avoid overshoot. However, MB-DQN-RL has failed to give steady EPO value. The events of missing dosages are introduced through time steps 112 to 115 and 150 to 153 days. Both control policies are able to recover the Hgb level due to the missing dosages; however, the frequency of EPO dosages is high in this range. It shows that how difficult these scenarios could be handled in the real world. Overall, the MB-DQN-RL provides unstable EPO dosages which result in high values of Hgb, which is not an ideal situation for personalized medicine.

To test the proposed control policies, the results of the second V-CKD patient are shown in Fig. 4.10. The cell maturity period of this virtual patient is 54 days, total blood volume is 5100 ml and $S_0 = 5.3 \times 10^5$. The initial Hgb level for this patient is 10.68 g/dl . The AMPC provides an initial EPO dosage of 500 units and MB-DQN-RL suggests varying EPO dosages. The Hgb level remains in the desired range for both AMPC and MB-DQN-RL approaches. The Hgb level drops due to bleeding at 70^{th} time step. Both proposed control policies increase the EPO dosage to recover the Hgb

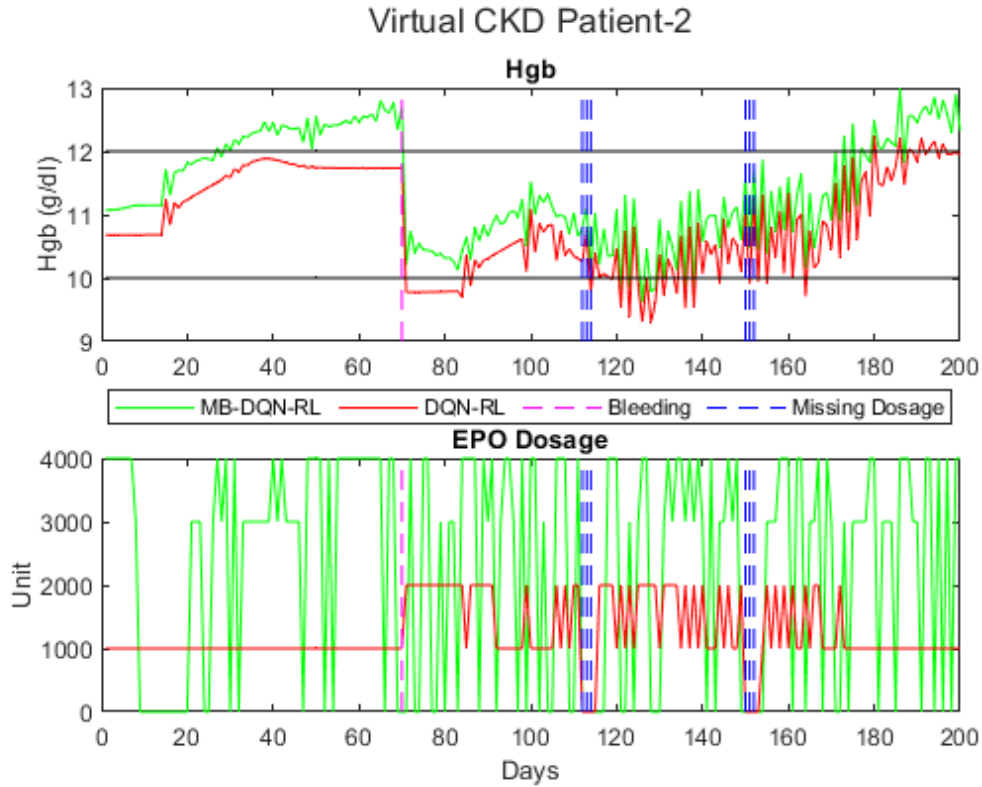


Figure 4.10: Results of MB-DQN-RL and AMPC for the V-CKD Patient-2.

level. The results show that MB-DQN-RL has more frequency in the change of EPO dosage as compared to the AMPC. The event of missing dosage introduced through time steps 112 to 115 and 150 to 153 days results in a drop in the Hgb level. However, MB-DQN-RL is not able to provide stable EPO dosages while the AMPC controller can suggest steady EPO dosages to recover the Hgb level.

This concludes that data-driven adaptive control methods, such as AMPC and MB-DQN-RL, is able to handle serious conditions of bleeding and missing dosage for V-CKD patients. To reduce the number of data points required for training the agent, model-based reinforcement learning (MBRL) is introduced. However, MB-DQN-RL has failed to provide steady EPO dosages.

CHAPTER 5

CONCLUSION AND FUTURE WORK

5.1 Summary

Personalized adaptive system identifications and adaptive controllers are studied for patients with warfarin and anemia management. In this research work, four recursive system identification techniques have been proposed: (1) semi-blind robust system identification with Kalman filter, (2) semi-blind robust system identification with model (In)validation (3) semi-blind robust system identification without model (In)validation, and (4) ARX with Kalman filter. Simulation results show that semi-blind robust system identification with Kalman filter is able to adapt the personalized patient model to represent the patient's true dose-response characteristics with the lowest error with using the limited number of patient-specific data as time progresses during the treatment. For controller design, four different types of control policies are studied for drug dosing in virtual CKD patients: (1) Adaptive model predictive control (AMPC), (2) extremum seeking control (ESC), (3) model-free reinforcement learning and (4) model-based reinforcement learning. The results show that AMPC outperforms the other control policies in order to provide steady EPO dosages to keep the Hgb level in the desired range. Furthermore, AMPC has an advantage over the reinforcement learning method on the merit of a low number of data points required to design the control policy.

5.2 Future Work

The field of data-driven Control Systems has revolutionized personalized medicine from artificial pancreas to mapping of patient dynamics. There are many opportunities in the research area such as: (1) selecting dosage in patients with comorbidities is one of the major challenges. The effect of Drugs can be altered by interacting with other medications when consumed simultaneously. The response of patients in this scenario can be predicted and observed by designing model identification methods for multi-input-multi-output (MIMO) models. The next can be the design of adaptive model identification methods for these complex models. Furthermore, one of the major challenges in the development of personalized dosing protocols is the availability of data and restriction of clinical testing. Therefore, it is important to develop cell-level virtual models of patient dose response which can be used in simulations to validate the performance of proposed methods. Personalized dosing protocols need to be tested in different scenarios such as bleeding, missing dosages, and many others. Therefore, it is important to identify more complex and realistic simulation scenarios. For control methods, more robust and auto-tuneable methods are required. Also, it is important to design wearable

sensors to sense the patient's vitals such as Hgb levels in real-time.

REFERENCES

- [1] S. Rogg, D. H. Fuertinger, S. Volkwein, F. Kappel, and P. Kotanko, “Optimal epo dosing in hemodialysis patients using a non-linear model predictive control approach,” *Journal of Mathematical Biology*, vol. 79, no. 6, pp. 2281–2313, 2019.
- [2] D. H. Fuertinger, F. Kappel, S. Thijssen, N. W. Levin, and P. Kotanko, “A model of erythropoiesis in adults with sufficient iron availability,” *Journal of mathematical biology*, vol. 66, no. 6, pp. 1209–1240, 2013.
- [3] M. Grissinger, “The five rights: a destination without a map,” *Pharmacy and Therapeutics*, vol. 35, no. 10, p. 542, 2010.
- [4] A. S. Levey and J. Coresh, “Chronic kidney disease,” *The lancet*, vol. 379, no. 9811, pp. 165–180, 2012.
- [5] E. Moore and R. Bellomo, “Erythropoietin (epo) in acute kidney injury,” *Annals of intensive care*, vol. 1, no. 1, pp. 1–10, 2011.
- [6] M. Panjeta, I. Tahirovic, J. Karamehic, E. Sofic, O. Ridic, and J. Coric, “The relation of erythropoietin towards hemoglobin and hematocrit in varying degrees of renal insufficiency,” *Materia socio-medica*, vol. 27, no. 3, p. 144, 2015.
- [7] “Data on anemia or iron deficiency,” <http://https://www.cdc.gov/nchs/fastats/anemia.htm>, accessed: 2022-07-01.
- [8] A. Hämmerlein, H. Derendorf, and D. T. Lowenthal, “Pharmacokinetic and pharmacodynamic changes in the elderly,” *Clinical pharmacokinetics*, vol. 35, no. 1, pp. 49–64, 1998.
- [9] W. L. West, E. M. Knight, S. Pradhan, and T. S. Hinds, “Interpatient variability: genetic predisposition and other genetic factors,” *The Journal of Clinical Pharmacology*, vol. 37, no. 7, pp. 635–648, 1997.
- [10] G. Ocak, M. Rookmaaker, A. Algra, G. De Borst, P. Doevendans, L. Kappelle, M. Verhaar, F. Visseren, S. S. Group, Y. van der Graaf *et al.*, “Chronic kidney disease and bleeding risk in patients at high cardiovascular risk: a cohort study,” *Journal of Thrombosis and Haemostasis*, vol. 16, no. 1, pp. 65–73, 2018.

- [11] R. Bellazzi, “Drug delivery optimization through bayesian networks: an application to erythropoietin therapy in uremic anemia,” *Computers and Biomedical Research*, vol. 26, no. 3, pp. 274–293, 1993.
- [12] M. Moscoso-Vásquez, P. Colmegna, N. Rosales, F. Garelli, and R. Sanchez-Pena, “Control-oriented model with intra-patient variations for an artificial pancreas,” *IEEE journal of biomedical and health informatics*, vol. 24, no. 9, pp. 2681–2689, 2020.
- [13] A. E. Gaweda, A. A. Jacobs, M. E. Brier, and J. M. Zurada, “Pharmacodynamic population analysis in chronic renal failure using artificial neural networks—a comparative study,” *Neural networks*, vol. 16, no. 5-6, pp. 841–845, 2003.
- [14] J. D. M. Guerrero, E. S. Olivas, G. C. Valls, A. J. S. López, J. J. P. Ruixo, and N. V. J. Torres, “Use of neural networks for dosage individualisation of erythropoietin in patients with secondary anemia to chronic renal failure,” *Computers in Biology and Medicine*, vol. 33, no. 4, pp. 361–373, 2003.
- [15] A. E. Gaweda, “Improving management of anemia in end stage renal disease using reinforcement learning,” in *2009 International Joint Conference on Neural Networks*. IEEE, 2009, pp. 953–958.
- [16] M. K. Muezzinoglu, “Approximate dynamic programming for anemia management,” Ph.D. dissertation, University of Louisville, 2006.
- [17] J. D. Martín-Guerrero, G. Camps-Valls, E. Soria-Olivas, A. J. Serrano-López, J. J. Pérez-Ruixo, and N. V. Jiménez-Torres, “Dosage individualization of erythropoietin using a profile-dependent support vector regression,” *IEEE Transactions on Biomedical Engineering*, vol. 50, no. 10, pp. 1136–1142, 2003.
- [18] Y. Chait, M. J. Germain, C. V. Hollot, and J. Horowitz, “The role of feedback control design in developing anemia management protocols,” *Annals of biomedical engineering*, vol. 49, no. 1, pp. 171–179, 2021.
- [19] A. Affan, J. M. Zurada, and T. Inanc, “Adaptive individualized modeling from limited clinical data for precise anemia management,” *IEEE Access*, vol. 9, pp. 119 466–119 475, 2021.
- [20] A. Affan and T. Inanc, “Robust system identification for anemia management,” *IFAC-PapersOnLine*, vol. 54, no. 7, pp. 328–333, 2021.
- [21] A. E. Gaweda, A. A. Jacobs, G. R. Aronoff, and M. E. Brier, “Model predictive control of erythropoietin administration in the anemia of esrd,” *American Journal of Kidney Diseases*, vol. 51, no. 1, pp. 71–79, 2008.
- [22] J. McAllister, Z. Li, J. Liu, and U. Simonsmeier, “Erythropoietin dose optimization for anemia in chronic kidney disease using recursive zone model predictive

- control,” *IEEE Transactions on Control Systems Technology*, vol. 27, no. 3, pp. 1181–1193, 2018.
- [23] R. S. Riley, D. Rowe, and L. M. Fisher, “Clinical utilization of the international normalized ratio (inr),” *Journal of clinical laboratory analysis*, vol. 14, no. 3, pp. 101–114, 2000.
- [24] J. Hirsh and L. Poller, “The international normalized ratio: a guide to understanding and correcting its problems,” *Archives of internal medicine*, vol. 154, no. 3, pp. 282–288, 1994.
- [25] N. A. Limdi, “Warfarin pharmacogenetics: challenges and opportunities for clinical translation,” *Frontiers in Pharmacology*, vol. 3, p. 183, 2012.
- [26] N. Eriksson and M. Wadelius, “Prediction of warfarin dose: why, when and how?” *Pharmacogenomics*, vol. 13, no. 4, pp. 429–440, 2012.
- [27] S. L. Booth and M. A. Centurelli, “Vitamin k: a practical guide to the dietary management of patients on warfarin,” *Nutrition reviews*, vol. 57, no. 9, pp. 288–296, 1999.
- [28] T. Khan, H. Wynne, P. Wood, A. Torrance, C. Hankey, P. Avery, P. Kesteven, and F. Kamali, “Dietary vitamin k influences intra-individual variability in anticoagulant response to warfarin,” *British journal of haematology*, vol. 124, no. 3, pp. 348–354, 2004.
- [29] B. F. Gage and L. J. Lesko, “Pharmacogenetics of warfarin: regulatory, scientific, and clinical issues,” *Journal of thrombosis and thrombolysis*, vol. 25, no. 1, pp. 45–51, 2008.
- [30] I. W. P. Consortium, “Estimation of the warfarin dose with clinical and pharmacogenetic data,” *New England Journal of Medicine*, vol. 360, no. 8, pp. 753–764, 2009.
- [31] J. A. Johnson, L. Gong, M. Whirl-Carrillo, B. F. Gage, S. A. Scott, C. Stein, J. Anderson, S. E. Kimmel, M. T. M. Lee, M. Pirmohamed *et al.*, “Clinical pharmacogenetics implementation consortium guidelines for cyp2c9 and vkorc1 genotypes and warfarin dosing,” *Clinical Pharmacology & Therapeutics*, vol. 90, no. 4, pp. 625–629, 2011.
- [32] B. Gage, C. Eby, J. Johnson, E. Deych, M. Rieder, P. Ridker, P. Milligan, G. Grice, P. Lenzini, A. Rettie *et al.*, “Use of pharmacogenetic and clinical factors to predict the therapeutic dose of warfarin,” *Clinical Pharmacology & Therapeutics*, vol. 84, no. 3, pp. 326–331, 2008.
- [33] H. Furuya, P. Fernandez-Salguero, W. Gregory, H. Taber, A. Steward, F. J. Gonzalez, and J. R. Idle, “Genetic polymorphism of cyp2c9 and its effect on warfarin

- maintenance dose requirement in patients undergoing anticoagulation therapy,” *Pharmacogenetics and Genomics*, vol. 5, no. 6, pp. 389–392, 1995.
- [34] D. S. Budnitz, M. C. Lovegrove, N. Shehab, and C. L. Richards, “Emergency hospitalizations for adverse drug events in older americans,” *New England Journal of Medicine*, vol. 365, no. 21, pp. 2002–2012, 2011.
- [35] M. Pirmohamed, S. James, S. Meakin, C. Green, A. K. Scott, T. J. Walley, K. Farrar, B. K. Park, and A. M. Breckenridge, “Adverse drug reactions as cause of admission to hospital: prospective analysis of 18 820 patients,” *Bmj*, vol. 329, no. 7456, pp. 15–19, 2004.
- [36] S. M. Öztaner, T. T. Temizel, S. R. Erdem, and M. Özer, “A bayesian estimation framework for pharmacogenomics driven warfarin dosing: a comparative study,” *IEEE journal of biomedical and health informatics*, vol. 19, no. 5, pp. 1724–1733, 2014.
- [37] S. R. Johnson, J. T. Granton, G. A. Tomlinson, H. A. Grosbein, T. Le, P. Lee, M. E. Seary, G. A. Hawker, and B. M. Feldman, “Warfarin in systemic sclerosis-associated and idiopathic pulmonary arterial hypertension. a bayesian approach to evaluating treatment for uncommon disease,” *The Journal of rheumatology*, vol. 39, no. 2, pp. 276–285, 2012.
- [38] D. F. Wright and S. B. Duffull, “A bayesian dose-individualization method for warfarin,” *Clinical pharmacokinetics*, vol. 52, no. 1, pp. 59–68, 2013.
- [39] A.-K. Hamberg, J. Hellman, J. Dahlberg, E. N. Jonsson, and M. Wadelius, “A bayesian decision support tool for efficient dose individualization of warfarin in adults and children,” *BMC medical informatics and decision making*, vol. 15, no. 1, pp. 1–9, 2015.
- [40] K. E. Hines, T. R. Middendorf, and R. W. Aldrich, “Determination of parameter identifiability in nonlinear biophysical models: A bayesian approach,” *Journal of General Physiology*, vol. 143, no. 3, pp. 401–416, 2014.
- [41] R. De Levie, *Advanced Excel for scientific data analysis*. Oxford University Press, USA, 2004.
- [42] A. Sharabiani, A. Bress, E. Douzali, and H. Darabi, “Revisiting warfarin dosing using machine learning techniques,” *Computational and mathematical methods in medicine*, vol. 2015, 2015.
- [43] A. Chocron, J. Oster, S. Biton, F. Mandel, M. Elbaz, Y. Y. Zeevi, and J. A. Behar, “Remote atrial fibrillation burden estimation using deep recurrent neural network,” *IEEE Transactions on Biomedical Engineering*, vol. 68, no. 8, pp. 2447–2455, 2020.

- [44] A. Sharabiani, H. Darabi, A. Bress, L. Cavallari, E. Nutescu, and K. Drozda, “Machine learning based prediction of warfarin optimal dosing for african american patients,” in *2013 IEEE international conference on automation science and engineering (CASE)*. IEEE, 2013, pp. 623–628.
- [45] T. Inanc, M. Sznaier, P. A. Parrilo, and R. S. S. Peña, “Robust identification with mixed parametric/nonparametric models and time/frequency-domain experiments: Theory and an application,” *IEEE Transactions on Control Systems Technology*, vol. 9, no. 4, pp. 608–617, 2001.
- [46] W. Ma, M. Yilmaz, M. Sznaier, and C. Lagoa, “Semi-blind robust identification/-model (in) validation with applications to macro-economic modelling,” *IFAC Proceedings Volumes*, vol. 38, no. 1, pp. 886–891, 2005.
- [47] W. Ma, “Semi-blind robust identification and model (in) validation,” Ph.D. dissertation, The Pennsylvania State University, 2007.
- [48] M. Yilmaz, “Robust systems theory applications to macroeconomic stabilization problems,” Ph.D. dissertation, The Pennsylvania State University, 2005.
- [49] A. Affan, J. M. Zurada, and T. Inanc, “Control-relevant adaptive personalized modeling from limited clinical data for precise warfarin management,” *IEEE Open Journal of Engineering in Medicine and Biology*, vol. 3, pp. 242–251, 2022.
- [50] L. Ljung, “System identification,” in *Signal analysis and prediction*. Springer, 1998, pp. 163–173.
- [51] K. S. Narendra and A. M. Annaswamy, *Stable adaptive systems*. Courier Corporation, 2012.
- [52] F. Borrelli, A. Bemporad, and M. Morari, *Predictive control for linear and hybrid systems*. Cambridge University Press, 2017.
- [53] J.-S. Kim, “Recent advances in adaptive mpc,” *ICCAS 2010*, pp. 218–222, 2010.
- [54] S. Zhang, L. Dai, and Y. Xia, “Adaptive mpc for constrained systems with parameter uncertainty and additive disturbance,” *IET Control Theory & Applications*, vol. 13, no. 15, pp. 2500–2506, 2019.
- [55] Z.-S. Hou and Z. Wang, “From model-based control to data-driven control: Survey, classification and perspective,” *Information Sciences*, vol. 235, pp. 3–35, 2013.
- [56] K. B. Ariyur and M. Krstic, *Real-time optimization by extremum-seeking control*. John Wiley & Sons, 2003.
- [57] A. Coronato, M. Naeem, G. De Pietro, and G. Paragliola, “Reinforcement learning for intelligent healthcare applications: A survey,” *Artificial Intelligence in Medicine*, vol. 109, p. 101964, 2020.

- [58] C. Yu, J. Liu, S. Nemati, and G. Yin, “Reinforcement learning in healthcare: A survey,” *ACM Computing Surveys (CSUR)*, vol. 55, no. 1, pp. 1–36, 2021.
- [59] A. E. Gaweda, M. K. Muezzinoglu, G. R. Aronoff, A. A. Jacobs, J. M. Zurada, and M. E. Brier, “Reinforcement learning approach to individualization of chronic pharmacotherapy,” in *Proceedings. 2005 IEEE International Joint Conference on Neural Networks, 2005.*, vol. 5. IEEE, 2005, pp. 3290–3295.
- [60] J. M. Malof and A. E. Gaweda, “Optimizing drug therapy with reinforcement learning: The case of anemia management,” in *The 2011 International Joint Conference on Neural Networks*. IEEE, 2011, pp. 2088–2092.
- [61] P. Escandell-Montero, M. Chermisi, J. M. Martinez-Martinez, J. Gomez-Sanchis, C. Barbieri, E. Soria-Olivas, F. Mari, J. Vila-Francés, A. Stopper, E. Gatti *et al.*, “Optimization of anemia treatment in hemodialysis patients via reinforcement learning,” *Artificial intelligence in medicine*, vol. 62, no. 1, pp. 47–60, 2014.

CURRICULUM VITAE

Affan Affan

Mailing Address: 2330 Crittenden Dr., 113-A, Louisville 40217, KY, USA. Email:affan.affan@louisville.edu
Mobile : +1 (502)-999-2388

Education

- **University of Louisville**, Louisville, United States Jan. 2020 – Dec. 2023
Doctor of Philosophy (Ph.D.) in Electrical and Computer Engineering
Research Area: Personalized medicine, Artificial Intelligence, Control Systems
CGPA:4.00/4.00
- **Lahore University of Management Sciences**, Lahore, Pakistan Sep. 2017 - Jun. 2019
Master of Science (MS) in Electrical Engineering
Research Area: State Estimation, System Modelling.
CGPA:3.38/4.00
- **COMSATS Institute of Information Technology**, Lahore, Pakistan Aug. 2017
Bachelor of Science in Electrical (Telecommunication) Engineering
CGPA:3.25/4.00

Journal Articles:

1. **A. Affan**, J. M. Zurada and T. Inanc, "Control-Relevant Adaptive Personalized Modeling From Limited Clinical Data for Precise Warfarin Management," in IEEE Open Journal of Engineering in Medicine and Biology, vol. 3, pp. 242-251, 2022, doi: 10.1109/OJEMB.2023.3240072.
2. **A. Affan**, J. M. Zurada and T. Inanc, "Adaptive Individualized Modeling From Limited Clinical Data for Precise Anemia Management," in IEEE Access, vol. 9, pp. 119466-119475, 2021, doi: 10.1109/ACCESS.2021.3106856.
3. **A. Affan**, H. M. Asif, and N. Tarhuni, "Machine-learning-based indoor localization under shadowing condition for P-NOMA VLC Systems," Sensors, vol. 23, no. 11, p. 5319, 2023. doi:10.3390/s23115319
4. **A. Affan**, H. A. Nasir, T. Manzoor, and A. Muhammad, "Mobile sensing for estimation of Hydro-dynamic parameters for minimally gauged open channels," Computers and Electronics in Agriculture, vol. 198, p. 107072, 2022.

5. H. M. Asif, **A. Affan**, N. Tarhuni, and K. Raahemifar, “Deep Learning-Based Next-Generation Waveform for Multiuser VLC Systems,” *Sensors*, vol. 22, no. 7, p. 2771, Apr. 2022, doi: 10.3390/s22072771.
6. **A. Affan**, S. Mumtaz, H. M. Asif and L. Musavian, ”Performance Analysis of Orbital Angular Momentum (OAM): A 6G Waveform Design,” in *IEEE Communications Letters*, vol. 25, no. 12, pp. 3985-3989, Dec. 2021, doi: 10.1109/LCOMM.2021.3115041.

Peer-Reviewed Conference Papers

1. **A. Affan**, and T.Inanc, “Learning Enabled Control for Optimal EPO Dosage in Virtual CKD Patients: Case of Bleeding and Missing Dosage,” 2024 American Control Conference (ACC). (under review)
2. **A. Affan**, T.Inanc and J. M. Zurada, “Patient-Specific Modeling and Model Predictive Control Approach to Personalized Optimal Anemia Management,” 2023 45th Annual International Conference of the IEEE Engineering in Medicine & Biology Society (EMBC), 2023.
3. **A. Affan** and T.Inanc, “Personalized EPO Dose Guidance using Adaptive Control Methods: Case of Bleeding and Missing Dosage,” 2023 45th Annual International Conference of the IEEE Engineering in Medicine & Biology Society (EMBC), 2023.
4. **A. Affan** and T. Inanc, ”Clinically Relevant Adaptive Modeling for Personalized Drug Dosing,” 2021 IEEE/ACM Conference on Connected Health: Applications, Systems and Engineering Technologies (CHASE), Washington, DC, USA, 2021, pp. 128-129, doi: 10.1109/CHASE52844.2021.00029.
5. **A. Affan**, J. M. Zurada, M. E. Brier and T. Inanc, ”Adaptive Individualized Drug-Dose Response Modeling from a Limited Clinical Data: Case of Warfarin Management,” 2021 43rd Annual International Conference of the IEEE Engineering in Medicine & Biology Society (EMBC), Mexico, 2021, pp. 4448-4451, doi: 10.1109/EMBC46164.2021.9630158.
6. S. I. Ali Meerza, **A. Affan**, H. Mirinejad, M. E. Brier, J. M. Zurada and T. Inanc, ”Precise Warfarin Management through Personalized Modeling and Control with Limited Clinical Data,” 2021 43rd Annual International Conference of the IEEE Engineering in Medicine & Biology Society (EMBC), Mexico, 2021, pp. 5035-5038, doi: 10.1109/EMBC46164.2021.9629945.
7. **A. Affan** and T. Inanc, “Robust system identification for anemia management,” *IFAC-PapersOnLine*, vol. 54, no. 7, pp. 328–333, 2021.

8. H. M. Asif, **A. Affan** and N. Tarhuni, "Spatial Distribution Waveform Design for an Efficient Optical Communication System," 2022 4th West Asian Symposium on Optical and Millimeter-wave Wireless Communications (WASOWC), Tabriz, Iran, 2022, pp. 1-5, doi: 10.1109/WASOWC54657.2022.9798427.
9. **A. Affan**, U. Khan, H. M. Asif and K. Raahemifar, "Multiuser Visible Light Communication System using Hybrid OFDM-PWM," 2020 International Symposium on Networks, Computers and Communications (ISNCC), Montreal, QC, Canada, 2020, pp. 1-6, doi: 10.1109/ISNCC49221.2020.9297203.
10. **A. Affan**, H. A. Nasir, and A. Muhammad, "State estimation in 2D hydrological models using lagrangian sensors and low resolution elevation maps," IFAC-PapersOnLine, vol. 53, no. 2, pp. 16549–16554, 2020.
11. **A. Affan**, H. A. Nasir, B. Shafiq, and A. Muhammad, "Data assimilation of mobile sensors in hydrological models of unsteady flow," IFAC-PapersOnLine, vol. 52, no. 23, pp. 29–36, 2019.
12. M. H. Riaz, M. K. Yousaf, T. Izhar, T. Kamal, M. Danish, **A. Affan**, and M. H. Qasmi, "Micro Hydro Power Plant Dummy Load Controller," 2018 1st International Conference on Power, Energy and Smart Grid (ICPESG), 2018.